Development of a 1K facility and modeling of a superfluid magnetic pump with no moving parts

by

Amir E. Jahromi

A thesis submitted in partial fulfillment of

the requirements for the degree of

Master of Science

(Mechanical Engineering)

at the

UNIVERSITY OF WISCONSIN – MADISON

2011

This thesis has been approved by

Prof. Franklin K. Miller, Assistant Professor (Advisor)	**Date**
Prof. Gregory F. Nellis, Associate Professor (Co-Advisor)	**Date**

Abstract

Sub Kelvin refrigeration systems are a key device in current and future x-ray and astrophysics missions. These missions enable space science agencies to explore the origin and structure of the universe. A new sub Kelvin refrigeration cycle, a pulse tube superfluid cycle, has been proposed as a more reliable alternative to current state of the art sub Kelvin coolers. The new pulse tube superfluid refrigeration system will have no moving parts and will be able to run continuously unlike other sub Kelvin refrigerators. This refrigerator uses a superfluid magnetic pump that is the main focus of this research.

This thesis describes the design, fabrication, and the test run of the low temperature facility along with the integrated 1 Kelvin refrigeration facility that has been built to support the superfluid magnetic pump "proof of concept" experiment. This test demonstrated that the system was fully capable of producing subcooled, superfluid helium. This verified the integrity of the test facility components and instrumentation at a nominal temperature of 1 Kelvin. The ultimate temperature attained with this refrigerator is 1.392 K with a cooling power of 200 mW at 1.72 K. Improvements in the 1 Kelvin facility are identified in order to further increase the cooling power at lower temperatures.

This thesis also describes the development of a model for the superfluid magnetic pump. This pump is proposed to operate between 1.5 and 1.9 K and between applied magnetic fields of 0 and 2 Tesla. The modeling of the superfluid magnetic pump lead to the conclusion that it is capable of producing a mass flow rate that will be useful to compress and expand ^{3}He in a ^{3}He-^{4}He mixture during future validation of the newly proposed superfluid pulse tube refrigerator.

Acknowledgements

This thesis is dedicated to my Mom, Shahrzad, my Dad, Hamid, my uncle, Shahram, my grandparents, Lagha and Javad, and my fiancée, Amanda. I miss you Grandpa….

First I would like to thank my primary advisor, Franklin Miller. I feel quite honored when you selected me to work with you. I have enjoyed working with you a lot and I look forward to working with you more in the future. Franklin is not only my primary advisor, but he is a dear friend and I am quite honored to be his first graduate student, and first "to be" graduating student. Our friendship deepens because of this unique first student-professor relationship. Thank you for your patience, kindness and time to explain all the details I needed to know in low temperature physics and cryogenics. I have learned a ton from you and thank you is simply not enough to express my appreciation…

I would like to thank my second advisor, Greg Nellis. Greg, I am honored to work for you. You made me to be what an engineer is supposed to be because of your constructive criticisms, concerns, and your patience explaining different problems I came up with during the modeling and experimentation. I am glad that I have vastly improved as a writer during my Masters career. Also I have something to tell you about your Heat transfer textbook: Your book is the best in heat transfer, an exemplary work and one of a kind in engineering. That's why I was among the first to purchase the book before I showed up at Wisconsin. I am also grateful that I had the opportunity to take two heat transfer classes with you. Without exaggeration, you are the best instructor I have ever had for a class in my life! Thanks a lot…

I would like to sincerely thank Sandy Klein for initially making a generous offer to hire me at the UW – Madison and at the Solar Energy Lab (SEL). Had it not been for Sandy I probably would

have not ended up here. But if I have to repeat this all over again I will still make the same decision I made two years ago, to come to Wisconsin and to work in the SEL group. Despite the fact that plans changed and I had to switch gears in the research topic I still had the honor to take your classes and learn much from you. Whenever I get results from EES, I call it the "miracle of EES". Ample thanks to you Sandy, I have the highest respect for you.

I also would like to thank John Pfotenhauer for his constructive advice during the 1 K facility tests. I am also grateful for taking your Vacuum Science class. It helped me better understand the proper vacuum procedures and explained the confusing results I was getting when I used to purge the 1 K line with helium. Thanks John.

Jacob Leachman, former SEL PhD student and current assistant professor at Washington State University, I thank you for taking me down the cold valleys of cryogenics when I started at UW. I'll never forget the many fine conversations we had in the office. Thank you for being so patient explaining all the details in cryogenics and telling me little points I had to consider when assembling my research apparatus. I miss you a lot, you are one of my best friends, Jake.

Harrison Skye, former SEL PhD student, I thank you for being so patient with me at times. Thank you for letting me borrow many of your tools and equipment from your lab. I enjoyed many of the fine conversations we had about different points of the project.

Dad and Mom, I don't know what to say, really! I am indebted to your encouragements, your patience answering all my questions when I was growing up. I feel honored being born in a family of engineers. Thank you is simply and obviously an understatement… I really don't know how to thank both of you; I hope I have answered part of your wishes with my work.

Shahram, without you I would not have had all of these great opportunities I had in this land of opportunity! I am now a US citizen because you paved this path for me with your thoughtfulness long ago. Thanks my beloved uncle.

Amanda, my lovely fiancée, without you I would not have been able to manage myself during the last months of my research. Thank you for your encouragement, love and support and to provide a stress free atmosphere every day I came back from school.

Thank you to my former undergraduate assistants Zheming Tong, Aaron Conger, and foremost and specifically the following: Bradley Moore, Jim Trauba and Dan Lawler. Brad, I'm sorry for the accident you had, I'm glad the "finger part" worked well with the rest of the components!

In the end I would like to thank Amanda Pertzborn, Dan Potratz, Dan O'Connor, Dan Schick, Bryant Mueller, and the rest of the SEL group for their friendship and support. Keith Griego, "my brother" thank you for your encouragement and showing me to believe in who I can be.

Greatly acknowledged financial support was provided by the Chester E. and Flora Jane LeRoy fellowship through my Master's career.

Table of Contents

Table of figures

List of tables

Nomenclature

A_c	Cross sectional area (m^2)
A_s	Surface area (m^2)
B	External applied magnetic field (Tesla)
Bi	Biot number (-)
b	Internal magnetic field (Tesla)
$\dot{C}$	Capacitance rate (W/K)
c	Heat capacity (J/kg-K)
D,d	Diameter (m)
Dev	Absolute deviation
E_b	Blackbody emissive power (W/m^2)
E	Energy (J)
ΔE	Energy resolution (J)
F	View factor (-)
f	Friction factor (-)
f_{th}	Film thickness (m)
g	Gravitational acceleration
H	Height (m)
h	Heat transfer convection coefficient (W/m^2-K)
h_k	Kapitsa conductance (W/m^2-K)
I	Electric current (Amp)
i	Enthalpy (J/kg)
J	Spin number (-)
j	Number of (in numerical model)
k	Thermal conductivity (W/m-K)
L	Length (m)
L_v	Latent heat of vaporization (J/kg)
MAT	Measurement accuracy temperature
MAV	Measurement accuracy voltage
MW	Molecular weight (kg/mol)
m	Mass (kg)
$\dot{m}$	Mass flow rate (kg/s)
N	Number of
NTU	Number of Transfer Units (-)
Nu	Nusselt number (-)
P	Pressure (Pa)
Q	Heat (J)
$\dot{q}$	Heat transfer rate (W)

R	Thermal resistance (K/W)
RR	Relative roughness (-)
r	Radius (m)
S_{pump}	Diaphragm Pumping speed (m^3/s)
$SenSen$	Sensor sensitivity (ohm/K)
$SenRdg$	Sensor reading
s	Entropy (J/kg-K)
T	Temperature (K)
$\bar{T}$	Averaged temperature (K)
t	Time (s)
UA	Conductance (W/K)
u	Velocity (m/s)
u_{He}	Internal energy of helium (J/kg)
V	Volume (m^3)
$\dot{V}$	Volumetric flow rate (m^3/s)
x	Location (m)
y	Yield (-)
Z	Flow impedance ($1/m^3$)

Greek Symbols

β	Bohr Magneton
ε	Emissivity (-)
λ	Wavelength (micron)
μ	Viscosity (Pa-s)
v	Specific volume ($1/m^3$)
ρ	Density (kg/m^3)
σ	Stefan-Boltzmann's constant ($W/m^2\text{-}K^4$)
τ	Period (s)
ψ	Standard deviation

1 INTRODUCTION

Sub-Kelvin refrigeration systems are a key device in current and future x-ray and astrophysics missions. These missions enable space science agencies to explore the origin and structure of the universe. Helium is the only element capable of producing sub-Kelvin temperatures using various thermodynamic refrigeration cycles, therefore an understanding of helium and its properties play an important role in understanding sub-Kelvin refrigeration systems. A new sub-Kelvin refrigeration cycle, a pulse tube superfluid cycle, has been proposed as a more reliable alternative to current state of the art sub-Kelvin coolers. The new pulse tube superfluid refrigeration system uses a pump, the superfluid magnetic pump, which is one of the main focuses of this work.

1.1 The need for sub-Kelvin refrigeration

Space instruments need to be cooled to sub Kelvin temperatures for new infrared and x-ray astrophysics missions. The current state of the art detectors for infrared and x-ray astrophysics missions are cryogenic detectors; either Microwave Kinetic Inductance Detectors (MKID) or micro-calorimeters. These detectors, integrated in a larger system, will enable space science agencies to discover the origin, structure, evolution and destiny of the universe. Both detector types require operation at sub-Kelvin temperatures for the highest sensitivity applications. Figure 1-1 shows a finished micro-colorimeter array bonded to a sensor board (PTB 2008).

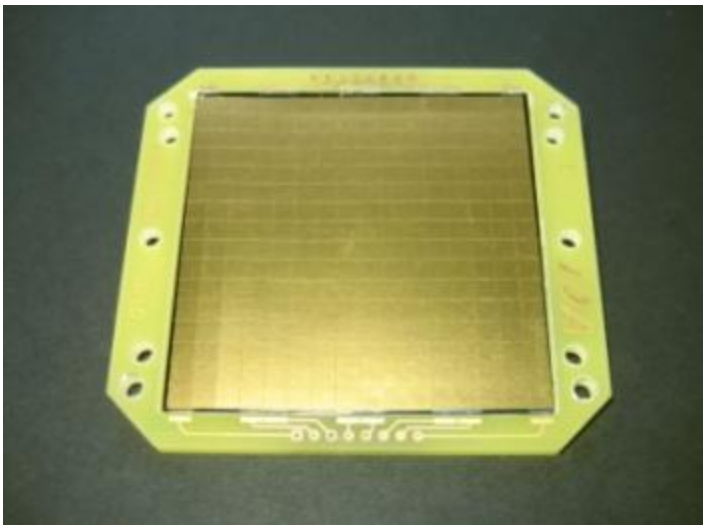

Figure 1-1 A finished micro-calorimeter array bonded to a sensor board (PTB 2008)

The structure of a micro-calorimeter consists of an absorber plate, a thermometer, and a weak thermal link that connects the absorber plate to a platform operating at temperatures below 1 Kelvin. A simplified schematic of a micro-calorimeter is depicted in Figure 1-2.

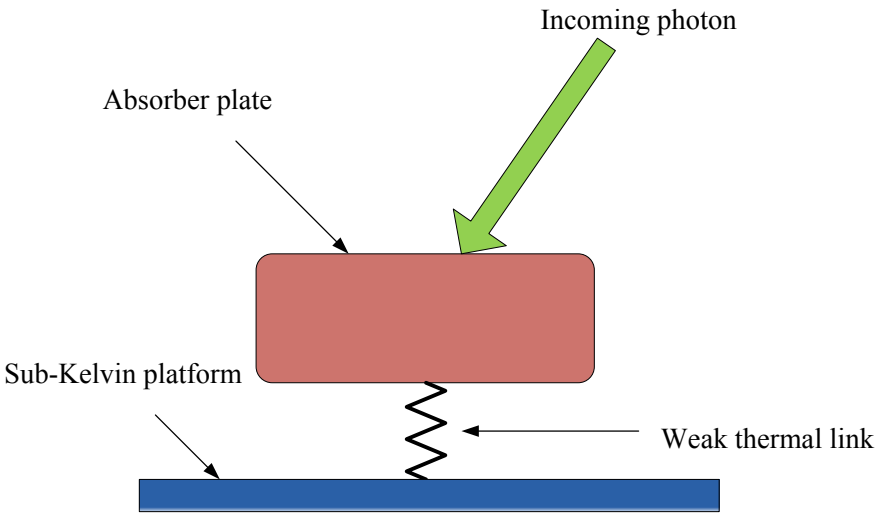

Figure 1-2 A simplified schematic of a micro-calorimeter

When a photon hits the absorber plate, the energy caused by the impact is converted into heat. This energy conversion will yield a temperature rise in the absorber material. Once the temperature increase is registered by a sensitive thermometer, the absorber material must be returned to its quiescent state. In order to return to the initial temperature heat is transferred from the absorber plate to a platform cooled by a sub-Kelvin cooler through a weak thermal link.

The objective of a micro-calorimeter is to measure the energy of photons hitting the absorber plate. Each micro-calorimeter is built for a specific bandpass that is, the maximum energy of an incoming photon. For typical x-ray applications the bandpass varies between 100 eV and 10 keV (ECAL - MIT 2009). Each micro-calorimeter also provides a specific energy resolution. For instance, if a photon with 5 keV energy hits the absorber plate of a micro-calorimeter, built for a bandpass of 10 keV and an energy resolution of 1 eV, then the reading provided by this micro-calorimeter will be 5 keV +/- 1eV. The energy resolution that a micro-calorimeter can provide is proportional to the absorber plate temperature and bandpass of the device. The energy resolution of a micro-calorimeter is approximated as (ECAL- MIT 2009):

$$\Delta E \simeq 2.35\sqrt{4\,\sigma\,T\,E_{\max}} \tag{1.1}$$

where σ is the Stefan-Boltzmann's constant ($5.67\text{x}10^{-8}$ W/m^2-K^4), T is the absorber plate temperature and E_{max} is the bandpass. For a fixed value of the bandpass, this implies that a lower temperature in the absorber plate results in a higher energy resolution. The energy resolution as a function of temperature for different constant values of bandpass is shown in Figure 1-3. At an average outer space temperature of 2.7 K and a bandpass of 10 keV, the energy resolution is 7.2 eV, whereas at 100 mK the energy resolution is 1.4 eV (an 80% improvement in energy resolution) assuming the same bandpass.

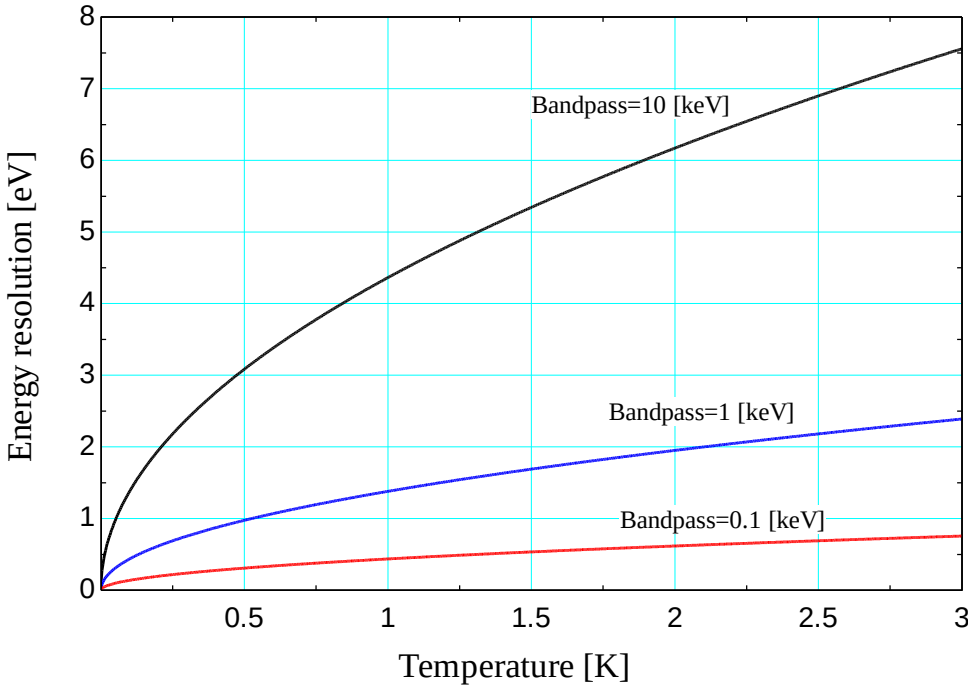

Figure 1-3 Energy resolution as a function of temperature at constant values of bandpass for a micro-calorimeter

The thermometer used in micro-calorimeters is a Transition Edge Sensor (TES). Its purpose is to measure the temperature rise of the absorber plate. These sensors are made from superconducting materials. A superconductor has a finite electrical resistance above its transition temperature (T_c). Once the temperature drops below its transition temperature the electrical resistance drops to zero. The transition from a finite value to a value of zero occurs in a narrow temperature range, typically in the order of a few milli-Kelvins. At its transition temperature, a small change in temperature produces a much greater change in resistance. This implies a high sensitivity in measurement readings. A qualitative plot of electrical resistance versus temperature for such superconductors is shown in Figure 1-4.

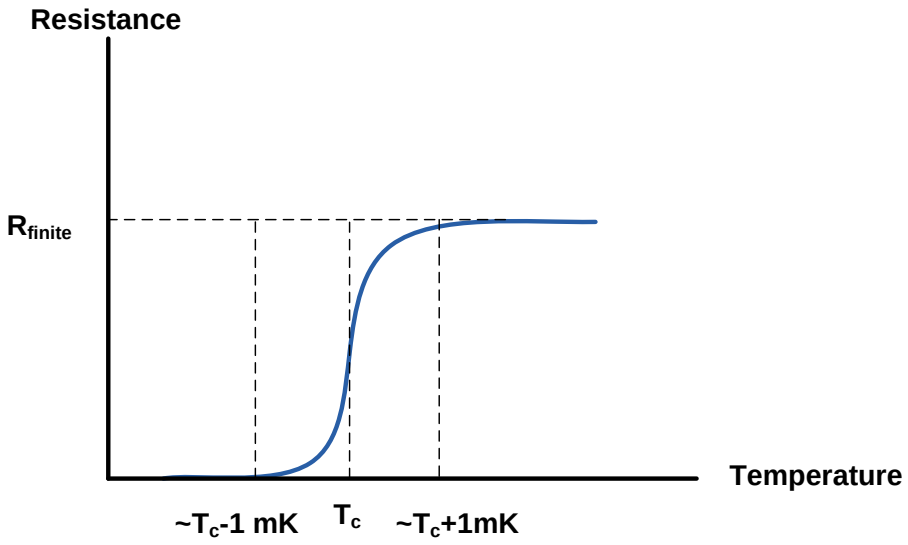

Figure 1-4 Qualitative resistance as a function of temperature plot for a superconductor used in a TES

The two most important parameters that are considered in the design of a micro-calorimeter are the ultimate low temperature that a sub-Kelvin cooler can attain and the selection of a superconductor. Lower absorber plate temperatures in a micro-calorimeter produce a higher energy resolution, and the superconductor material used in a TES is selected such that its transition temperature lies within the operating temperature range of the sub-Kelvin cooler. Therefore sub-Kelvin coolers are an important and integral part of space science detectors and sensors.

1.2 Helium

Helium is an odorless, colorless element. It enjoys weak intermolecular potential. Helium was first liquefied by Dutch physicist Heike Kammerlingh Onnes in 1908 (Wilks 1967). Of all the cryogenic fluids, helium has the lowest critical temperature and boiling point. Its phase diagram, shown in Figure 1-5, does not have a triple point. This is because helium does not solidify under its own vapor pressure even at temperatures close to zero Kelvin. A pressure greater than 25 atm

must be exerted on the liquid phase at temperatures near zero Kelvin in order to solidify helium. This characteristic of helium makes it the only cryogenic fluid capable of producing sub-Kelvin temperatures using various thermodynamic refrigeration cycles. Some facts about helium are listed in Table 1-1.

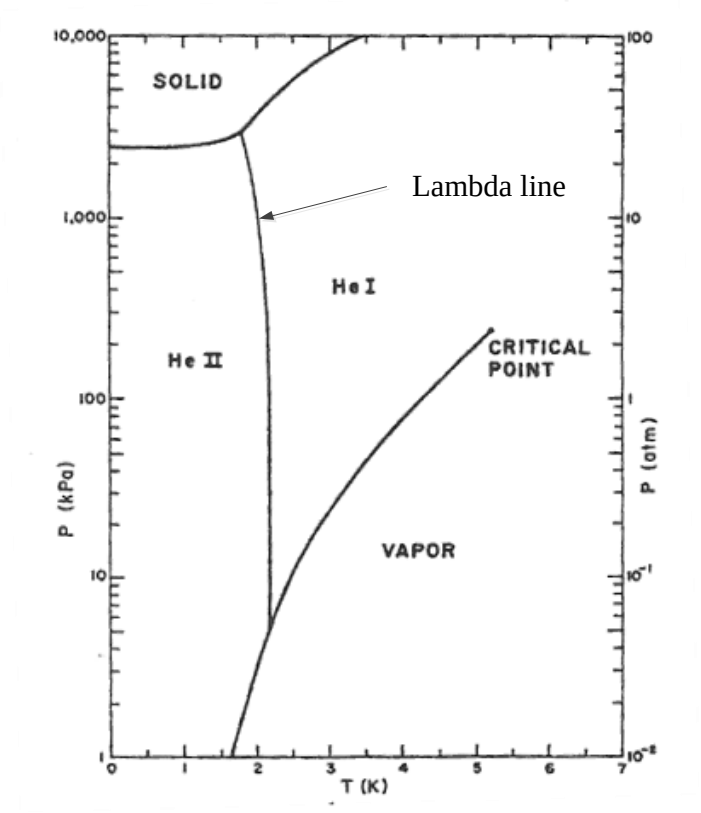

Figure 1-5 Phase diagram for helium (Van Sciver 1986)

Critical point	5.2 K
Boiling point	4.22 K
Lambda point	2.172 K
Triple point	Does not exist

Table 1-1 Some facts about helium (all values at atmospheric pressure)

1.3 He I and He II

Helium, when liquefied, remains a normal fluid until its temperature is decreased to a transition temperature that is known as the lambda point (and labeled the lambda line) at which point helium undergoes a phase transition. The lambda line has its name due to its resemblance to the Greek letter lambda when tracing the specific heat versus temperature plot of helium at the transitional region (Van Sciver 1986). The lambda line is shown in Figure 1-5. Liquid helium above the lambda line is known as He I or the "warmer liquid helium". He I is regarded as a normal fluid because it behaves as a Newtonian fluid. There is no specific volume change or latent heat associated with the lambda transition.

The term He II or the "cooler liquid helium" is used for liquid helium when it is subcooled to temperatures below the lambda line. At these temperatures, He II no longer behaves as a Newtonian fluid; it demonstrates some remarkably odd properties, which are mostly due to its quantum effects. Kapitsa reported that there is no measurable resistance to flow when he studied the flow of He II through small capillaries. This fact implies that He II has no viscosity. As a result, Kapitsa named it "superfluid". Later on, other experiments done by Keesom and Meyer revealed another odd property of superfluid helium: during an oscillating disk experiment, they demonstrated the existence of a viscous drag in He II. The contradicting results of the two experiments, one showing He II as an inviscid and the other as a viscous fluid, led to the development of the two fluid model by Landau and Tisza.

1.4 Superfluid Helium – He II

Liquid helium exists in two different phases: He I, the normal fluid, and He II, the superfluid. The two phases are separated by the lambda line. At either end of this line, helium has two lambda points: a lower lambda point, which is the intersection of the vapor pressure curve with the lambda line and an upper lambda point, which is the intersection of the solid phase line and the lambda line. The lower lambda point is 2.172 K at saturated vapor pressure and the upper lambda point is 1.763 K at 29.3 atm. Once subcooled to temperatures below the lambda line, normal liquid helium does not undergo an abrupt transition to a superfluid, but rather a gradual transition. As the temperature is further decreased below the lambda line, more and more normal fluid becomes superfluid. At 1 K, 98.7% of the fluid has transitioned to superfluid. This phenomenon is depicted in Figure 1-6 which shows the ratio of each fluid component as a function of temperature.

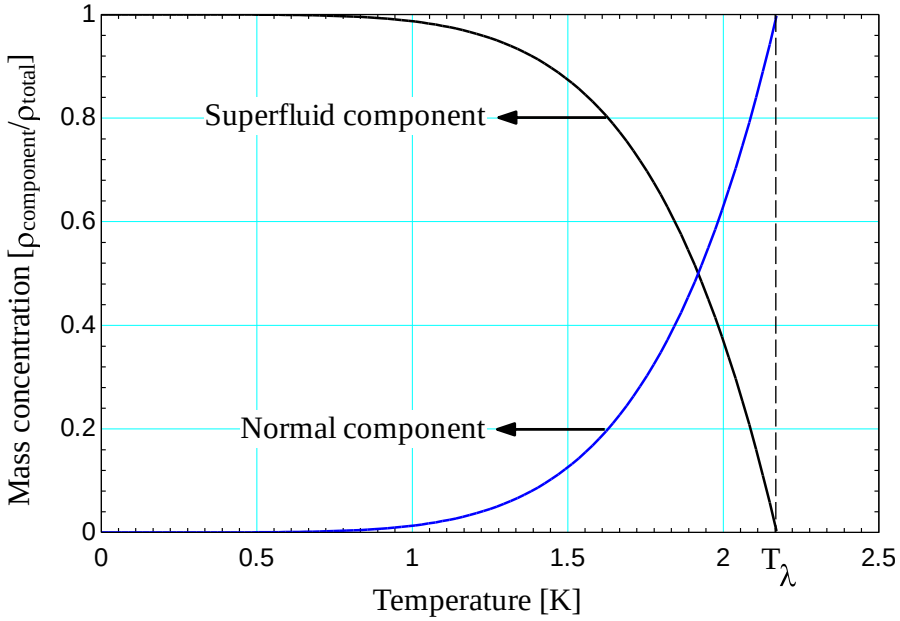

Figure 1-6 Mass concentration as a function of temperature below the lambda point

The specific heat of liquid helium varies unlike any other fluid. As shown in Figure 1-7, the heat capacity of liquid helium increases to a large value as the temperature approaches the lambda point. Also, the thermal conductivity of liquid helium behaves in a unique manner. Above the lambda point, the thermal conductivity decreases as the temperature is decreased. This behavior is consistent with that of a gas. Below the lambda point the heat transport properties of He II become quite interesting. When a container filled with He I is being pumped on in order to reduce the liquid helium pressure and therefore the temperature, one can observe nucleate boiling as a result of a temperature gradient in the bulk fluid. As the temperature is decreased through the lambda point the violent bubbling suddenly stops and the liquid becomes stable; however, the boiling process has not stopped. In fact, boiling and evaporation still continues even when helium is subcooled below the lambda point. Due to an incredibly high thermal conductivity there is no temperature gradient within the fluid and therefore there is no chance for a bubble to form and float as a result of natural convection within the fluid. The thermal conductivity of He II is orders of magnitude higher than copper at room temperature; the apparent thermal conductivity can be as high as 100 kW/m-K (Van Sciver 1986).

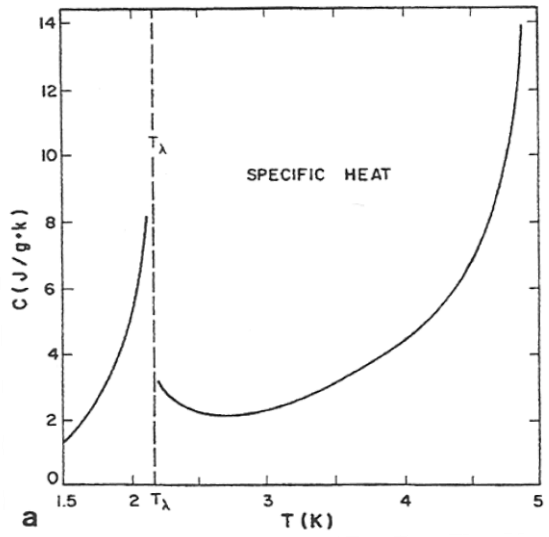

Figure 1-7 Specific heat vs. temperature in liquid helium (Van Sciver 1986)

1.5 Sub-Kelvin refrigeration background

Temperatures below 1 K (sub Kelvin temperatures) are not only applicable for X-ray and astrophysics missions, but also apply to fields as diverse as particle physics (for cooling polarized targets and advanced detectors), surface chemistry (for enhancing Nuclear Magnetic Resonance sensitivity), materials science, and condensed-matter physics. Such low temperatures are only attainable through using helium or magnetic materials. Any other substance is either in solid state or does not have useful amounts of entropy for refrigeration purposes. Various types of sub Kelvin refrigeration systems such as Adiabatic Demagnetization Refrigerators (ADR), ^{3}He evaporative coolers, and ^{3}He-^{4}He dilution refrigerators have been developed and used in the past several decades. It is important to provide a background for these various types of refrigeration systems before discussing the new Pulse tube Superfluid Refrigeration (PSR) system. The focus of this section is to provide a very brief review of each refrigeration method

The oldest method for reaching sub Kelvin temperatures is by using the ADR: cooling takes place as a result of the adiabatic demagnetization of a suitable paramagnetic salt. This technique was first proposed independently by Debye (1926) and by Giauque (1927) but was first put into practice by De Haas, Wiersma and Kramers (1933). In early stages of development the salt was the subject to be cooled in this type of refrigeration system. Later, the main interest shifted to cooling substances to milli-Kelvin temperatures by thermally putting the substance in contact with the salt. The disadvantage of an ADR is that it cannot run continuously thus it needs to be recycled periodically and it frequently requires magnetic shielding between the specimen and the refrigerator. An image of an ADR built at NASA Goddard (2010) is shown in Figure 1-8.

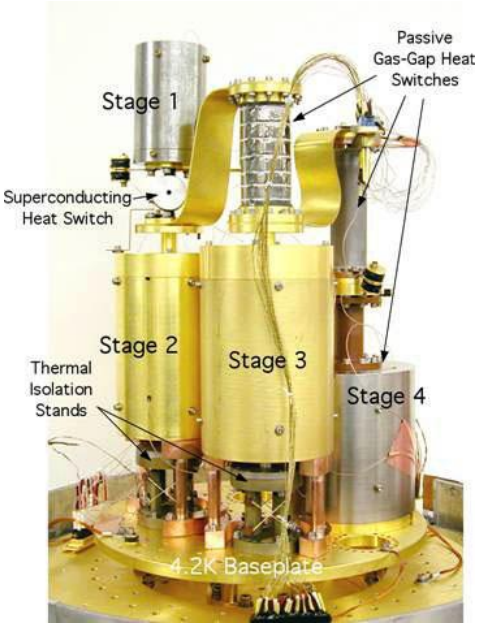

Figure 1-8 An ADR built at NASA Goddard

Another method for reaching sub Kelvin temperatures is by using a ^{3}He evaporative cooler: any heat transferred from a warm body to a pot containing liquid ^{3}He, the rare isotope of helium (1 ppm of atmospheric helium), will directly evaporate the more energetic molecules of ^{3}He in the pot. Therefore the vapor carries some energy away from the liquid. Note that the same refrigeration technique can be implemented by using pure ^{4}He as the liquid in the pot, the common isotope of helium, however the lowest practical temperature that can be achieved with ^{4}He is 940 mK instead of 300 mK with ^{3}He (Lounasmaa 1974). The disadvantages of this type of cooling with ^{3}He are: at lower temperatures the vapor pressure is too low to provide significant cooling power, ^{3}He is mainly obtained from the byproducts of tritium decay in a nuclear facility thus it is very expensive ($4,000 per gram as of this writing). A schematic of a single stage ^{3}He evaporative refrigerator (Janis 2011) is shown in Figure 1-9.

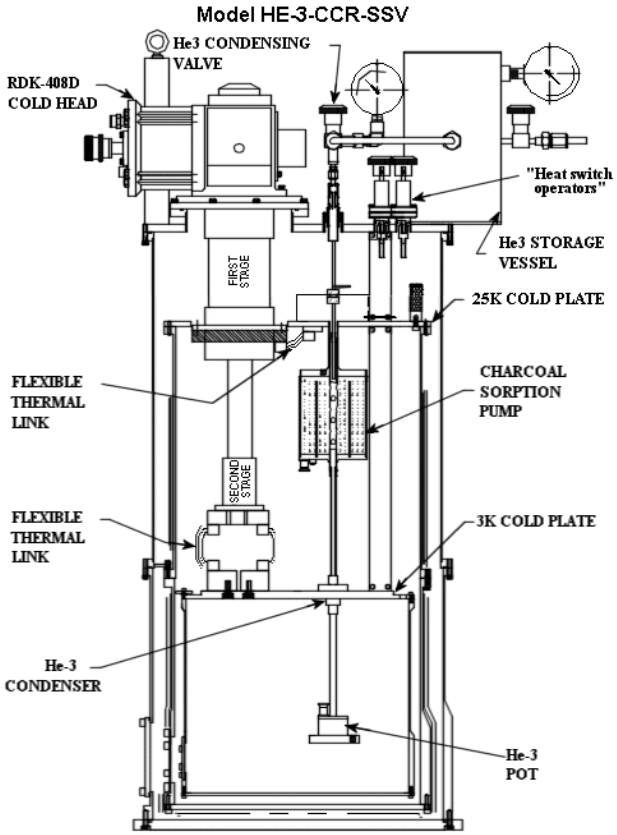

Figure 1-9 A ^{3}He evaporative refrigerator developed at Janis (2011)

A more recent and more widely used sub Kelvin refrigerator is the ^{3}He-^{4}He dilution refrigerator. A mixture of ^{3}He and ^{4}He is subcooled to temperatures below 870 mK so that it undergoes a spontaneous phase separation to form a ^{3}He-rich phase and a ^{3}He-poor phase. Just like in evaporative cooling, energy is required to transport ^{3}He atoms from the ^{3}He-rich phase into the ^{3}He-poor phase. The mixture cools if the atoms can be made to continuously cross the boundary between this rich and poor phase. The principle of dilution refrigerator was originally suggested by London (1951) and later by London, Clarke and Mendoza (1962). The first prototype of this type refrigerator, reaching a temperature of 220 mK, was built by Ouboter and Taconics (1965). The low temperature record using a dilution refrigerator is held at present by Dr. Will Oliver (MIT-Lincoln Lab 2010) of 4.1 mK. There are two main disadvantages of using a dilution refrigerator: it typically consumes several kW of electrical power to produce several μW of

cooling power and it requires an expensive room temperature pumping system. Figure 1-10 shows a dilution refrigerator built at Brookhaven National Lab (2010).

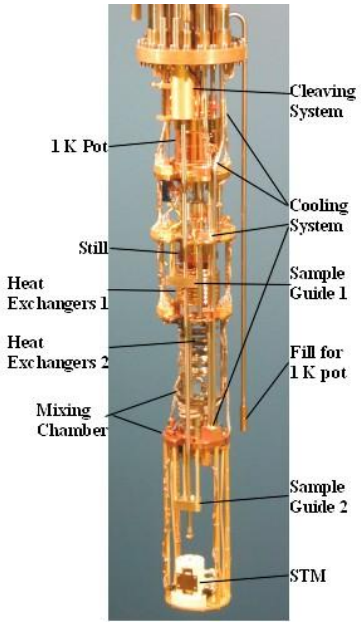

Figure 1-10 A dilution refrigerator built at Brookhaven National Lab (2010)

In summary, sub Kelvin temperatures can be achieved by various refrigeration methods: ADR's, ^{3}He evaporative coolers, and dilution refrigerators. Each type of refrigerator discussed in this section has its own unique disadvantages but they all share one disadvantage: they all use mechanical moving parts and need to be recycled periodically. The new PSR will replace all moving parts with non-moving parts and will be able to operate continuously. A general description of the PSR is presented in the next section. Table 1-2 shows the general characteristics of each traditionally used sub Kelvin refrigerator.

Refrigerator type	Typical operating temperature	Typical cooling power
ADR	60 mK	0.5 μW
^{3}He evaporative	300 mK	10 μW
Dilution refrigerator	100 mK	0.1 μW

Table 1-2 Various sub Kelvin refrigerator characteristics

1.6 The new pulse tube refrigeration system with no moving parts

A new type of sub Kelvin refrigeration system, the Superfluid Stirling Refrigerator (SSR), was first introduced by Greg Swift and Kotsubo in 1991 at Los Alamos National Lab. This refrigerator works based on the Stirling cycle and the working fluid is a mixture of ^{3}He-^{4}He. Just like any other "first" prototype, the first prototype of the SSR was a proof of concept. In order to make the SSR more reliable and efficient, the same group along with John G. Brisson modified the system in 1994 and built a second prototype that had double acting pistons on the warm and cold ends, thus increasing the cooling power and improving the lowest temperature achieved by this refrigeration system. Later in 1996 further improvements were made by Watanabe, Swift and Brisson to eliminate moving parts from the cold end of the SSR. A new refrigeration system evolved from the SSR, the Pulse tube Superfluid Refrigerator (PSR): in this new refrigerator the bellows and pistons were substituted by pulse tubes in the cold end of the refrigeration system. Details of these changes are discussed throughout this section. In 2008, Franklin K. Miller proposed to eliminate the remaining moving parts in the warm end of the PSR by replacing it with a superfluid Magnetic Pump (SMP), making it the first true continuously operating sub Kelvin refrigeration system with no moving parts in the world. The SMP is the focus of this research.

The Stirling cycle can be used to provide cooling. The operation of a Stirling cooler (a type of heat pump) is the reverse of a Stirling engine. A simplified Stirling refrigerator consists of a regenerator, a thermal reservoir that cyclically exchanges heat with the working fluid (i.e. ideal gas), and a cold and hot piston cylinder assembly. Figure 1-11 shows the four processes that

occur in a Stirling cooler: A) During the isothermal compression process the hot piston moves to the left compressing the fluid in the hot side of the chamber. Heat is rejected to the surroundings in order to keep this an isothermal process. B) During the constant volume regenerative heat rejection process both pistons, cold and hot side, move to the left in order to keep the working fluid at a constant volume. The working fluid is pushed through the regenerator, therefore rejecting its heat to the material in the regenerator. C) During isothermal expansion the cold piston moves to the left allowing the working fluid to absorb heat from the surroundings. D) During a constant volume regenerative heat absorption process both pistons return to their original positions and the working fluid absorbs the heat that was once stored in the regenerator during process B in order to return the working fluid to the original thermodynamic state.

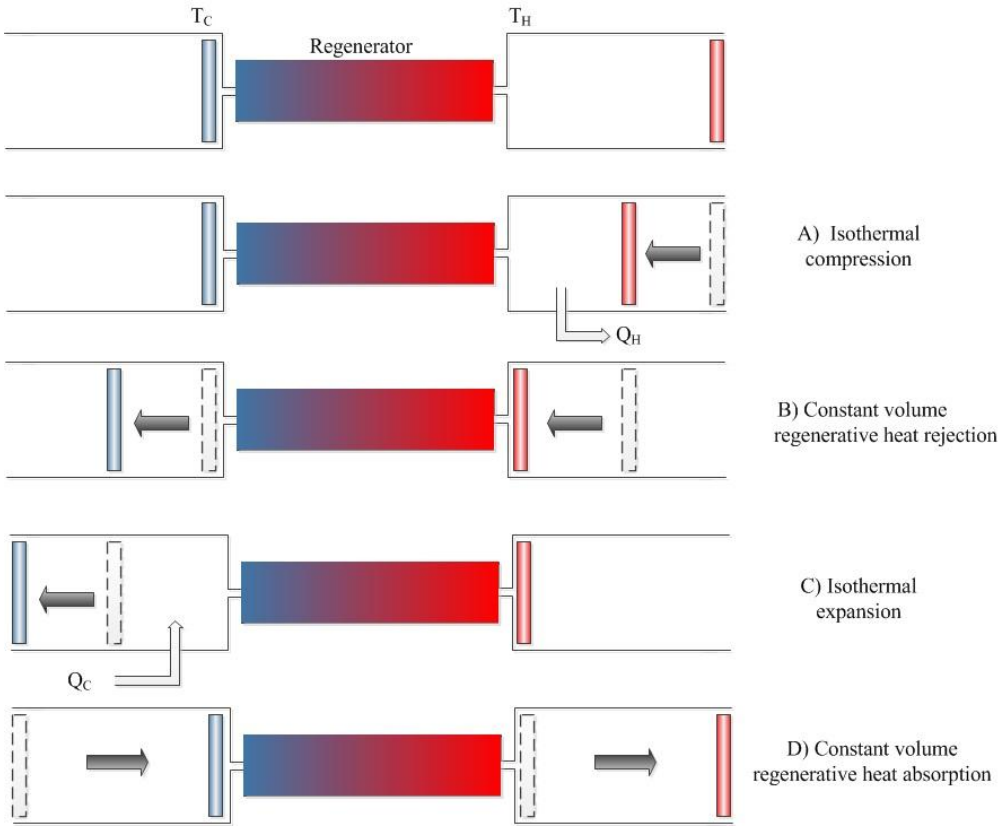

Figure 1-11 Stirling cooler

Figure 1-12 shows a schematic of the first prototype of the SSR that was built by Swift and Kotsubu in 1991. This refrigerator works based on the same principle that was discussed earlier for the simplified Stirling cooler shown in Figure 1-11. The warm end of the first type SSR, right hand side branch on Figure 1-12, is connected to the cold end, left hand side branch on Figure 1-12, via a regenerator. The regenerator consists of an array of capillaries stuffed into a bigger tube. Both ends of this refrigerator consist of a bellows piston assembly with a cylindrical vycor glass superleak inserted in the center of each piston. Each piston bellows assembly is displaced by a rod that is connected to a cam system. The warm end of this refrigerator is anchored to a heat sink at 1.2 K.

All the lines within the refrigeration system are filled with a mixture of ^{3}He-^{4}He. The vycor glass superleak in each piston only allows Superfluid ^{4}He to pass through it (Note that ^{3}He is not a superfluid at temperatures higher than 1 mK which is significantly lower than the operation temperature of the SSR). Thus one side of the bellows always acts as a reservoir for superfluid ^{4}He. Figure 1-13 shows a simplified version of the SSR configuration. Superfluid ^{4}He provides an inert background for the ^{3}He solute in the mixture. Therefore superfluid ^{4}He can be thought of as a vacuum space where the ^{3}He molecules act as an ideal gas in the "vacuum space" because of the large intermolecular distance in ^{3}He. It is now apparent how the SSR works: During this Stirling cycle, heat is rejected from the mixture when ^{3}He atoms are compressed between the two pistons and vice versa when the ^{3}He atoms are expanded. This first prototype of the SSR achieved a low temperature of 590 mK and provided a cooling power of 20 μW.

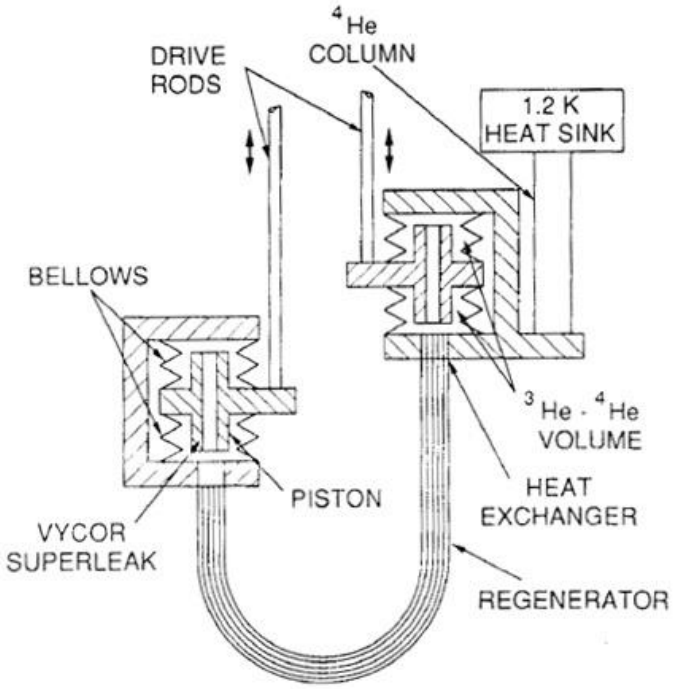

Figure 1-12 First prototype of SSR , Los Alamos 1991

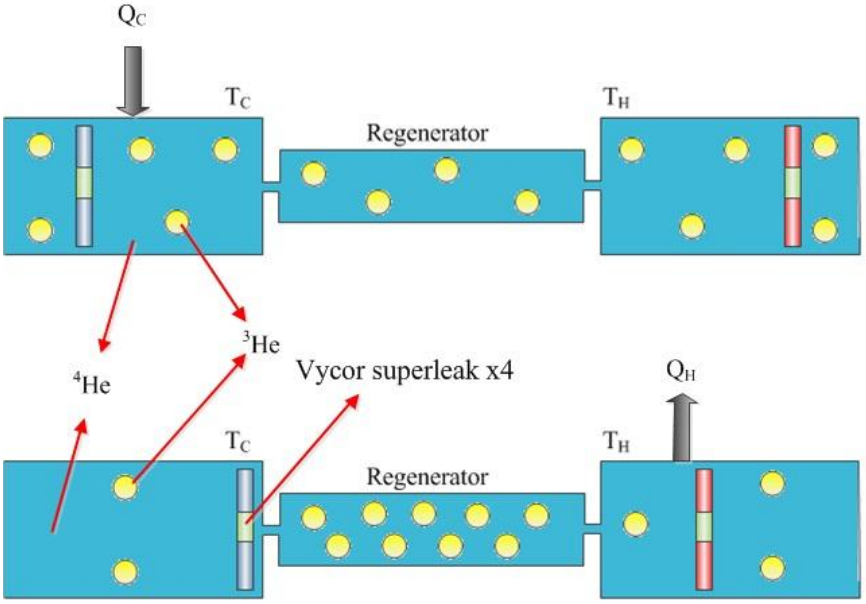

Figure 1-13 Compression-expansion of ^{3}He in the SSR

When Brisson joined the Condensed Matter and Thermal Physics group at Los Alamos National Lab in 1994, he, along with Kotsubo and Swift, proposed a new SSR that can achieve temperatures lower than 500 mK and provide improved cooling power. Thus the second SSR is a modified version of the first. A schematic of the second SSR is shown in Figure 1-14. The second SSR was two refrigerators that operate 180 degrees apart from each other. The ^{3}He-^{4}He working fluid occupied both sides of the pistons, making them a double acting piston in this design. The regenerator was a heat exchanger between the counterflowing fluids in each half of the SSR. The capillaries were arranged in alternating rows that correspond to each half of the SSR. The second SSR achieved a low temperature of 340 mK and provided a net cooling power of 160 μW.

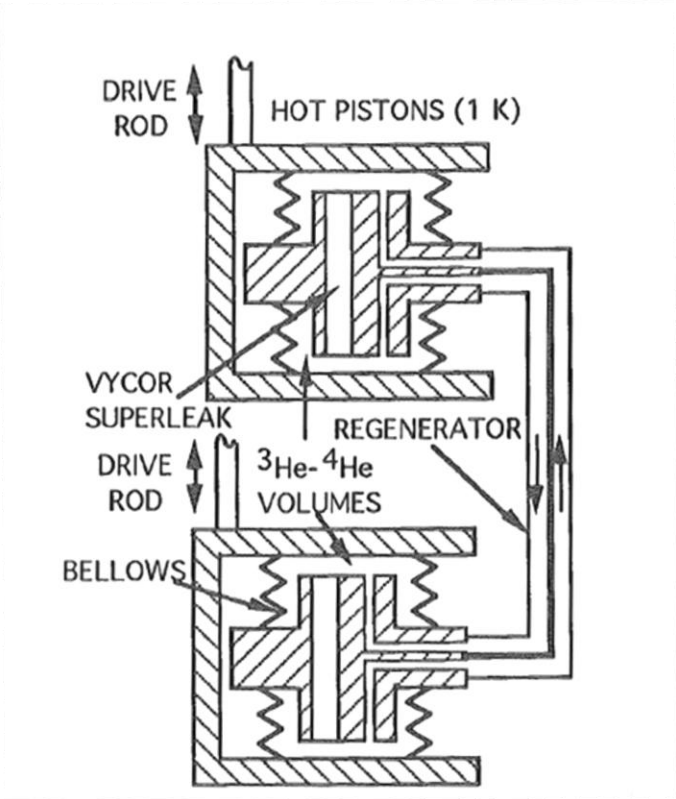

Figure 1-14 Second SSR

Watanabe, Swift and Brisson made a slight modification to the second SSR in 1996. The major modification was the addition of an independent refrigeration system, a ^{3}He evaporative cooler, that cools the hot platform on which the hot pistons were mounted. With this arrangement the hot platform temperature could be maintained at temperatures between 300 mK and 1 K. Everything else throughout the modified second SSR is the same as the original second SSR. A schematic of the modified version of the second SSR is shown in Figure 1-15. This refrigerator achieved a low temperature of 168 mK.

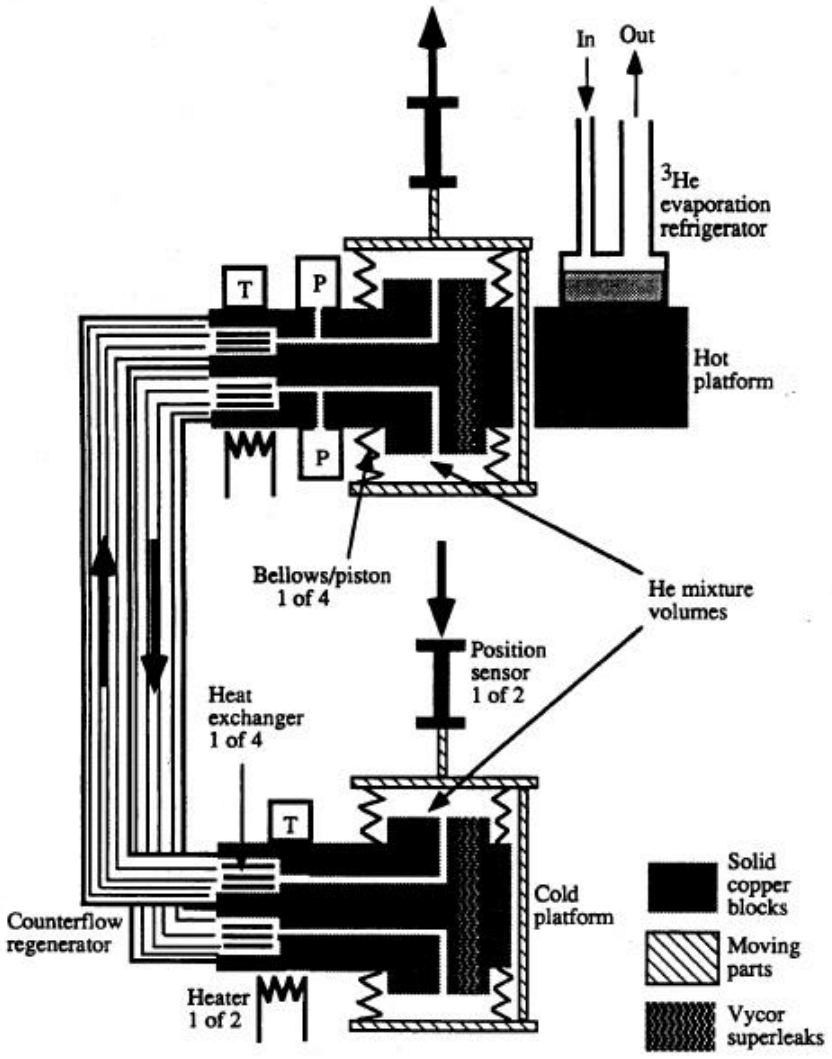

Figure 1-15 Modified version of the second SSR

A new generation of sub Kelvin refrigeration system was introduced by Watanabe, Swift and Brisson in 1996 at Los Alamos National Lab. This was a pulse tube superfluid refrigerator (PSR), a modified version of the SSR. The only difference between the PSR and the SSR is the addition of two heat exchangers and the substitution of bellows pistons at the cold end of the system with 2 pulse tubes that are connected by an orifice.

Figure 1-16 shows a simplified schematic of the pulse tube configuration in comparison to the traditional bellows piston configuration in a Stirling cooler. The cold piston has been replaced by a pulse tube, an orifice, and a tank (buffer volume). The working fluid is pushed by the hot piston and energy is dissipated as the fluid passes through the orifice. This energy dissipation manifests itself in the form of heat; therefore this additional heat must be removed by a heat exchanger that is connected to the hot platform. The pulse tube thermally isolates the orifice's dissipation from the cold end while transmitting fluid motion. Therefore moving parts have been eliminated from the cold end of the refrigerator in this design.

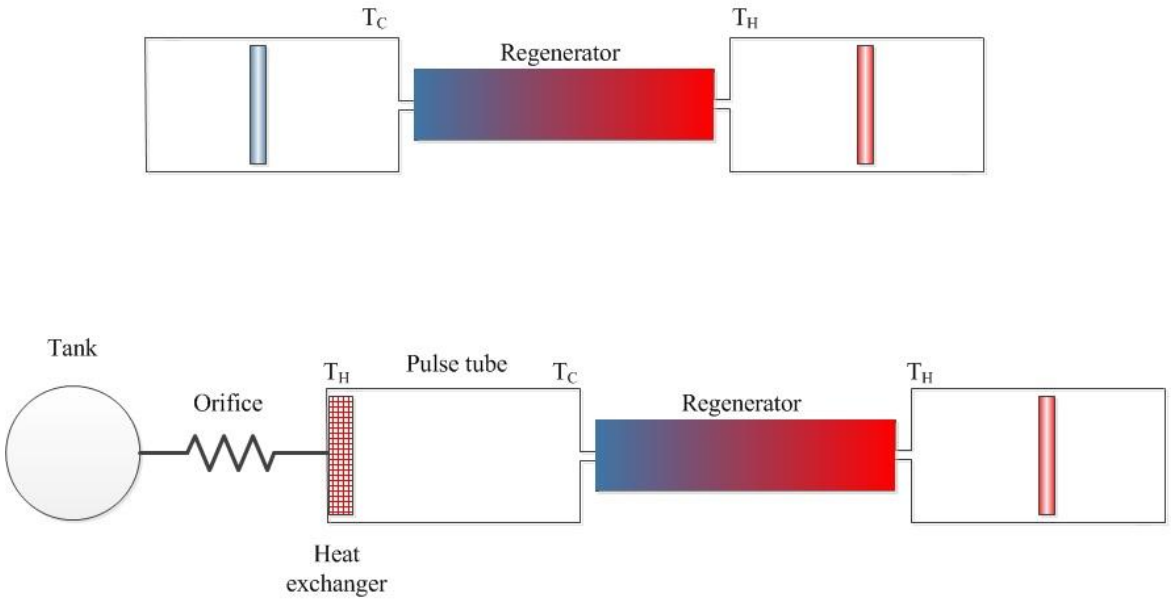

Figure 1-16 Piston configuration vs. pulse tube configuration in a Stirling cooler

Figure 1-17 shows a schematic of the PSR that was built by Watanabe, Swift and Brisson in 1996. The cold end of the refrigerator was replaced by two pulse tubes and two heat exchangers. The rest is the same as the modified version of the second SSR. When the mixture is pushed through one pulse tube the other pulse tube acts as a buffer volume for the other half of the cycle and vice versa. The lowest temperature attained with this first prototype was 640 mK. It is unknown whether a second prototype was made to improve the lowest temperature attained with this type refrigerator.

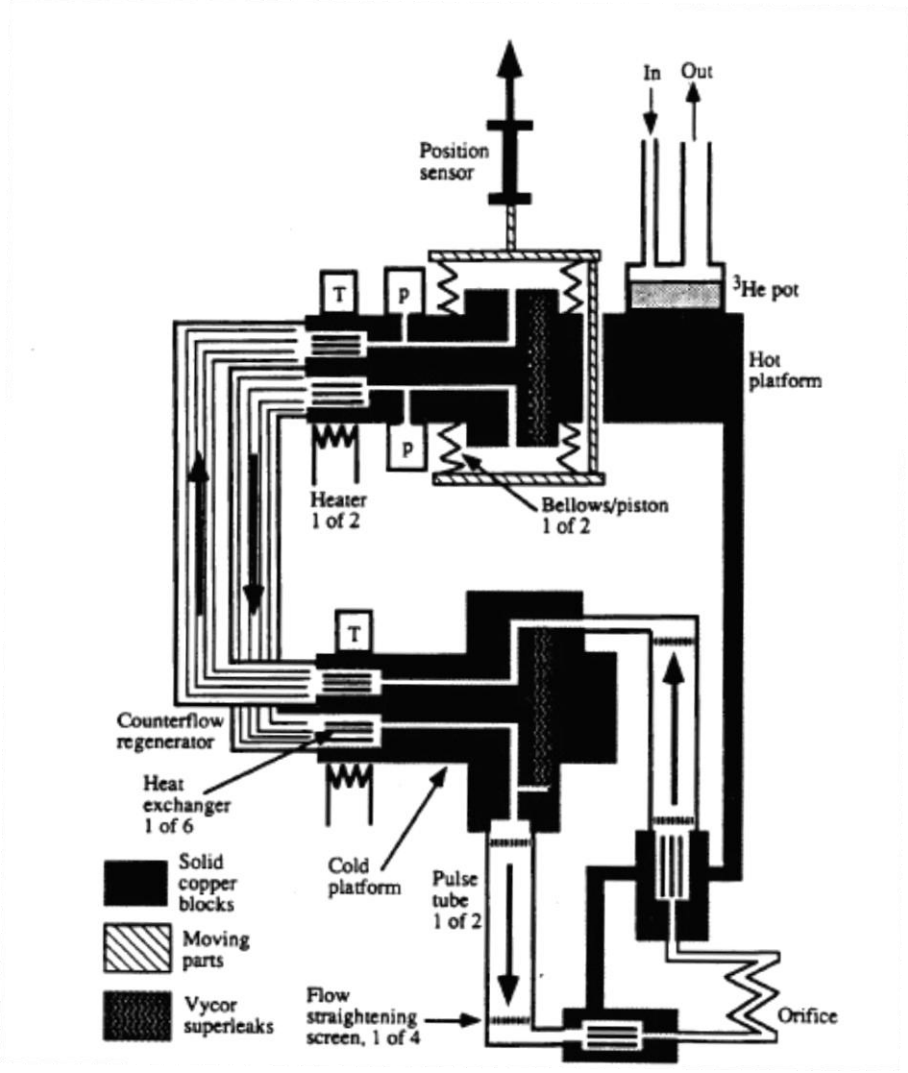

Figure 1-17 A schematic of the first prototype of the PSR built at Los Alamos 1996

In 2008, Miller proposed a new PSR system that has no moving parts and can run continuously. He proposed to use a Superfluid Magnetic Pump (SMP) instead of the bellows piston assembly in the warm end of the PSR. Thus two SMP's are incorporated in the new design each working for one half of the refrigerator that operates 180 degrees apart from each other. Each SMP will pump superfluid ^{4}He into and out of the canisters. Therefore these pumps can be thought of as imaginary double acting pistons. Figure **1-18** shows a schematic of this newly proposed PSR. The rest of this new PSR is exactly identical to the original PSR. The main focus of this research is on the SMP and its development. This refrigeration system is expected to perform identical to the original PSR. Once the SMP is independently demonstrated by experimental methods, the new PSR will be demonstrated with the SMP's and the performance will be compared against theoretical models.

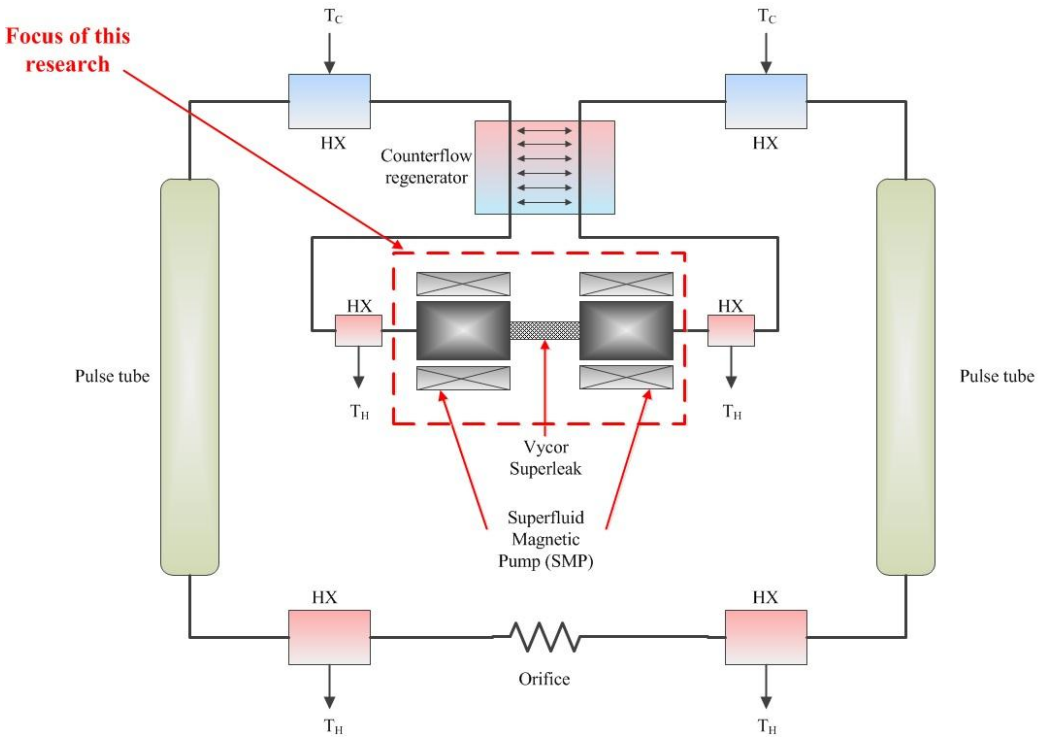

Figure 1-18 **New PSR proposed by Miller (2008)**

1.7 References

Brisson, J.G., "The superfluid Stirling refrigerator, a new method for cooling below 0.5 K", Physica B (1994) Pg. 45-46

ECAL (Experimental Cosmology and Astrophysics Laboratory), website, MIT-Figueroa Group, 2009

Janis Research Group, website, 2011

Lounasmaa, O.V. , Experimental principles and methods below 1 K, Academic Press, New York, 1974

Miller, F.K. , "Sub-Kelvin space cryocooling without moving parts", Proposal: NASA, 2008

Miller, F.K. , Brisson, J.G. , "A superfluid pulse tube driven by a thermodynamically reversible magnetic pump", Conference: CEC, 2009

MIT-Lincoln National Labs, website, 2009

NASA-Goddard, Website, 2010

PTB, website, contact: Kobusch, M. , 2008,

Swift, G.W., Kotsubo, V., "Superfluid Stirling cycle refrigeration below 1 Kelvin, Journal of low temperature physics, Vol. 83 (1991)

Van Sciver, S.W., Helium cryogenics, Plenum Press, New York, 1986

Watanabe, A. , Swift, G.W., Brisson, J.G. , "Measurements with a recuperative superfluid Stirling refrigerator", Advances in cryogenic engineering, Vol. 41 (1996), Pg. 1527-1533

Watanabe, A. , Swift, G.W., Brisson, J.G. , “Superfluid orifice pulse tube refrigerator below 1 Kelvin”, Advances in cryogenic engineering, Vol. 41 (1996), Pg. 1519-1526

Wilks, J., The properties of liquid and solid helium, Oxford University Press, 1967

2 DEVELOPMENT OF A LOW TEMPERATURE FACILITY AND INSTRUMENTATION IN SUPPORT OF THE 1 K FACILITY

2.1 Cryogenic Dewar and heat exchange platforms

When carrying out cryogenic experiments it is important to minimize heat flow from the ambient to the low temperature components due to all three modes of heat transfer: conduction, convection, and radiation. This task can be accomplished by thermally isolating the experimental space from the ambient by using a cryogenic Dewar. Weak thermal links, used to structurally support the experimental assembly from the cryogenic Dewar, reduce heat loads due to conduction. A vacuum in the cryogenic Dewar significantly reduces heat loads due to convection. Lastly, proper radiation shielding substantially reduces heat loads due to radiation.

The author participated in the design, specification, procurement, and assembly of the cryogenic Dewar. Different components of the Dewar used in this work are labeled in Figure 2-1. The supports are bolted to the head in order to elevate it to the required height. The head has four feed-throughs: two ISO-63 and two KF-40 ports. The two heat exchange platforms are suspended from the head via G-10 supports. The cylindrical shields are then bolted to their corresponding heat exchange platforms. Finally, o-rings are used to create a tight vacuum seal in the bolted joints between the main body, port rim, and the head. The port rim has six uniformly distributed feed-throughs, all of type KF-50. The engineering drawings of the Dewar assembly are presented in Appendix A.

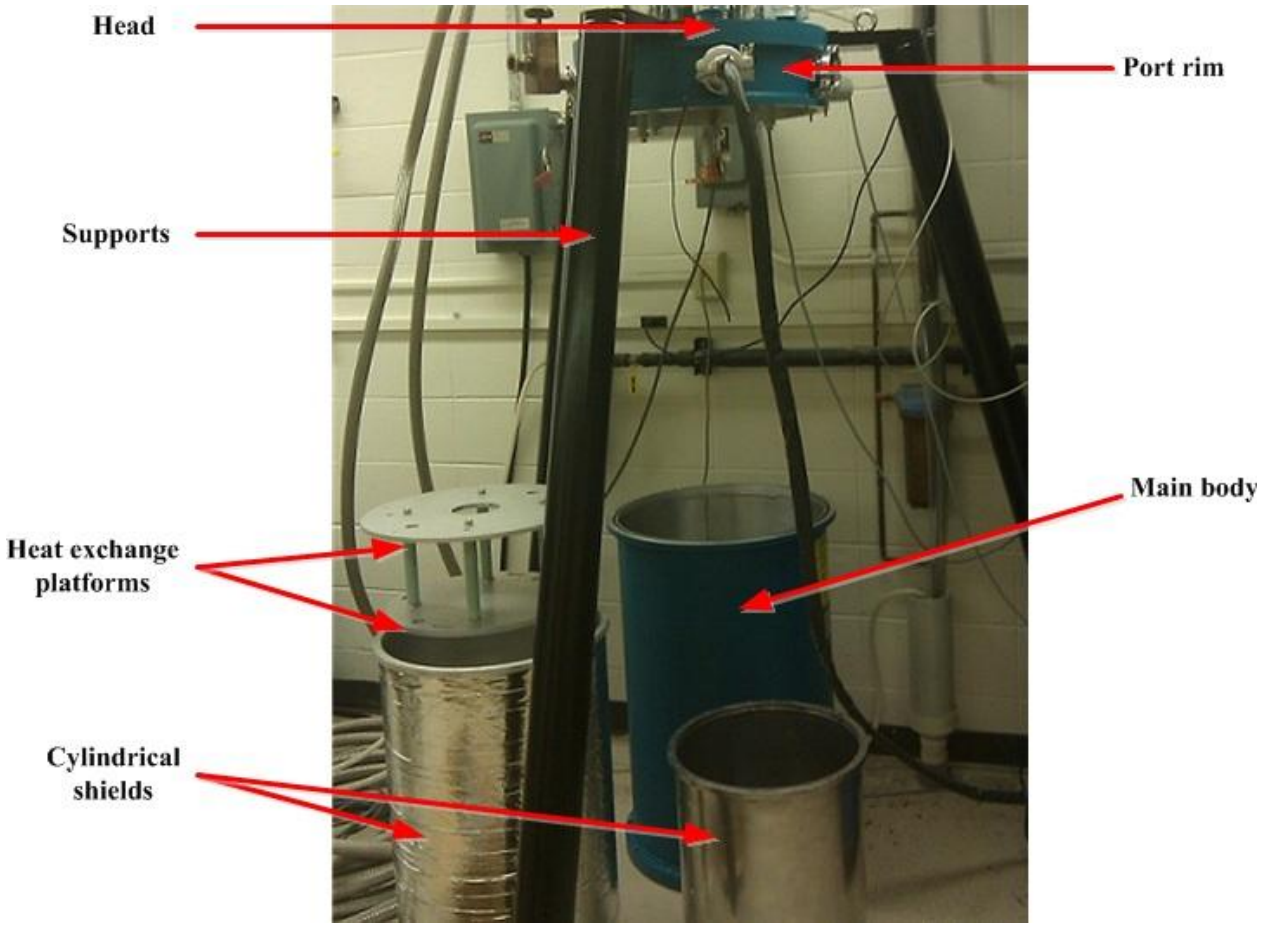

Figure 2-1 An image of the Dewar used in this work with labeled parts

2.1.1 Heat exchange platforms

The two heat exchange platforms: the first stage (the warmer stage), and second stage (colder stage), serve as a low temperature surface for the experiments that will be conducted in the Dewar. They were initially received as blank aluminum disks. The heat exchange platforms needed to be modified in order to accommodate experimental components. A list of modifications made to each platform along with their purpose is presented in Table 2-1 and Table 2-2. Engineering drawings of the platforms are also available in Appendix B.

Modifications	Purpose
1-15/16” center hole	Clearance for cryocooler
20x 4-40 helicoil pattern at radius=8.25”	Accommodates experimental components
20x 4-40 helicoil pattern at radius=7.75”	Accommodates experimental components
2x 1” hole	Clearance for experimental components sent through the top KF-40 ports (rods, tube, etc.)
6x 8-32 helicoil pattern at radius=2.38”	Accommodates heat straps

Table 2-1 Modifications made to the first stage heat exchange platform

Modifications	Purpose
1” by 1” 4-40 helicoil grid pattern	Accommodates experimental components
4x rectangular slots	Houses electric connectors (D-connector)
2x 1” hole	Clearance for experimental components sent through the top KF-40 ports (rods, tube, etc.)
8x 4-40 helicoil offset pattern	Accommodates heat straps

Table 2-2 Modifications made to the second stage heat exchange platform

2.2 Turbo-Roughing pump station

Convective heat loads in the cryogenic Dewar can be substantially reduced by utilizing a properly sized pumping station. A combination of a roughing pump “first stage” and a turbo-molecular pump “second stage” constitutes a pumping station. The roughing pump is first activated to pull a “rough” vacuum on the cryogenic Dewar, typically in the range of several hundred Pascal. Once a crossover pressure has been achieved (i.e., the pressure at which it is considered safe to activate the second stage of pumping) the turbo pump is activated in order to attain a very high vacuum in the Dewar (between $1x10^{-7}$ and $1x10^{-4}$ Pa). The cryocooler can be activated once the pressure in the Dewar falls into the very high vacuum range.

The roughing pump used in this work is a Pfeiffer diaphragm pump, model MVP-040-2. This is a two stage dry compressor vacuum pump. The advantage of this type of pump over traditionally

used vacuum pumps such as rotary vane and other oil sealed pumps is the elimination of oil mist that might back stream into the vacuum chamber. The turbo pump that is used in series with the diaphragm pump is a Pfeiffer turbo drag pump, model TMU 071. Some general properties of both pumps are presented in Table 2-3 and Table 2-4. The turbo pump was directly attached to the Dewar via an ISO-63 port. The roughing pump is connected to the turbo pump's exhaust via a 1/4 inch tube. This system setup is shown in Figure 2-2.

Properties	**Values**
Nominal pumping speed	2.5 m^3/hr
Ultimate low pressure	400 Pa
Exhaust maximum pressure	110 kPa
Rotation speed	1800 rpm

Table 2-3 Some general properties of the diaphragm pump

Properties	**Values**
Nominal rotation speed	1500 Hz
Cross over pressure	1 kPa
Volume flow rate – air	212 m^3/hr
Compression ratio	>1e11
Ultimate pressure	1e-6 Pa

Table 2-4 Some general properties of the turbo pump

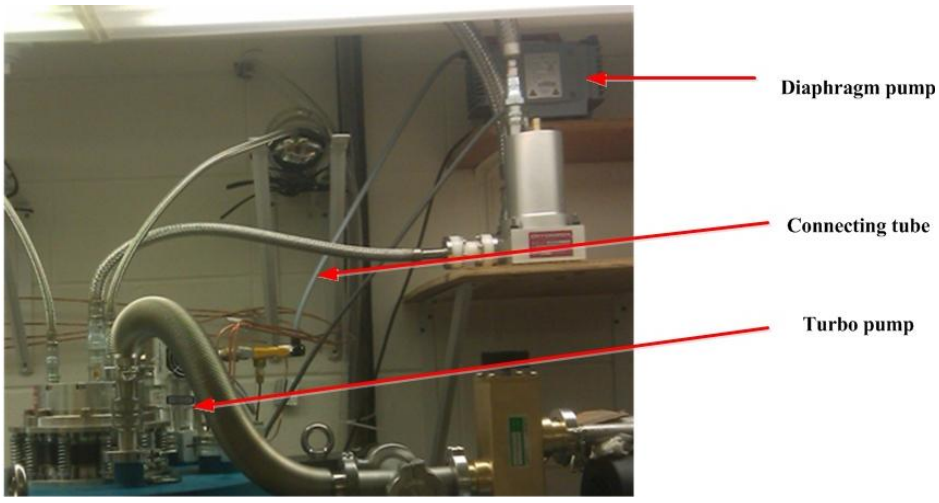

Figure 2-2 Vacuum pumping station setup

It is useful to know approximately how long it will take before the pressure in the Dewar (P_{Dewar}) reaches the crossover pressure. The volume of the Dewar (V_{Dewar}) and the pumping speed of the diaphragm pump (S_{pump}) are known, allowing the time (t) required to get from atmospheric pressure (P_0) to the crossover pressure to be estimated using Eq. (2.1) (O'Hanlon 2003). The pressure as a function of time is plotted from the time of diaphragm pump activation to the time it reaches the crossover pressure in Figure 2-3.

$$P_{dewar} = P_0 \, e^{\left(\frac{-S_{pump}}{V_{dewar}} t\right)} \tag{2.1}$$

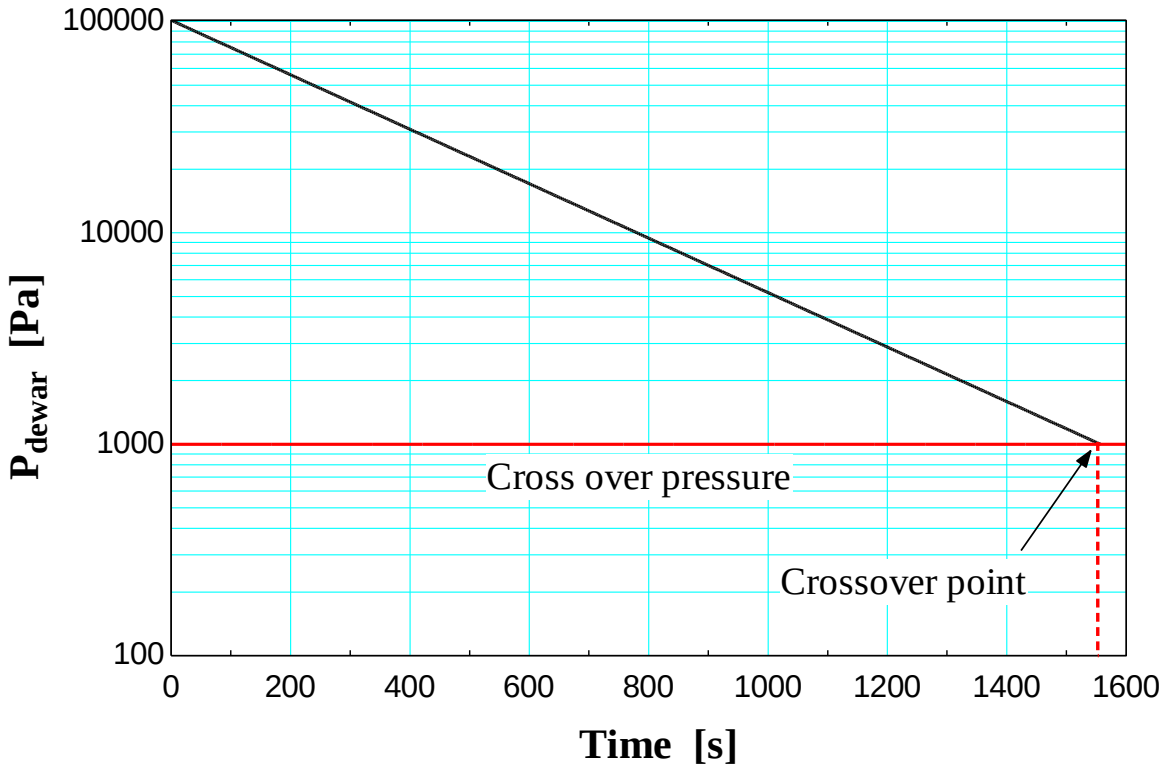

Figure 2-3 Predicted pressure in the Dewar as a function of time during roughing stage. Note the cross over pressure of 1 kPa for this pump setup

An initial testing of the pumping station was conducted by plugging all the ports on the Dewar and pulling a vacuum on the empty space. During this test, it took the roughing pump

approximately 35 minutes (2100 seconds) to reduce the pressure in the Dewar from atmospheric to crossover pressure. The ultimate pressure achieved with the turbo pump was $1x10^{-4}$ Pascal. Therefore the result of this test confirmed a tight vacuum seal within the Dewar as well as ensured the performance of the pumping station.

2.3 Pulse tube cryocooler

A cryocooler is a device used to reach cryogenic temperatures. There are several types of cryocoolers available, including Stirling, Gifford-McMahon, pulse tube, etc. The moving displacers in Stirling and Gifford-McMahon cryocoolers are a source of vibration, reduce the lifetime and reliability of the cryocooler, and contribute to axial heat conduction. These problems are eliminated in a pulse tube cryocooler because it has no moving parts. This absence of moving parts will also be consistent with the superfluid magnetic pump with no moving parts when used in conjunction for the experiment. Thus, a pulse tube cryocooler was selected to be used in this work; specifically, a Cryomech pulse tube cryocooler, model PT410 was installed.

The cryocooler system consists of a CP 2880 compressor, the cold head with first stage and second stage heat exchangers, a rotary valve, a reservoir for the first stage and second stage, and flexes line hoses to connect different components of the assembly. A schematic of the assembled unit is shown in Figure 2-5. The specifications of these pulse tube cryocoolers slightly vary from one unit to another; however, when no load is applied, the first and second stage of all PT410 cryocoolers is certified to reach 31 K and 2.8 K respectively. The cooling capacity curve of one of the first prototypes tested and published by Cryo-mech is shown in Figure 2-4 (Cryomech 2010).

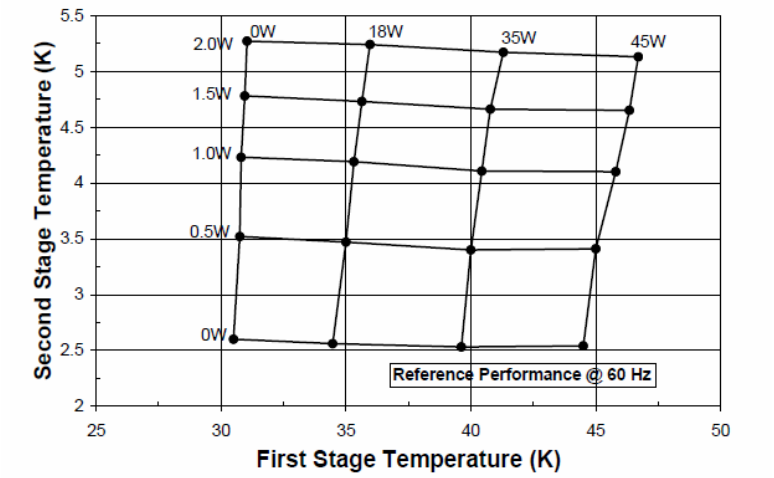

Figure 2-4 Cooling capacity curve for the pulse tube cryocooler

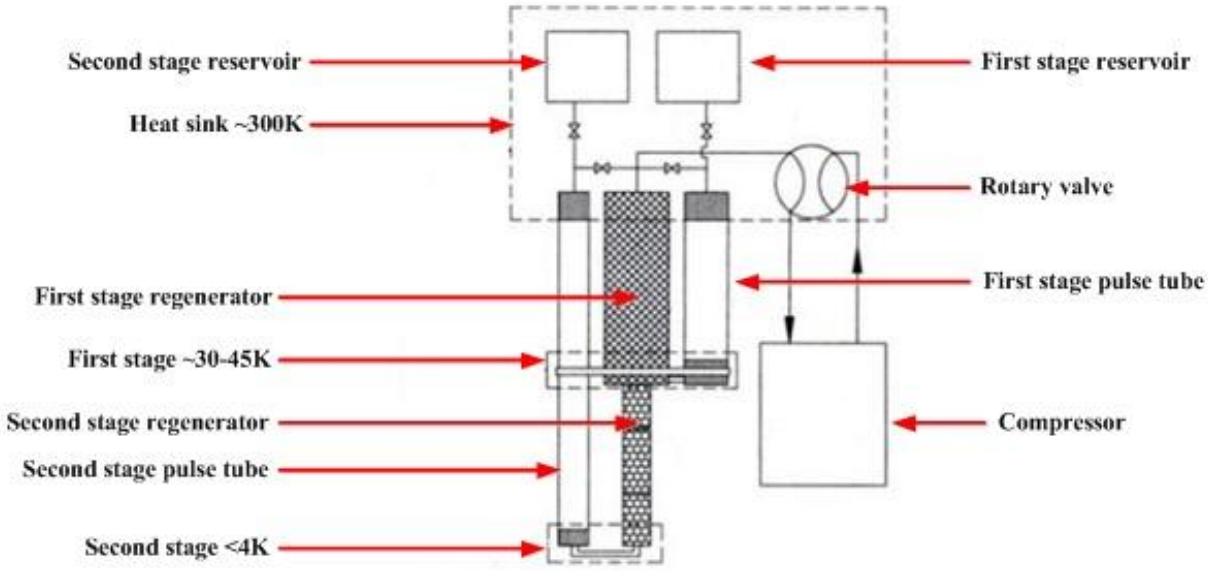

Figure 2-5 An assembled schematic of the pulse tube cryocooler with different components labeled

An initial test of the cryocooler performance was conducted. The cryocooler components were assembled and the cold head was flanged to the Dewar head. Aluminized Mylar sheets were temporarily wrapped around the cold head in stacked layers to act as a radiation shield. The Dewar was evacuated to a pressure of 1e-4 Pa before activating the cryocooler. It took the first stage heat exchanger approximately 100 minutes to reach 36 K and the second stage 40 minutes

to reach 3.8 K. The performance of the cryocooler during this test was compared to the published data for consistency, showing that the two sets of data were consistent, as shown in Figure 2-6.

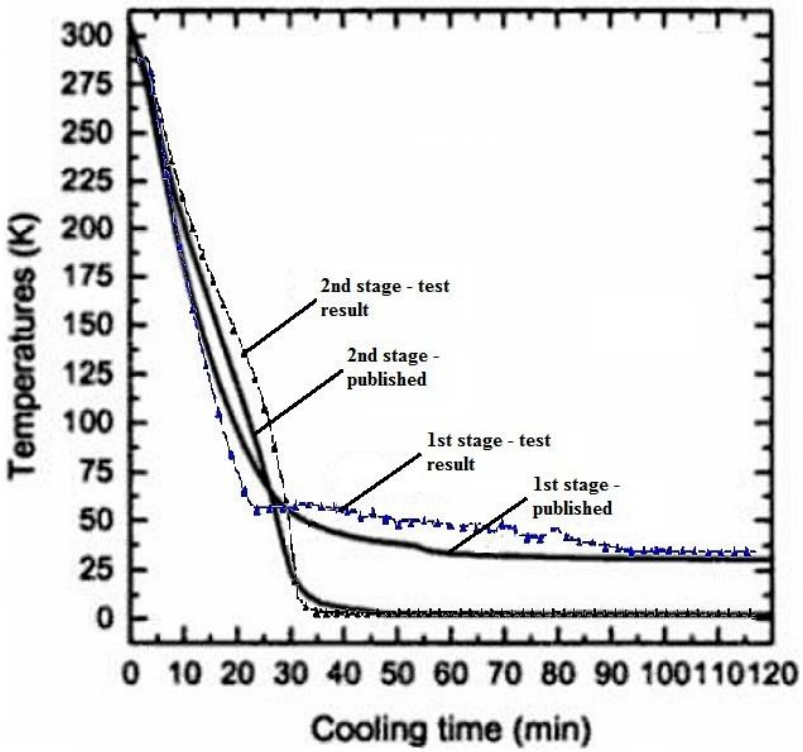

Figure 2-6 The performance of the cryocooler vs. published data for the same model cryocooler (lines with symbols are the test results and solid lines are the published data)

2.4 Heat straps

Heat straps are flexible conductive linkages that are used to thermally integrate a cryocooler with cryogenic experimental components. Flexible heat straps alleviate mechanical issues such as side loads on the cold head, stresses due to differential thermal contraction, mechanical vibration, and misalignments. Two sets of heat straps, one linking the first stage cryocooler heat exchanger with the first stage heat exchange platform and the other linking the second stage cryocooler heat

exchanger with the second stage heat exchange platform, are needed to carry the heat away from the two cylindrical radiation shields and experimental components mounted to the platforms.

2.4.1 Design and fabrication of the first stage heat straps

The material used for a heat strap must be a good thermal conductor. Oxygen Free High Conductivity (OFHC) copper has a very high thermal conductivity even at low temperatures, thus this material was selected to be used for the heat straps. Six heat straps were used for the first stage. The structure of each heat strap consists of a copper wire welded to two L-shaped copper brackets at either end, as shown in Figure 2-7. The wire used in the structure of the heat strap is 1.17 cm in diameter (4/O AWG). A very thin layer of indium was compressed between the mating surfaces when installing the heat straps in order to reduce thermal contact resistance. A preliminary model showed that it will take approximately 9 hours to cool the first stage heat exchange platform and the cylindrical shield attached to it. After fabrication and installation of the heat straps, a cool down test showed that it takes approximately 11 hours to cool the first stage assembly down to ~37 K.

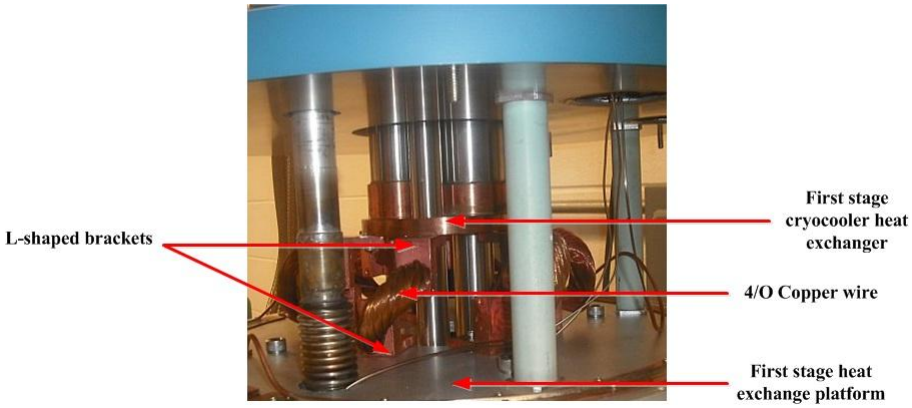

Figure 2-7 First stage heat strap configuration

2.4.2 Second stage heat straps

The heat straps used for the second stage have a different configuration than the first stage heat straps. The S-shaped second stage heat straps are made out of 70 layers of rectangular OFHC copper foils that are tape welded to each other at either end. The performance of the two second stage heat straps used in this work was tested in a previous work by Nellis, et al (2004). A preliminary model estimated a cool down time of approximately 7 hours for the second stage heat exchange platform and cylindrical shield attached to it. In the same test run conducted for the first stage, the cool down time to ~4 K was found to be 10 hours. An image of the second stage heat straps is shown in Figure 2-8.

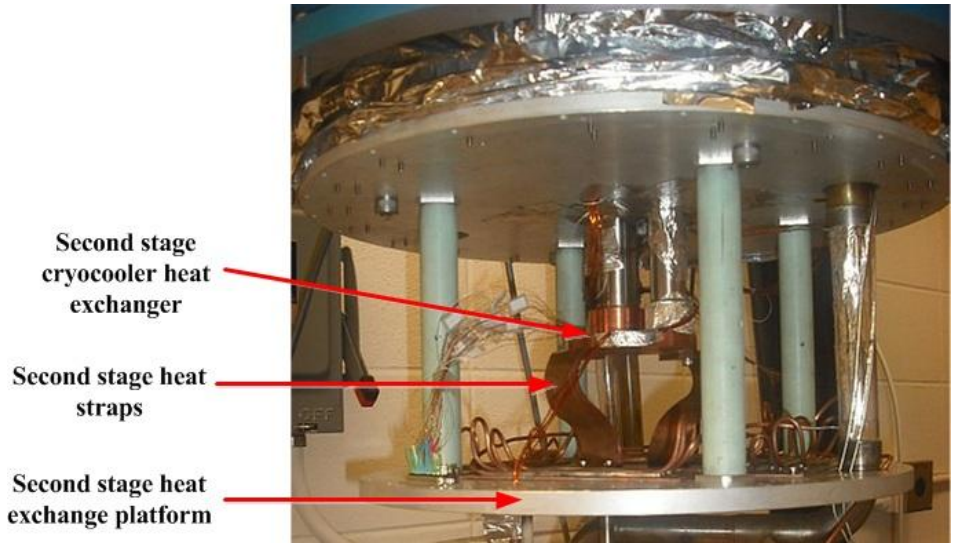

Figure 2-8 Second stage heat strap configuration

2.5 Radiation shielding

Radiative heat loads can be substantially reduced by introducing radiation shields in the cryogenic Dewar. Radiation shields consist of surfaces with very low emissivity, which creates a

barrier for radiative head transfer when placed between two surfaces at different temperatures. It was noted earlier that the cryocooler is equipped with a first stage heat exchanger that is thermally linked to the first stage heat exchange platform and the cylindrical radiation shield attached to it. This "can" assembly is used both as a radiation shield for the second stage components and also as a precooler. However, the first stage assembly is directly exposed to room temperature surfaces, thus it must be protected from the radiation heat transfer received from these surfaces. For this reason, a Multi Layer Insulation (MLI) shield, composed of aluminized Mylar sheets, is placed over the cylinder and on top of the first stage platform, surrounding the entire assembly. The number of layers required to reduce the radiative heat load on the first stage assembly can be calculated. The radiative load between two surfaces at temperatures T_1 and T_2 with corresponding emissivity, ε_1 and ε_2, is expressed as:

$$\dot{q}_{1to2} = \frac{A_{s1} F_{12} \sigma \left(T_1^4 - T_2^4 \right)}{\frac{1}{\varepsilon_1} + \frac{1}{\varepsilon_2} - 1} \tag{2.2}$$

where A_{s1} is the area of surface 1, F_{12} is the view factor from surface 1 to 2, and σ is the Stefan-Boltzmann's constant. Figure 2-9 shows the radiation resistance network between two surfaces with N radiation shields between them. Radiation heat transfer between surfaces 1 and 2 for this network can be written as:

$$\left(\dot{q}_{1to2} \right)_N = \frac{E_{b1} - E_{b2}}{R_{total}} = \frac{E_{b1} - E_{b2}}{\frac{1-\varepsilon_1}{A_{s1}\varepsilon_1} + \frac{1}{A_{s1}F_{12}} + \frac{1-\varepsilon_{3,1}}{A_{s3}\varepsilon_{3,1}} + \frac{1-\varepsilon_{3,4}}{A_{s3}\varepsilon_{3,4}} + \ldots + \frac{1-\varepsilon_{N,N-1}}{A_{sN}\varepsilon_{N,N-1}} + \frac{1-\varepsilon_{N,2}}{A_{sN}\varepsilon_{N,2}} + \frac{1}{A_{sN}F_{N2}} + \frac{1-\varepsilon_2}{A_{s2}\varepsilon_2}} \tag{2.3}$$

where R_{total} is the total radiation heat transfer resistance between surfaces 1 and 2, and E_b is the blackbody emissive power:

$$E_b = \sigma T^4 \tag{2.4}$$

Assuming a view factor of 1 between the adjacent surfaces and area *A* for all surfaces, Eq. (2.3) can be simplified and rearranged:

$$\left(\dot{q}_{1\,to\,2}\right)_N = \frac{A\sigma(T_1^4 - T_2^4)}{\left(\frac{1}{\varepsilon_1} + \frac{1}{\varepsilon_2} - 1\right) + \left(\frac{1}{\varepsilon_{3,1}} + \frac{1}{\varepsilon_{3,4}} - 1\right) + \ldots + \left(\frac{1}{\varepsilon_{N,N-1}} + \frac{1}{\varepsilon_{N,2}} - 1\right)} \tag{2.5}$$

In the special case where the emissivity of the inner and outer surfaces of the MLI sheets are the same, $\varepsilon_{MLI\ \text{sheet}}$ Eq. (2.5) can be rewritten as:

$$\left(\dot{q}_{1\,to\,2}\right)_N = \frac{A\sigma(T_1^4 - T_2^4)}{\left(\frac{1}{\varepsilon_1} + \frac{1}{\varepsilon_2} - 1\right) + N\left(\frac{2}{\varepsilon_{MLI\ sheet}} - 1\right)} \tag{2.6}$$

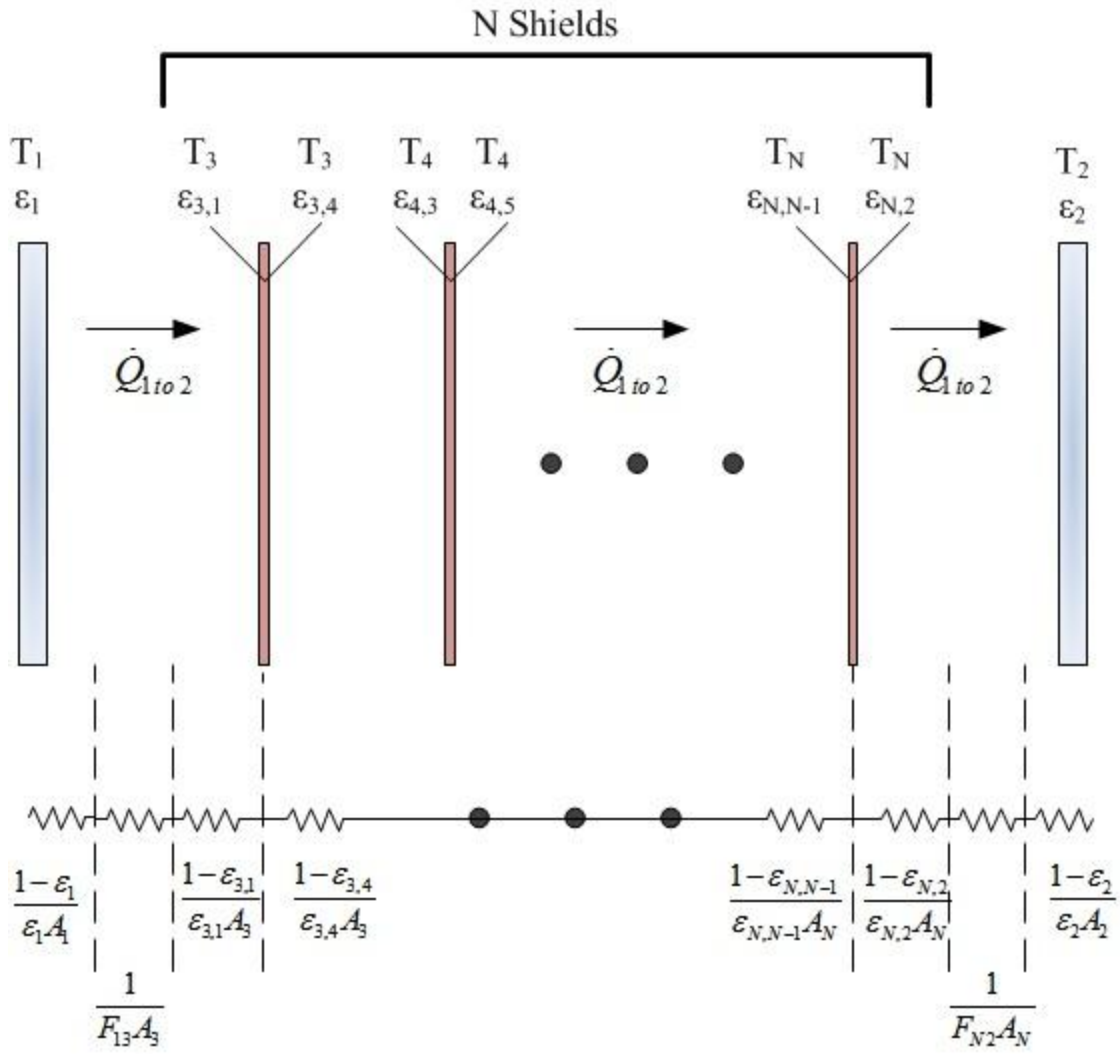

Figure 2-9 Radiation resistance network between two surfaces with N radiation shields between them

The inner surface of the Dewar and the cylindrical shield are made from unpolished commercial aluminum sheets. Fermi Lab (2010) reports that the the emissivity of a commercial aluminum sheet is approximately equal to 0.09. Musilova et al. (2004) suggests that the emissivity of aluminized polyester foils "Mylar sheets" is approximately 0.017. Using these values, the radiation heat load versus number of radiation shields is plotted in Figure 2-10. As can be seen from this plot, the radiation between the two surfaces could be reduced by more than 98% by

using 10 layers of aluminized Mylar sheets. Thus, 10 layers of insulating sheets were used, resulting in a predicted 423 mW of heat load on the first stage due to radiation.

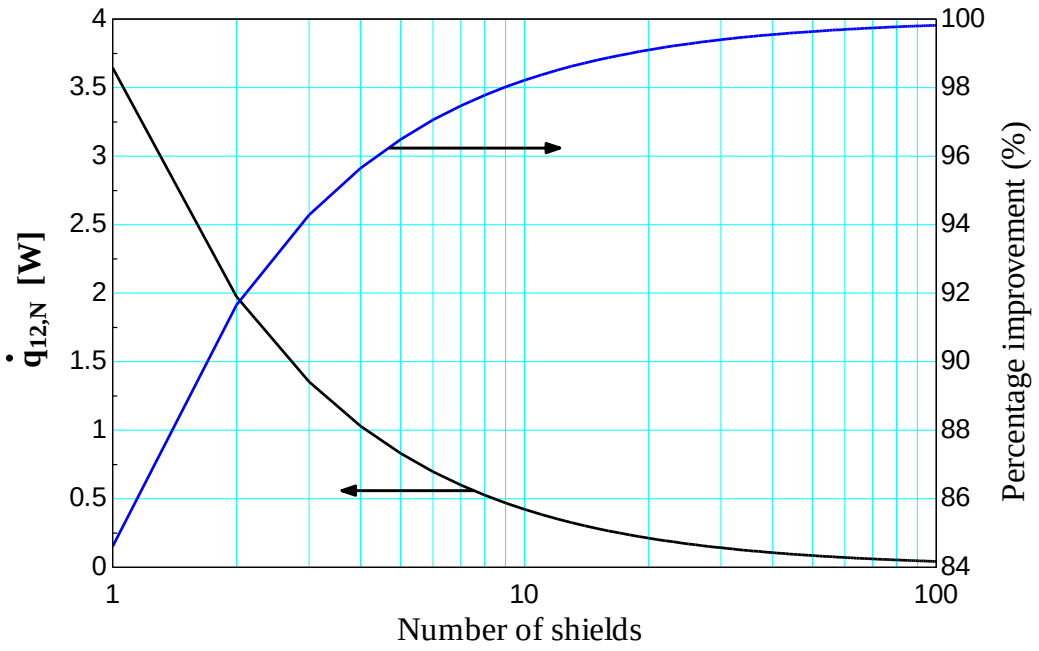

Figure 2-10 Heat load due to radiation between the outer surface of the Dewar and the first stage assembly vs. number of aluminized Mylar sheets used as the MLI

It is tempting to take similar measures to protect the second stage assembly from the radiation heat load that is received from the first stage assembly. However it is not useful to use MLI sheets for this purpose. To understand this, the wave like behavior of radiation must be reviewed. The radiation emitted by any surface at a certain temperature has a unique spectral distribution. Blackbody emissive power from a surface at temperature T can be obtained from Planck's law (Nellis 2009):

$$E_{b,\lambda} = \frac{C_1}{\lambda^5 \left[\exp\left(\frac{C_2}{\lambda T} \right) - 1 \right]} \tag{2.7}$$

where C_1=3.742 x 10^8 W-μm^4/m^2, C_2=14,388 μm-K, and λ is the wavelength in microns. In order to compare the spectral distribution of radiation emitted from two surfaces at two different temperatures, it is useful to non-dimensionalize the blackbody emissive power so that it varies between 0 and 1:

$$E_{b,\lambda-ND} = \frac{E_{b,\lambda}}{\max(E_{b,\lambda})} \tag{2.8}$$

The spectral distribution of radiation for two different surfaces; one at room temperature and one at 40 K is shown in Figure 2-11. As can be seen from this plot, almost all the radiation emitted from a room temperature surface (the solid shaded area) has a wavelength smaller than the thickness of an MLI sheet (60 micron thickness), whereas most of the radiation emitted from the 40 K surface has a wavelength bigger than the thickness of an MLI sheet (the light shaded area).

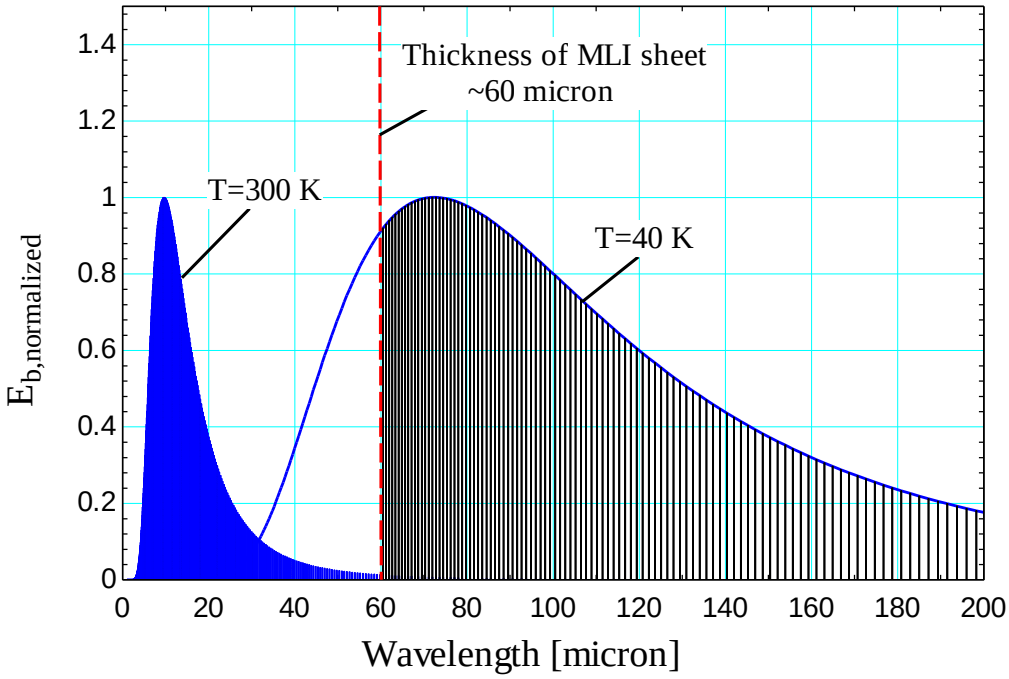

Figure 2-11 Normalized blackbody emissive power for two surfaces; 300K (solid shaded area) and 40K (light shaded area)

The radiation emitted from warmer surfaces has a shorter wavelength than the radiation emitted from colder surfaces. The longer the wavelength, the further these waves can penetrate through a material. For instance, Figure 2-12 shows three different situations; labeled A, B and C. In case A, radiation is emitted from a surface at room temperature. The wavelength in this case is shorter than the thickness of the MLI sheets. Therefore the wave is absorbed as it travels through the sheet. In case B, radiation is emitted from a surface at 40 K, approximately the same temperature as the first stage shield. Due to the longer wavelength of the radiation, the wave penetrates through the sheets. In case C, the same wave as in case B is absorbed as the wave travels through the second stage cylindrical shield's wall because the wavelength is shorter than the thickness of the wall. Thus, instead of using MLI sheets to protect the second stage assembly from radiative heat loads, the emissivity of the inner and outer surfaces of the second stage cylindrical shield must be reduced as much as possible by polishing the surfaces with an aluminum buffing compound. The use of MLI sheets is not effective because the radiation passes through these sheets as if they were not present.

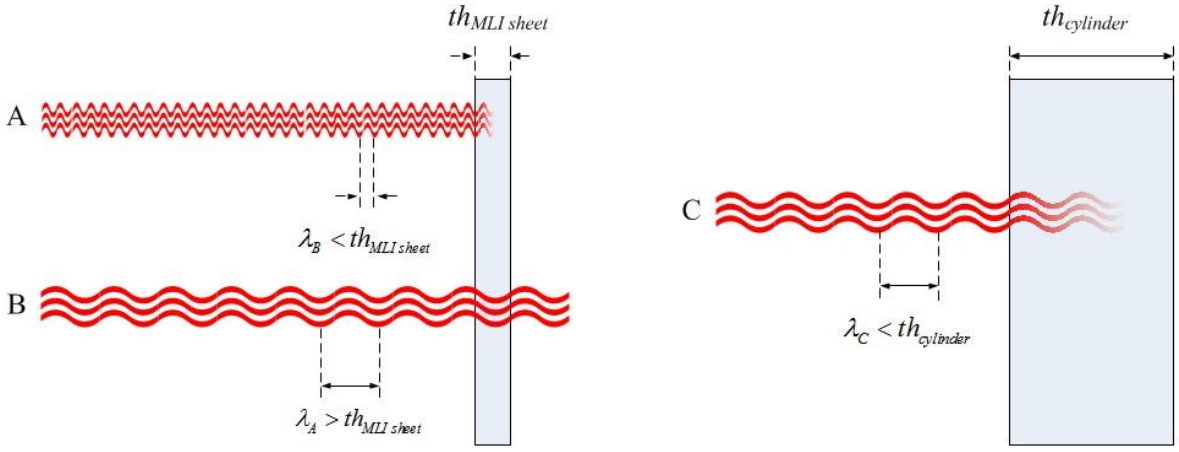

Figure 2-12 Penetration depth: A) radiation from room temperature surface, B & C) radiation from 40 K surface

2.6 Electrical wiring and connections

A hermetically sealed electrical connector is used when a bundle of wire needs to be introduced from room conditions into a vacuum space. For this work, a hermetic feedthrough was made from a blank KF-50 stub. The connector was machined to house a 41 pin round connector, and an o-ring is used between the connector and the stub to ensure a tight vacuum seal. The engineering drawing of this connector housing is available in Appendix C.

Unlike a wire in room conditions, where the heat generated because of electrical resistance is carried away by convection with the surrounding air, a wire placed in a vacuum space cannot be cooled by convection. One common technique for taking heat away from the wire in such situations is to tie them down to the cold surfaces in the Dewar. However, there is still a section of wire that is not attached to any cold surface. To counteract this, measures must be taken to correctly size the wires in a vacuum space based on the electrical current sent through them. One consideration in sizing electrical wires is to make them as short as possible in order to reduce the electrical resistance and subsequently generated heat; however, a wire that is too short leads to a large conductive heat load from room conditions. This implies that there should be an optimum length or diameter for wires for this purpose. When one end of the wire is at 290 K and the other is tied to 4.2 K the optimum length and diameter could be determined from (Ekin 2006):

$$\frac{L_{wire} I_{lead}}{A_c} \cong 5 \times 10^6 \left(amp/m \right) \tag{2.9}$$

where L_{wire} is the length of the wire, I_{lead} is the current sent through the wire, and A_c is the cross sectional area of the wire. Three groups of wires run into the Dewar; one for thermometry, one for the superconducting magnetic coil and the other for the heaters. The wires used for

thermometry are not a concern here because the current sent through them is small, so a 0.12 mm diameter Cu-Ni clad stainless steel wire is selected for this purpose. The wires used for running the superconducting magnetic coils carry 3 amperes. Therefore per 1 meter length of these wires the optimum diameter is 0.86 mm (size AWG 20). The heaters are designed such that they can safely carry a maximum of 0.5 ampere (6.25 W power with a 25 ohm resistor heater or 12.5 W with a 50 ohm resistor heater). Therefore a 0.35 mm (size AWG 27) is selected to be used for this purpose.

2.7 Measurement and control instrumentation

Thermometry in cryogenics involves the use of temperature sensors, whether diode, Resistance Temperature Detector (RTD), thermocouple, etc, and a device for displaying the temperature called a temperature monitor. A temperature controller could be used to control a heater that adjusts the temperature of the cold components.

When running experiments it is useful to know the temperature of the shields and the first stage heat exchange platform, but it is not crucial to know the temperatures at these locations with a very high accuracy. Thus silicon diode sensors are used for these “housekeeping” applications. Diodes provide +/- 1K accuracy when cooled to temperatures below 100 K; therefore, the use of these sensors for more accurate measurements is not a good option. Cernox sensors, a type of RTD, are used in locations where high accuracy measurements are needed. Some properties of both types of sensors are presented in Table 2-5 and Table 2-6.

Property	Range	Value
Minimum temperature	-	100 mK
Maximum temperature	-	325 K
Accuracy	100 mK to 77 K	+/- 25 mK
Accuracy	77 K to 300 K	+/- 153 mK

Table 2-5 Properties of Cernox sensor

Property	Range	Value
Minimum temperature	-	1.4 K
Maximum temperature	-	500 K
Accuracy	2 K to 100 K	+/- 1 K
Accuracy	100 K to 305 K	+/- 1% of temperature

Table 2-6 Properties of Diode sensor

Two model 44 Cryo-con temperature controllers are used as both temperature monitor and controller. Each temperature controller has four channel readings, compatible with cryogenic temperature sensors and two heater loops, each capable of providing a power output of 50 W when used with a 50 ohm resistor heater.

A 2700 Keithley multi-meter unit is used to measure voltage, current or resistance. A 7700 Keithley multiplexer provides 20 channels of 2-pole (2-lead wire measurements) or 10 channels of 4-pole (4-lead wire measurements) and is interfaced to the multi-meter unit. The multiplexer is ideal for RTD, thermistor, and thermocouple applications. Proper operation and resistance reading of the temperature controllers was verified by comparing the measured values with those provided by the multi-meter.

A computer is used for data acquisition and data logging. The instruments are connected to the computer via General Purpose Interface Bus (GPIB) cables. Once communication between the computer and instruments was established, a visual programming software called LabView was used as an interface between the instruments and the user.

2.8 A Summary of the facility

A low temperature facility provides the platform that is used for the 1 K facility. The functionality and performance of each component was tested as they were integrated. The Dewar was designed and assembled and a properly sized pump station was installed in order to pull a vacuum on the Dewar before activating the cryocooler. The cryocooler's performance, as the heart of the facility, was tested and compared against the data published by the manufacturer. The behavior of the system during this test closely follows the predictions ensuring proper functioning of not only the cryocooler but the whole assembly. An operation manual for the low temperature facility including the operation of the 1 K facility is presented in Appendix D.

2.9 References

Cryomech, User's manual for PT-410 cryocooler, Cryomech, Syracuse, 2010

Ekin, J., Experimental techniques for low temperature measurements, Oxford University Press, 2006

Fermi-Lab National Laboratories, website, 2011

Musilova, V., Hanzelka, P., Kralik, T., Srnka, A., "Low temperature radiative properties of materials used in cryogenics", Cryogenics, Vol. 45 (2004) Pg. 529-536

Nellis, G.F., Klein, S.A., Heat transfer, Cambridge, New York, 2009

Nellis, G.F., Lachner, B.F., Lokken, O.D., Stahl, B.L., Crawford, L.D., "Thermal resistance measurements for flexible straps at cryogenic temperatures", Conference: Advances in cryogenics engineering, Vol. 710 (2004) pg. 651-658

O’Hanlon, J.F. , A user’s guide to vacuum technology, John-Wiley, New York, 3 Ed., 2003

3 MODELING OF THE 1 K FACILITY

3.1 Overview of 1 K facility system/setup

A 1 K pot is a device that is used to attain temperatures near 1 Kelvin. The pot contains liquid helium at a nominal temperature of 1 Kelvin and works based on the evaporative cooling principle; any heat transferred into the liquid would cause the more energized liquid helium molecules to depart the liquid surface (evaporation). These evaporated molecules must be removed from the pot in order to keep the pressure and subsequently the temperature down. Figure 3-1 shows the vapor pressure of helium as a function of its temperature and shows that in order to keep the temperature of the liquid helium at 1.5 K, the pressure in the pot must be kept at 451 Pa. The application of a 1 K pot is quite broad; it is commonly used in ^{3}He-^{4}He dilution refrigerators, where the pot acts as a condenser (precooler) for the helium mixture. It can also be used to cool superconducting magnets because helium, when subcooled to temperatures below the lambda point, exhibits excellent thermal transport properties.

The superfluid magnetic pump (SMP) must circulate liquid helium at temperatures lower than 2 Kelvin. Therefore, a refrigeration system must be used to subcool helium to the appropriate temperature range for the SMP experiment. The low temperature facility discussed in chapter 2 is only capable of attaining 3.8 K (and this temperature is only attainable when no heat load is applied to the second stage). Commercially available cryocoolers are not capable of producing temperatures below the lambda point due to the complexities introduced by superfluid helium in such systems. Therefore, a 1 K pot must be integrated with the low temperature facility discussed in chapter 2 in order to attain lower temperatures.

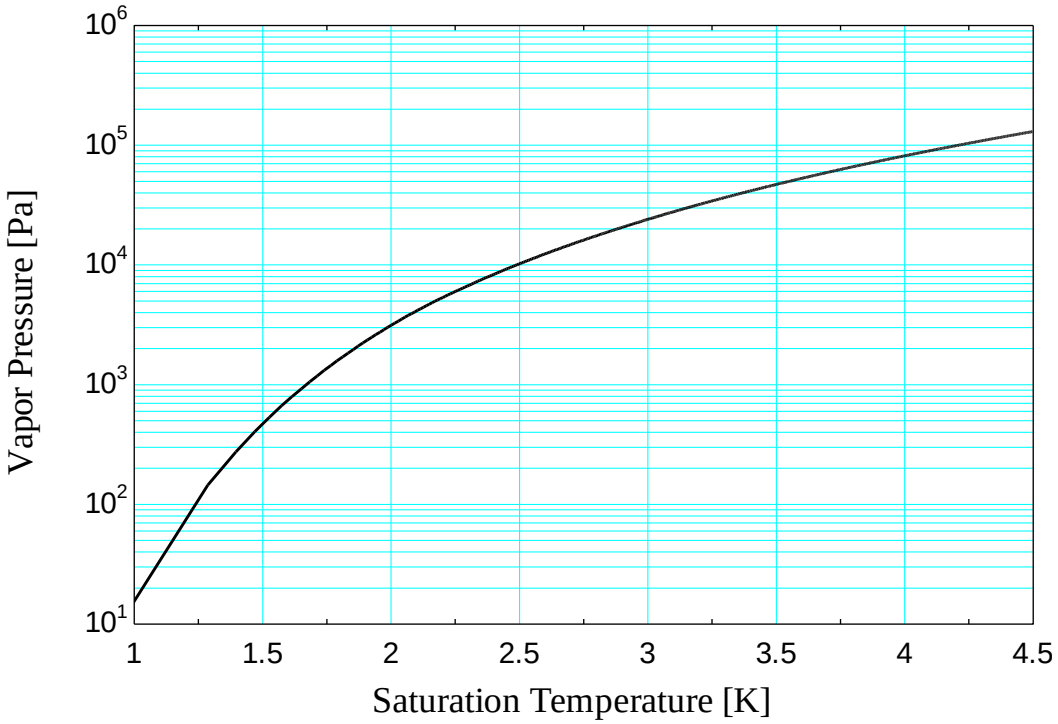

Figure 3-1 Vapor pressure of helium as a function of its temperature

The components of the 1 K facility are shown in Figure 3-2. The bold arrows in this figure represent the direction of helium flow in the system. Helium is first discharged from the reservoir at room temperature. After entering the Dewar, it is precooled by exchanging heat with the first stage heat exchange platform. Then it enters the first stage recuperator where helium is further precooled before exchanging heat with the second stage heat exchange platform (the liquefier). After liquefaction and subcooling, helium is further subcooled in a second stage recuperator. Then the Joule-Thompson (J-T) effect, a process explained more in detail later in this chapter, causes the helium temperature to drop after it exits the J-T restrictor. At this point, helium enters the pot at a nominal temperature of 1 Kelvin. Helium evaporating in the pot is pumped out by a rotary vane pump, keeping the vapor pressure above the liquid low. The helium pumped by the rotary vane pump is exhausted to the ambient.

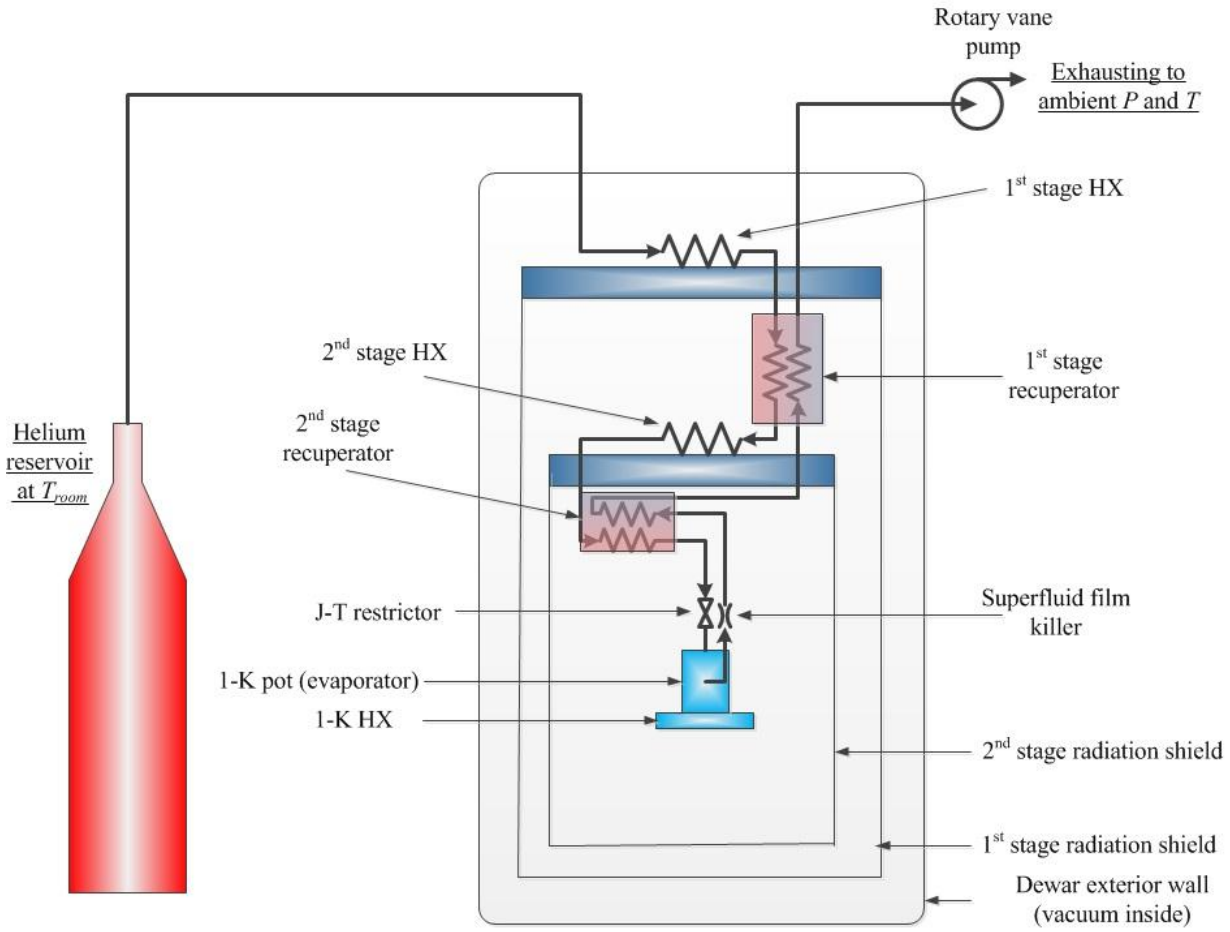

Figure 3-2 Schematic of the 1 K facility used in this work with different components labeled (HX: Heat Exchanger)

The 1 K pot is chosen to provide a power of 150 mW based on two factors: the power needed to precool the helium in the SMP experiment ($\dot{q}_{smp}$)and the heat leaks to the 1 K pot ($\dot{q}_{leaks-1K}$):

$$\dot{q}_{1K\ pot} = \dot{q}_{SMP} + \dot{q}_{leaks-1K} \tag{3.1}$$

The power needed to precool the helium in the SMP experiment is predicted and discussed in more detail in chapters 5 and 6. The heat loss from the 1 K pot depends on the geometry and the size of the different components attached to the pot. Therefore, the heat loss is estimated and discussed in the experimental setup details in chapter 4.

Any heat received by the 1 K pot will directly result in evaporating liquid helium in the pot. The evaporated helium must be replenished by the same amount of helium in order to maintain steady state operation in the 1 K pot. Thus the mass flow rate required for this system is calculated by dividing the power that the 1 K pot can provide by the latent heat of vaporization L_v:

$$\dot{m}_{1K} = \frac{\dot{q}_{1K\ pot}}{L_v} \tag{3.2}$$

The latent heat of vaporization for saturated superfluid helium is not a strong function of temperature between 1 and 4.4 K; it varies from 23,400 to 19,400 J/kg (Pfotenhauer 1992). Assuming an average latent heat of vaporization of 21,400 J/kg, the mass flow rate for the 1 K facility is found to be $7x10^{-6}$ kg/s. The mass flow rate throughout the system must be the same due to mass conservation. In this chapter, each component of the 1 K facility will be modeled using this mass flow rate and the state of the helium will be predicted from its entrance to the Dewar, through every component, until it is exhausted to ambient.

3.2 Modeling the first stage heat exchanger

A pressure regulator is attached to the helium reservoir, allowing the user to control the pressure of the incoming helium to the system. Helium is discharged from the reservoir at 2 atm and room temperature and enters the Dewar. The first component that the helium passes through is the first stage heat exchanger where it exchanges heat with the first stage heat exchange platform. A 1/8 inch tube with an internal diameter of 1/16 inch is thermally linked to the first stage heat exchange platform. Copper tube is selected because of its high thermal transport properties even

at low temperatures. The objective of this section is to find the appropriate tube length needed to precool the incoming helium.

As the fluid moves through the tube it is cooled; therefore, its thermodynamic properties such as temperature, density, etc. change. For this reason, Nellis and Klein (2009), suggest that the heat exchanger must be broken into sub heat exchangers, where the heat transferred between each sub heat exchanger and the first stage heat exchange platform are assumed to be equal. In order to find the heat transfer rate for each sub heat exchanger, the total heat transfer rate during the first stage heat exchange must be determined:

$$\dot{q}_{HX} = \dot{m}_{1K}\left(i_{in,HX} - i_{out,HX}\right) \tag{3.3}$$

where $i_{in,HX}$ is the specific enthalpy of the incoming helium and $i_{out,HX}$ is the specific enthalpy of helium exiting the heat exchanger. In this analysis, the first stage heat exchange platform is assumed to be at a constant temperature of 39K. If the approach temperature difference of the first stage heat exchanger, the temperature difference between the cold platform and the helium leaving the heat exchanger, is a very small value then the required length of the tube for the heat exchanger will be very long (approaching infinity for infinitesimal approach temperature difference). However if the approach temperature difference of the first stage heat exchanger is a large value, then helium leaving the first stage heat exchanger will put a higher heat load on the next heat exchanging component. Thus 1 K is chosen to be a sufficient value for the approach temperature difference in the first stage heat exchanger. The Engineering Equation Solver (EES) (Klein 2011) is used to model the first stage heat exchanger.

```
"!Known information"
T_H_in=298[K]                    "Inlet temperature"
T_H_out=40[K]                    "Outlet temperature"
```

```
T_c=39[K]                                   "First stage heat exchange platform
temperature"
m_dot=7e-6[kg/s]                            "Mass flow rate"
p_H=2[atm]*convert(atm,Pa)                  "Pressure within HX"

"!Finding the total heat transferred in HX1"
i_H_in=enthalpy('Helium', T=T_H_in, P=P_H)  "Inlet enthalpy"
i_H_out=enthalpy('Helium', T=T_H_out, P=P_H) "Outlet enthalpy"
q_dot=m_dot*(i_H_in-i_H_out)   "Total heat transfer during precooling at 1st stage"
```

The heat exchanger is broken into N sub heat exchangers, as shown in Figure 3-3. The heat transfer rate increases when moving from left to right. Subscript j denotes the number of the node:

$$\dot{q}_j = j\frac{\dot{q}_{HX}}{N} \quad for \quad j = 1 \, to \, N \tag{3.4}$$

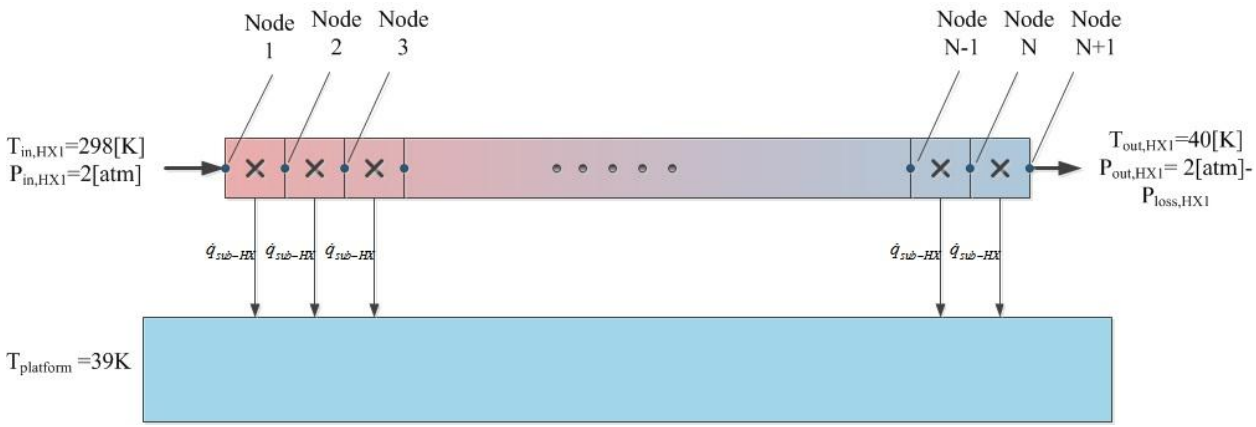

Figure 3-3 First stage heat exchanger is broken into *N* sub heat exchangers with *N+1* nodes

Since the heat transfer rate for each sub heat exchanger is known, it is possible to apply an energy balance and calculate the specific enthalpy of helium leaving each sub heat exchanger from:

$$i_j = i_{j-1} - \frac{\dot{q}_{HX}}{N\dot{m}_{1K}} \quad for \; j = 1 \, to \, N \tag{3.5}$$

The pressure drop within each sub heat exchanger can be computed from:

$$\Delta P_j = \left(\frac{2\dot{m}_{1K}}{\pi D_{tube}^3} \right) \left(f_j \Delta x_j u_j \right) \tag{3.6}$$

where f_j is the friction factor, Δx_j is the length, and u_j is the average velocity of helium in each sub heat exchanger. The first term on the right hand side of Eq. (3.6) is constant and found to be 1,114 among all sub heat exchangers. The second term on the right hand side is dependent on the fluid properties and dimensions of each sub heat exchanger. The velocity of helium within each sub heat exchanger can be calculated according to:

$$u_j = \frac{\dot{m}_{1K}}{\rho_j A_{c,tube}} \tag{3.7}$$

where ρ_j is the density of helium within each sub heat exchanger and $A_{c,tube}$ is the cross sectional area of the tube. The second term on the right hand side of Eq. (3.6) varies between 0.024 at 298 K and 0.0009 at 40K per cm length of sub heat exchanger, implying a pressure loss of only 27 and 1 Pa at the two temperature extremes. Thus the pressure loss in the helium is safely ignored and assumed to be at 2 atm throughout the first stage heat exchanger.

The temperature of helium leaving each sub heat exchanger can be found using the specific enthalpy and pressure at each node. The temperature of helium is found by EES internal routines. This information is entered in EES:

```
N=200[-]                                          "Number of sub heat exchangers"
"!Heat transfer rate increases from left to right"
duplicate j=1,N
    q_dot[j]=j*q_dot/N
end

T_H[1]=T_H_in                                     "Temperature of first node"
i_H[1]=i_H_in                                     "Enthalpy of first node"

"!Finding enthalpy and temperature of each node"
duplicate j=2,(N+1)
    i_H[j]=i_H[j-1]-q_dot/(N*m_dot)
```

```
    T_H[j]=Temperature('Helium', h=i_H[j], P=P_h)
end
```

Effectiveness (ε, the dimensionless heat exchanger performance) and the number of transfer units (NTU, dimensionless size of a heat exchanger) are used to build a bridge between the heat exchange parameters and the sizing of a heat exchanger. This method is known as the effectiveness-NTU method for analyzing heat exchangers. In order to be able to apply this method the capacitance rates of the cold (the first stage heat exchange platform) and hot stream (helium) within each sub heat exchanger must be computed.

$$\dot{C}_{H,j} = \dot{m}_{1K} \frac{\left(i_{H,j} - i_{H,j+1}\right)}{\left(T_{H,j} - T_{H,j+1}\right)} \quad for \quad j = 1 \, to \, N \qquad (3.8)$$

In the first stage heat exchanger the hot stream is a fluid and the cold stream is a solid. This implies that the capacitance rate of the first stage heat exchange platform must be a large value compared to the capacitance rate of the helium. Also the capacitance rate of the first stage heat exchange platform does not change because its temperature does not change.

```
"!Finding capacitance rate for helium in each sub HX"
duplicate j=1,N
    C_dot_H[j]=m_dot*(i_H[j]-i_H[j+1])/(T_H[j]-T_H[j+1])
end

"! Solid 'cold stream' - setting capacitance rate a large value"
C_dot_c=100
```

The effectiveness of each sub heat exchanger is:

$$\varepsilon_j = \frac{\dot{q}_j}{\dot{C}_{H,j}(T_{H,j} - T_{C,j+1})} \quad for \quad j = 1 to \; N \tag{3.9}$$

The number of transfer units required by each sub heat exchanger is found by the ε-NTU solution implemented by the function HX (Nellis and Klein, 2009). This function accepts either a parallel flow, counter flow, or cross flow heat exchanger configuration as one of its inputs. The configuration of the first stage heat exchanger is not important because the temperature of the cold stream is constant therefore any heat exchanger configuration can be chosen as an input in the HX function. The conductance in each sub heat exchanger is computed by applying:

$$UA_j = NTU_j \, \dot{C}_{H,j} \tag{3.10}$$

```
"!Applying effectiveness-NTU method"
duplicate j=1,N
    eff[j]=q_dot/(N*C_dot_H[j]*(T_H[j]-T_c))
    NTU[j]=HX('counterflow', eff[j],c_dot_H[j], C_dot_c, 'NTU')
    UA[j]=NTU[j]*C_dot_H[j]
end
```

The procedure *PipeFlow_local* in EES returns lower (assuming constant temperature of pipe wall) and upper (assuming constant heat flux) bounds on the local heat transfer coefficient and the local pressure gradient at axial position *x* for a specified mass flow rate through a circular tube of diameter *D* and length *L* (Nellis and Klein, 2009). The temperature and location in the center of each sub heat exchanger is determined by taking an average of the corresponding values between two adjacent nodes for this procedure. Relative roughness, the ratio of the dispersions on the wall of a tube (ε_d) to its diameter, must be provided for this procedure. Relative roughness for a tube is computed according to Eq. (3.11). Binder (1973) suggests that wall dispersions in a commercial copper tube wall is 1.5 micron.

$$RR = \frac{\varepsilon_d}{D_{tube}} \tag{3.11}$$

```
D=1[in]/16*convert(in,m)                                   "Inner diameter of tube"
epsilon_d=1.5e-6[m]                                        "Dispersions in tube wall"
RelRough=epsilon_d/D                                       "Relative roughness"
x[1]=0[m]                                                  "Location of first node"

duplicate j=1,N
    call PipeFlow_local('Helium',T_avg[j],P_h,m_dot,D,x_avg[j],RelRough:h_T_x[j], h_H_x[j], dPdx[j])
    x_avg[j]=(x[j]+x[j+1])/2                               "location of sub - HX"
    h_local[j]=h_T_x[j]                                    "Local convection coefficient"
    T_avg[j]=(T_H[j]+T_H[j+1])/2                           "Temperature in sub- HX"
    x[j+1]=x[j]+dx[j]                                      "Acuumilating length"
end
```

The tube will be soldered to a thin copper plate and joined to the first stage heat exchange platform as shown in the left hand side schematic in Figure 3-4. The configuration can be simplified to the one shown on the right hand side of Figure 3-4. The Biot number *Bi* is defined as the ratio of the resistance one would like to ignore to the resistance that one is considering in a model. The resistances to ignore in this case are the tube wall, the solder and the copper plate. The Biot number is:

$$Bi = \frac{R_{cond,tube} + R_{cond,solder} + R_{cond,plate}}{R_{conv}} \tag{3.12}$$

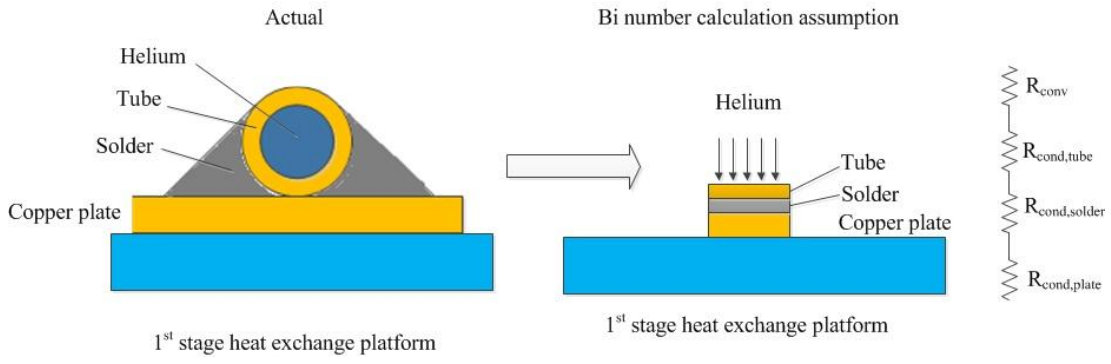

Figure 3-4 Resistance network between heat exchanger tube and first stage heat exchange platform

The Biot number is found to be in the range of 0.012 for all sub heat exchangers therefore the resistance in the tube wall, the solder and the plate are safely ignored. The conductance for each sub heat exchanger is the inverse of the total resistance between the helium and the first stage heat exchange platform. Ignoring the resistance of the tube wall, solder and plates yields:

$$UA_j = \frac{1}{R_{total}} = \left(\frac{1}{\pi D_{tube} \Delta x_j} \left[\frac{1}{h_{H,j}} \right] \right)^{-1} \tag{3.13}$$

Eq. (3.13) can be rearranged to obtain the length of each sub heat exchanger:

$$\Delta x_j = \frac{UA_j}{\pi D_{tube}} \left(\frac{1}{h_{H,j}} \right) \tag{3.14}$$

```
Duplicate j=1,N
    dx[j]=UA[j]/(h_local[j]*pi#*D)                    "Finding length of each sub-HX"
    P_loss[j]=dPdx[j]*dx[j]
end

P_sum=SUM(P_loss[j],j=1,N)
```

The required length of the first stage heat exchanger is found to be 30 cm. The temperature of helium along the tube as a function of position is shown in Figure 3-5. The pressure loss is also found by multiplying the pressure loss per unit length returned as an output of the procedure by the length of each sub heat exchanger and summing all the pressure losses throughout the tube. The total pressure loss is found to be a small value, only 96 Pascal (0.05% of inlet pressure).

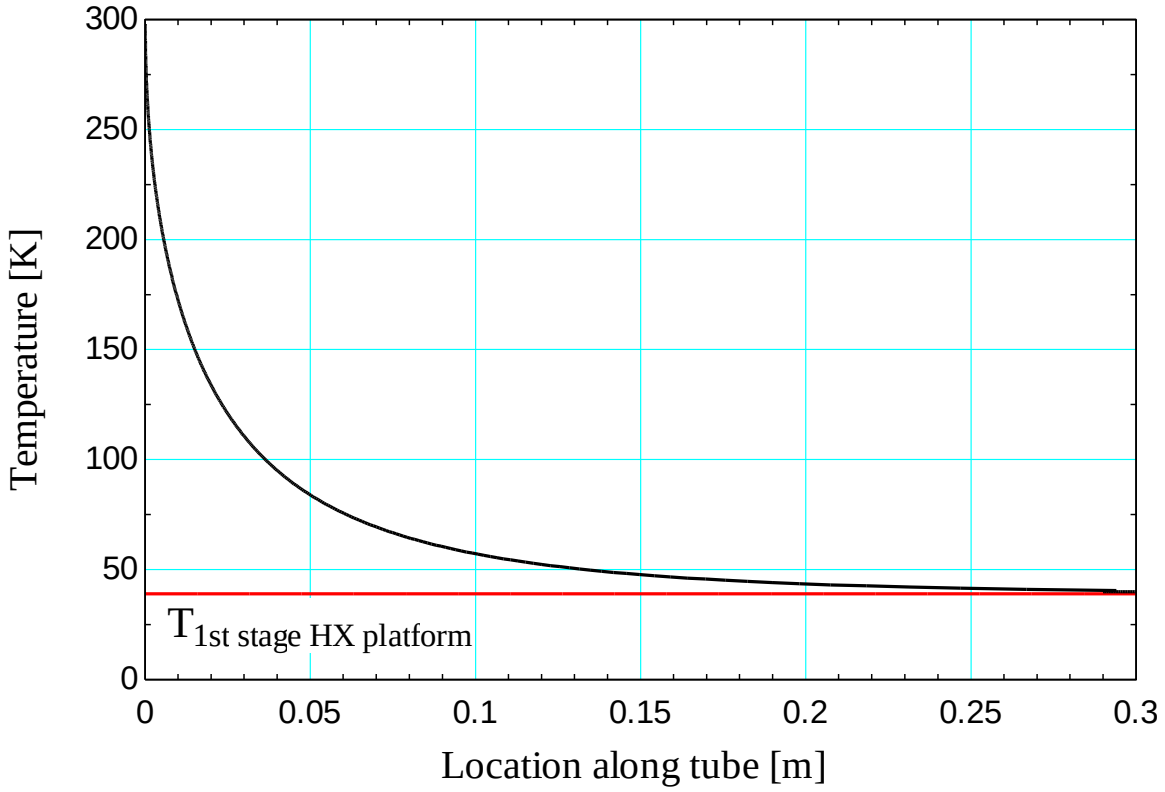

Figure 3-5 Temperature as a function of position along the tube for the first stage heat exchanger

3.3 Modeling the first stage recuperator

A recuperator is an energy recovery heat exchanger. It is often used in cryogenics to make use of a cold stream cryogenic fluid that is being exhausted to precool a hot stream of fluid within a system. In this case, the cold stream of helium is the gas that is evaporated from the 1 K pot and the hot stream is the helium leaving the first stage HX (for the first stage recuperator) and the helium leaving the second stage HX (for the second stage recuperator). The two recuperative heat exchangers can be constructed by shaping a smaller tube into two coils and inserting these coils into the exhaust tube, allowing the cold stream of helium to flow over these coils perpendicularly in order to form a cross flow heat exchanger. These two heat exchangers; one admitting the helium coming out of the first stage heat exchanger and the other admitting helium

coming out of the second stage heat exchanger will be referred to as the first stage and second stage recuperator respectively.

The analysis in this section focuses on the first stage recuperator. The objective is to demonstrate the necessity of using a first stage recuperator and to find the required length of tube needed to precool the helium before it enters the second stage heat exchanger. The reason for using a first stage recuperator can be justified by calculating the heat load applied to the second stage heat exchanger in the absence of a recuperator ($\dot{q}_{no-rec1}$) and comparing this value with the cooling capacity of the second stage, shown in Figure 2-4:

$$\dot{q}_{no\_rec1} = \dot{m}_{1K}\left(i_{out,HX1} - i_{out,HX2}\right) \tag{3.15}$$

where $i_{out,HX1}$ is the specific enthalpy of helium leaving the first stage heat exchanger and $i_{out,HX2}$ is the specific enthalpy of helium leaving the second stage heat exchanger. The heat load on the second stage heat exchange platform in the absence of a recuperator is found to be 1.5 W. This value corresponds to a second stage temperature of 4.75K when matched to the cooling capacity of the cryocooler, shown in Figure 2-4. However if a first stage recuperator is used that is capable of decreasing the temperature of helium to 10 K before entering the second stage heat exchanger then the heat load on the second stage will reduce by 75% (0.38 W) which corresponds to a second stage temperature of approximately 3.25 K according to Figure 2-4.

After helium has been precooled in the first stage heat exchanger, it enters the first stage recuperator at a temperature near 40 K. The recuperator design constrains the temperature of helium leaving the first stage recuperator to be at 10 K. Therefore the inlet and outlet temperatures of the hot stream are known. However, neither the inlet nor the outlet temperature of the cold stream is known. The inlet temperature of the cold stream can be found by applying

an energy balance on the second stage recuperator. Figure 3-6 shows a schematic of both recuperators with their inlet and outlet temperatures labeled.

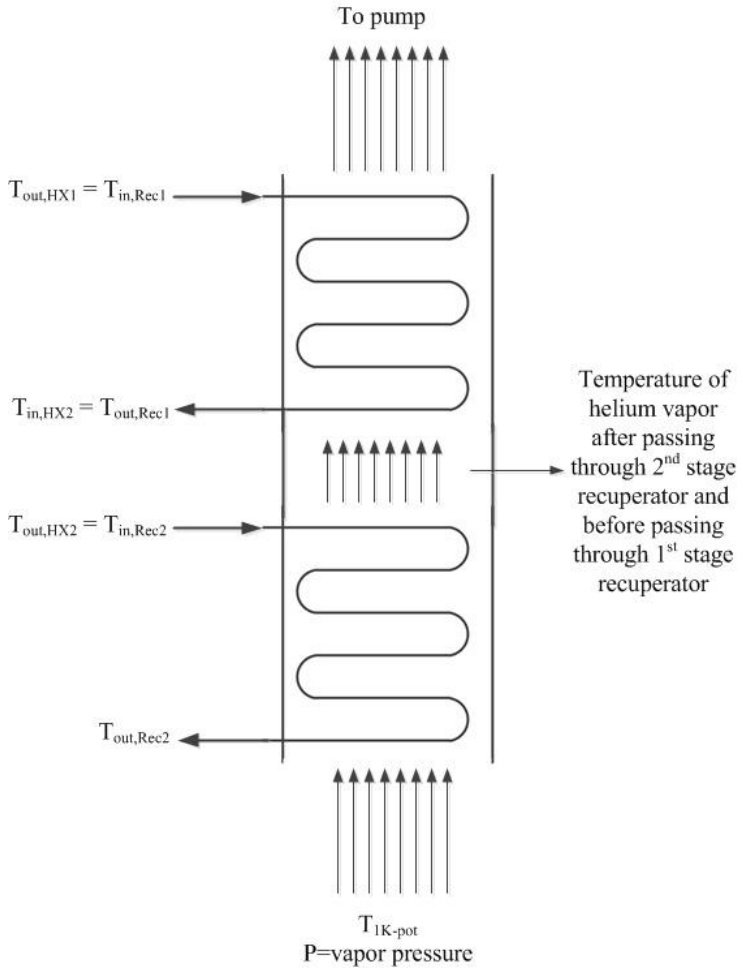

Figure 3-6 First and second stage recuperators. Subscripts HX1 and HX2 denote the first stage and second stage heat exchanger respectively, Rec1 and Rec2 denote first stage and second stage recuperator respectively.

The heat transfer rate from the hot stream must be equal to the heat transfer rate to the cold stream during the second stage recuperation:

$$\dot{m}_{1K}\left(i_{in,h,rec2} - i_{out,h,rec2}\right) = \dot{m}_{1K}\left(i_{in,c,rec2} - i_{out,c,rec2}\right) \tag{3.16}$$

where $i_{in,h,rec2}$ and $i_{out,h,rec2}$ are the inlet and outlet specific enthalpy of the hot stream of the second stage recuperator and $i_{in,c,rec2}$ and $i_{out,c,rec2}$ are the inlet and outlet specific enthalpy of the cold stream of the second stage recuperator, respectively. Liquid helium in the 1 K pot is assumed to be at 1.3 K. The corresponding vapor pressure is 158 Pa. The pressure loss in the cold stream is assumed to be negligible because pressure only affects the enthalpy, Prandtl number, viscosity and thermal conductivity in this model. These thermodynamic properties are not a strong function of pressure for helium at low pressure ranges. Thus for simplicity, 150 Pa will be used in the analysis. The temperature of the cold stream leaving the second stage recuperator and entering the first stage recuperator is found to be 2.23 K. The total heat transfer rate in the first stage recuperator is found by:

$$\dot{q}_{rec1} = \dot{m}_{1K}\left(i_{H,in} - i_{H,out}\right) \tag{3.17}$$

where $i_{H,in}$ and $i_{H,out}$ are the inlet and outlet specific enthalpy of the hot stream in the first stage recuperator respectively. The total heat transfer rate in the first stage recuperator is computed using EES:

```
p_H=2[atm]*convert(atm,Pa)                    "Pressure in hot stream"
p_C=150[Pa]                                   "Pressure in cold stream"
T_H_in=40[K]                                  "Inlet hot stream temperature"
T_C_in=2.23[K]                                "Inlet cold stream temperature"
T_H_out=10[K]                                 "Outlet hot stream temperature"

i_H_in=Enthalpy('Helium', T=T_H_in,P=p_H)     "Inlet enthalpy hot stream"
i_H_out=Enthalpy('Helium', T=T_H_out,P=p_H)   "Outlet enthalpy hot stream"

m_dot=7e-6[kg/s]                              "Mass flow rate"
q_dot=m_dot*(i_H_in-i_H_out)   "Total heat transfer in recuperator"
```

The specific enthalpy of the cold stream leaving the recuperator is found by an energy balance:

$$i_{C,out} = i_{C,in} + \frac{\dot{q}_{rec1}}{\dot{m}_{1K}} \tag{3.18}$$

where $i_{C,in}$ is the specific enthalpy of the cold stream entering the first stage recuperator. Thus the cold stream outlet temperature is found by EES internal property routines:

```
i_C_in=Enthalpy('Helium', T=T_C_in,P=p_C)          "Inlet enthalpy cold stream"
i_c_out=i_c_in+q_dot/m_dot                         "Outlet enthalpy cold stream"
T_c_out=Temperature('Helium', h=i_c_out,P=p_c)     "Outlet cold stream temperature"
```

Thermodynamic properties of helium in the cold and hot stream vary with temperature. Therefore, the recuperator is broken into N sub heat exchangers. The heat transfer rate between the two streams within each sub heat exchanger is equal among all sub heat exchangers. The sub heat exchanger setup is shown in Figure 3-7.

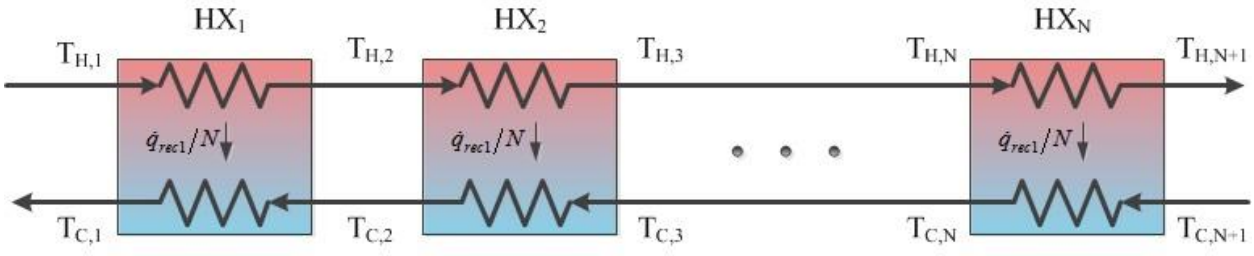

Figure 3-7 Sub heat exchanger setup for first stage recuperator

The total heat transfer increases when moving from left to right in Figure 3-7 according to:

$$\dot{q}_j = j\frac{\dot{q}_{rec1}}{N} \qquad j = 1 \, to \, N \tag{3.19}$$

```
N=100[-]                                           "Number of sub-HX"
duplicate j=1,N
    q_dot[j]=j*q_dot/N                             "Equal heat for each sub-HX"
end
```

The enthalpy leaving each sub heat exchanger can be found by applying an energy balance on the hot stream:

$$i_{H,j+1} = i_{H,j} - \frac{\dot{q}}{\dot{m}_{1K}} \tag{3.20}$$

The temperature of each node is found using the enthalpy and pressure of each node:

```
T_H[1]=T_H_in                                   "Temperature of first node in hot stream"
T_c[1]=T_c_out                                  "Temperature of first node in cold stream"
i_H[1]=i_H_in                                   "Enthalpy of first node in hot stream"
i_C[1]=i_C_out                                  "Enthalpy of first node in cold stream"

"Finding the temperature for each node in hot stream"
duplicate j=2,(N+1)
    i_H[j]=i_H[j-1]-q_dot/(N*m_dot)
    T_H[j]=Temperature('Helium', h=i_H[j],p=p_H)
end
```

The same procedure is applied to find the enthalpy and temperature for each node in the cold stream:

```
"Finding the temperature for each node in cold stream"
duplicate j=2,(N+1)
    i_C[j]=i_C[j-1]-q_dot/(N*m_dot)
    T_C[j]=Temperature('Helium',h=i_C[j],p=p_C)
end
```

Effectiveness-NTU method is used to analyze the first stage recuperator. In order to be able to apply this method the capacitance rates of the cold and hot stream within each sub heat exchanger must be computed:

$$\dot{C}_{H,j} = \dot{m}_{1K} \frac{\left(i_{H,j} - i_{H,j+1}\right)}{\left(T_{H,j} - T_{H,j+1}\right)} \quad for \quad j = 1 \, to \, N \tag{3.21}$$

$$\dot{C}_{C,j} = \dot{m}_{1K} \frac{\left(i_{C,j} - i_{C,j+1}\right)}{\left(T_{C,j} - T_{C,j+1}\right)} \quad for \quad j = 1 \, to \, N \tag{3.22}$$

```
"Calculating capacitance rates for hot and cold stream"
duplicate j=1,N
    C_dot_H[j]=m_dot*(i_H[j]-i_H[j+1])/(T_H[j]-T_H[j+1])
    C_dot_C[j]=m_dot*(i_C[j]-i_C[j+1])/(T_C[j]-T_C[j+1])
end
```

The effectiveness of each sub heat exchanger is:

$$\varepsilon_j = \frac{\dot{q}_{rec1}/N}{MIN(\dot{C}_{C,j}, \dot{C}_{H,j})(T_{H,j} - T_{C,j+1})} \quad for \quad j = 1 \, to \, N \tag{3.23}$$

The number of transfer units required by each sub heat exchanger is found by the ε-NTU solution for a cross-flow heat exchanger implemented by the function HX (Nellis and Klein, 2009). The conductance in each sub heat exchanger is computed by applying:

$$UA_j = NTU_j \; MIN(\dot{C}_{C,j}, \dot{C}_{H,j}) \tag{3.24}$$

```
"Applying effectiveness NTU method"
duplicate j=1,N
    eff[j]=q_dot/(N*MIN(C_dot_H[j],C_dot_C[j])*(T_H[j]-T_C[j+1]))
    NTU[j]=HX('crossflow_one_unmixed', eff[j], C_dot_H[j], C_dot_C[j], 'NTU')
    UA[j]=NTU[j]*MIN(C_dot_H[j],C_dot_C[j])
End
```

The procedure *PipeFlow_N_Local* in EES returns the local Nusselt numbers assuming constant temperature wall or constant heat flux for a given flow condition in a circular tube. The procedure requires the Reynolds and Prandtl numbers, the axial position to diameter ratio, and the relative roughness. The procedure also returns the local friction factor for these conditions (Klein 2011). This procedure can be used to obtain the local convection coefficient for each sub heat exchanger on the hot side by applying:

$$h_{H,j} = \frac{Nu_{H,j} \; k_{H,j}}{D_{tube}} \quad for \quad j = 1 \, to \, N \tag{3.25}$$

where $Nu_{H,j}$ is the Nusselt number on the hot side for each sub heat exchanger, $k_{H,j}$ is the conductivity of helium on the hot side for each sub heat exchanger, and D_{tube} is the inner diameter of the coil tube. The Reynolds number for each sub heat exchanger on the hot side can be calculated according to:

$$\mathrm{Re}_{H,j} = \frac{\dot{m}_{1K} D_{tube}}{A_H \mu_{H,j}} \tag{3.26}$$

where A_H is the tube's cross sectional area and $\mu_{H,j}$ is the viscosity of helium in each sub heat exchanger on the hot side. The local heat transfer coefficient for each sub heat exchanger on the hot side is computed in EES:

```
D_c=1[in]*convert(in,m)                                  "ID of cold stream tube"
A_c=pi#*D_c^2/4                                          "cross sectional area in cold stream tube"

D=0.03*convert(in,m)                                     "ID of hot stream tube"
A_h=pi#*D^2/4                                            "Cross sectional area in hot stream tube"
epsilon_d=0.015e-3[m]                                    "Dispersions in SS tube wall - hot stream tube"
RelRough=epsilon_d/D                                     "Relative roughness of hot stream tube"

x[1]=0[m]                                                "Location of first node"

Duplicate j=1,N
    "Hot stream"
    call PipeFlow_N_local(Re_H[j],Pr_H[j],xoverD[j],RelRough: Nusselt_T_x[j],Nusselt_H_x[j],f_x[j])
        Re_H[j]=m_dot*D/(A_h*mu_H[j])                    "Reynolds number-hot stream"
            mu_H[j]=Viscosity(Helium,T=T_H[j],P=P_H)     "Viscosity-hot stream"
        Pr_H[j]=Prandtl('Helium', T=T_H[j], p=P_H)       "Prandtl number - hot stream"
        xoverD[j]=x[j]/D                                 "Length to diameter ratio"
    Nusselt_H_x[j]=h_conv_h[j]*D/k_H[j]                  "Nusselt number - hot stream"
        k_H[j]=conductivity('Helium',T=T_H[j],p=p_H)     "Conductivity - hot stream"
end
```

The cross sectional area of the 1 inch tube is 256 times larger than the cross sectional area of the tube used as a coil, therefore for simplicity the cross sectional area of the cold side (A_c) is chosen to be of that of the 1 inch tube. The same procedure can be used to obtain the local heat transfer coefficient of the cold side of the sub heat exchangers using correlations for external flow over a cylinder:

```
Duplicate j=1,N
    "Cold stream"
    Call External_Flow_Cylinder_ND(Re_c[j],Pr_c[j]: Nusselt[j],C_d[j])
        Re_c[j]=m_dot*(D_c)/(A_c*mu_He_c[j])             "Reynolds number - cold stream"
            mu_He_c[j]=Viscosity(Helium,T=T_c[j],P=P_c)  "Viscosity - cold stream"
        Pr_c[j]=Prandtl('Helium', T=T_c[j], p=P_c)       "Prandtl number - cold stream"
```

```
    Nusselt[j]=h_conv_c[j]*D/k_c[j]                    "Nusselt number - cold stream"
        k_c[j]=conductivity('Helium',T=T_c[j],p=p_c)   "Conductivity - cold stream"
end
```

The resistance network between the cold and hot stream of the sub heat exchangers is shown in Figure 3-8. The resistance to ignore in this case is the hot side's tube wall resistance. Thus the Biot number is:

$$Bi = \frac{R_{cond,tube}}{R_{conv,H} + R_{conv,C}} = \frac{\frac{\ln\left(r_{tube,out}/r_{tube,in}\right)}{2\pi\, k_{tube}}}{\frac{1}{\pi D_{tube}}\left(\frac{1}{h_{H,j}} + \frac{1}{h_{C,j}}\right)} \tag{3.27}$$

where $R_{cond,tube}$ is the resistance of the tube wall, $R_{conv,H}$ and $R_{conv,C}$ are the convective resistance on the hot and cold side respectively, $r_{tube,out}$ and $r_{tube,in}$ are the outer and inner radius of the tube coil respectively, k_{tube} is the conductivity of the tube. A 1/16 inch stainless steel tube with an internal diameter of 0.03 inch is used as the coil tube. Stainless steel has a relatively low thermal conductivity. The tube extends from the outlet of the first stage to the inlet of the second stage heat exchanger, thus a lower thermal conductivity corresponds to a smaller heat load due to conduction from the first stage to the second stage heat exchange platform.

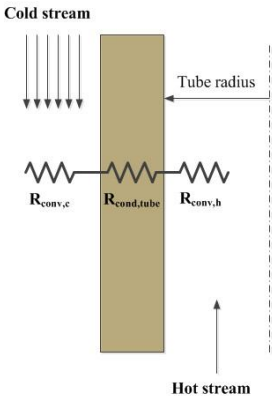

Figure 3-8 Resistance network in the recuperator

A different Biot number is computed for each sub heat exchanger. This number varies between 0.008 and 0.045; therefore, the resistance of the tube wall on the hot side of each sub heat exchanger is safely ignored in this model. The conductance for each sub heat exchanger is the inverse of the total resistance between the cold and hot streams:

$$UA_j = \frac{1}{R_{total}} = \left(\frac{1}{\pi D_{tube} \Delta x_j} \left[\frac{1}{h_{H,j}} + \frac{1}{h_{C,j}} \right] \right)^{-1} \tag{3.28}$$

Eq. (3.28) can be rearranged to obtain the required length of each sub heat exchanger:

$$\Delta x_j = \frac{UA_j}{\pi D_{tube}} \left(\frac{1}{h_{H,j}} + \frac{1}{h_{C,j}} \right) \tag{3.29}$$

```
Duplicate j=1,N
    "!Finding the length of each sub-HX"
    dx[j]=UA[j]/(pi#)*(1/(h_conv_h[j]*D)+1/(h_conv_c[j]*D))
    x[j+1]=x[j]+dx[j]
end
```

The total required length of tube needed for the first stage recuperator is found to be 58 cm. Figure 3-9 shows the temperature of the hot and cold stream as a function of position. The pressure loss in each sub heat exchanger is computed on the hot side according to:

$$\Delta P_{H,j} = \frac{f_{H,j} \Delta x_j \rho_{H,j} u_{H,j}^2}{2 D_{tube}} \tag{3.30}$$

where subscript H denotes hot stream, $f_{H,j}$ is the local friction factor, $\rho_{H,j}$ is the density of helium, and $u_{H,j}$ is the velocity of helium in each sub heat exchanger. Total pressure loss in the hot stream is found to be relatively small, 1 kPa, or 0.5% of the inlet pressure.

```
Duplicate j=1,N
    "Pressure loss in hot stream"
    f_x[j]=d_P[j]/dx[j]*2*D/(Density(Helium,T=T_H[j],P=P_H)*u_m[j]^2)
```

```
            m_dot=Density(Helium,T=T_H[j],P=P_H)*u_m[j]*A_h
end

P_loss=SUM(d_P[j],j=1,N)        "Calculating pressure loss in hot stream"
```

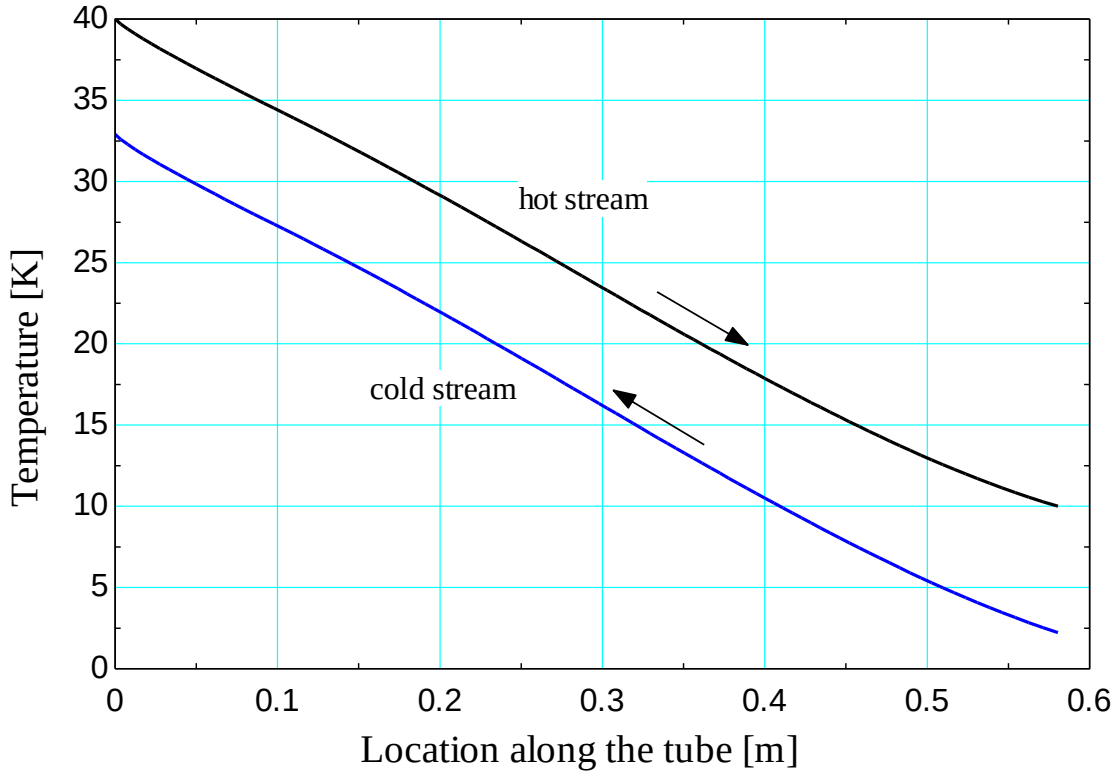

Figure 3-9 Temperature as a function of position along the hot stream tube for the first stage recuperator

3.4 Modeling of the second stage heat exchanger

The purpose of using a second stage heat exchanger is similar to using a first stage heat exchanger; to decrease the temperature of helium on its way to the 1 K pot. However, the cooling process in the second stage heat exchanger differs from the first stage heat exchanger because helium must be liquefied and subcooled before leaving the second stage heat exchanger. Thus the second stage heat exchanger must be broken into three sections as shown in Figure 3-10; a precooling stage where the temperature of the hot fluid decreases to the saturation temperature

(Pre-HX), a condensation stage where the hot side helium condenses (Cond-HX), and a subcooling stage where the temperature of the liquid helium is further decreased (SC-HX). In this section, the second stage heat exchanger model is developed.

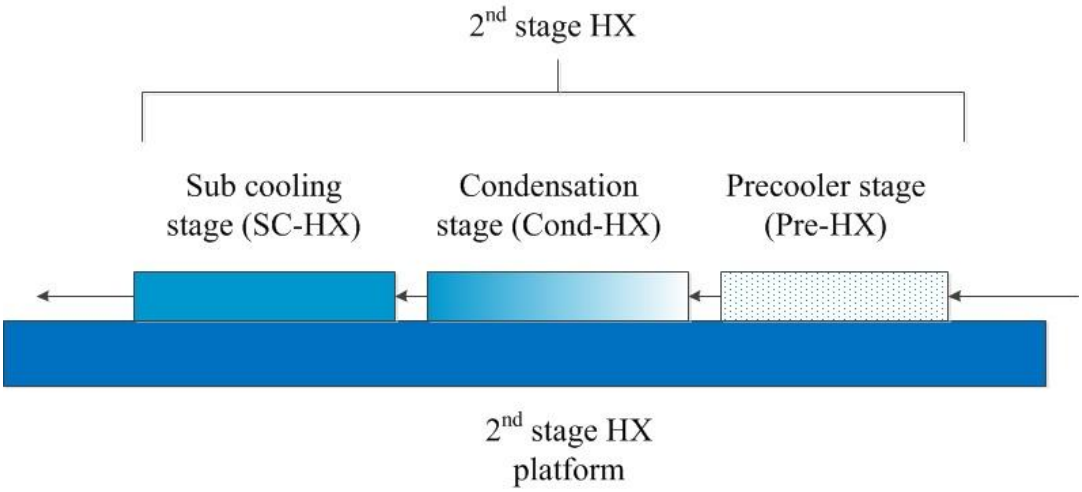

Figure 3-10 Three stages in the second stage heat exchanger

Figure 3-11 shows the operation of the 1 K facility during initial and steady state operation; at steady state operation, the inlet temperature of the second stage heat exchanger is the same as the outlet temperature of the hot stream in the first stage recuperator. However, during initial operation of the 1 K facility there is no liquid in the 1 K pot and therefore no evaporation occurs. As a result of this the temperature of helium remains unchanged in the first stage recuperator, thus the temperature of helium entering the second stage heat exchanger will be the same as the temperature of helium leaving the first stage heat exchanger. For this reason the second stage heat exchanger must be designed to be able to decrease helium's temperature from 40 K to 4 K.

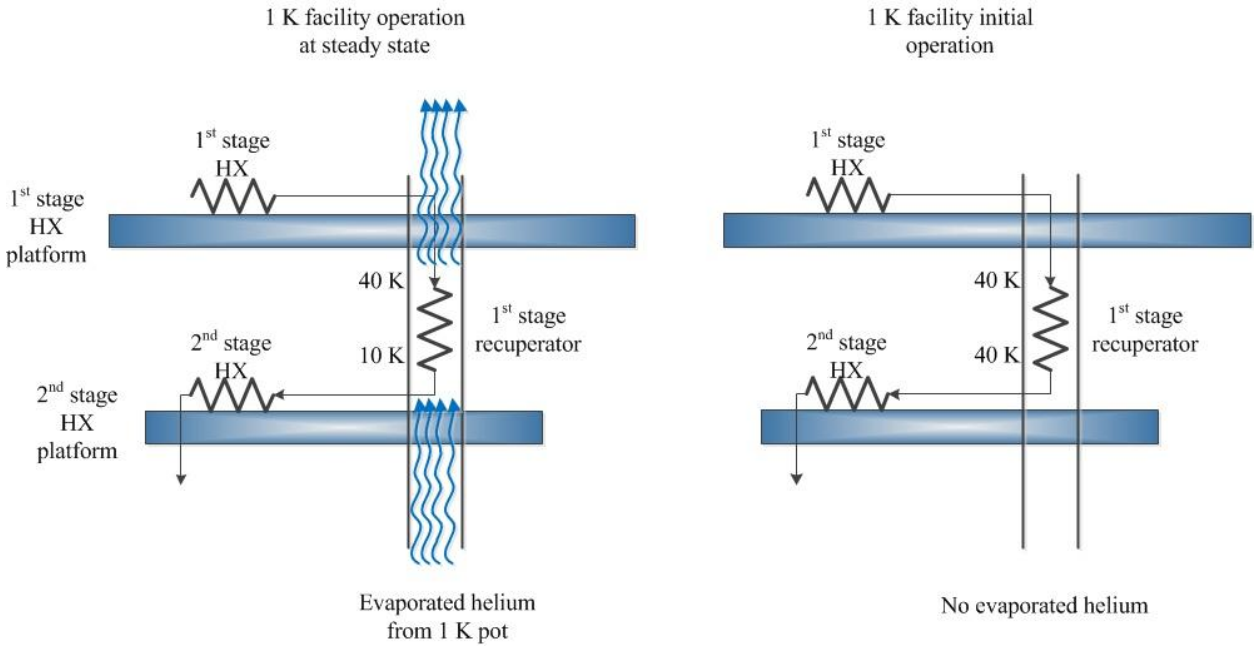

Figure 3-11 Second stage heat exchanger; steady state vs. initial operation

3.4.1 Precooler stage in second stage heat exchanger

The modeling starts by finding the required length of a 1/8 inch copper tube with an internal diameter of 1/16 inch in the Pre-HX. The temperature of helium in the Pre-HX for this model decreases from 40 K to the saturation temperature, however the thermodynamic state of helium is not well defined at the saturation temperature therefore the outlet temperature of the Pre-HX is constrained to a slightly higher temperature than the saturation temperature of helium at 2 atm. The temperature of the second stage heat exchange platform is assumed to be at 3.9 K. Similar to the modeling of the first stage heat exchanger, the inlet and outlet enthalpies and the total heat transfer rate are found in EES:

```
"!set condition 'precooler' -> precooler region , 'condensation' -> condensation region, ELSE -> subcooling region"
$IF condition$='precooler'
"!Known information"
T_c=3.9[K]
```

```
T_H_in=40[K]                                   "Inlet temperature"
T_H_out=T_sat('Helium',p=p_H)+0.1[K]           "Outlet temperature"
m_dot=7e-6[kg/s]                               "Mass flow rate"
p_H=2[atm]*convert(atm,Pa)                     "Pressure within HX"

"!Finding the total heat transferred in HX1"
i_H_in=enthalpy('Helium', T=T_H_in, P=P_H)     "Inlet enthalpy"
i_H_out=enthalpy('Helium', T=T_H_out, P=P_H)   "Outlet enthalpy"
q_dot=m_dot*(i_H_in-i_H_out)                   "Total heat transfer during precooling at 1st
stage"
```

The Pre-HX is broken into sub heat exchangers, where the heat transfer rate between each sub heat exchanger and the second stage heat exchange platform are equal to each other. The heat transfer rate increases when moving from left to right, as shown in Figure 3-3:

```
N=250                                          "Number of sub - HX"
"!Equal heat transfer rate for all sub-HX"
duplicate j=1,N
    q_dot[j]=j*q_dot/N
end
```

Each node's enthalpy and temperature is found by EES' internal routines:

```
T_H[1]=T_H_in                                  "Temperature of first node"
i_H[1]=i_H_in                                  "Enthalpy of first node"

"!Finding temperature of each node"
duplicate j=2,(N+1)
    i_H[j]=i_H[j-1]-q_dot/(N*m_dot)
    T_H[j]=temperature('Helium',h=i_H[j],p=p_H)
end
```

Similar to the method used in the first stage heat exchanger, the capacitance rates for the cold and hot stream are found by:

```
"! Finding capacitance rate for each sub-HX"
duplicate j=1,N
    C_dot_H[j]=m_dot*(i_H[j]-i_H[j+1])/(T_H[j]-T_H[j+1])
end

C_dot_c=100
```

The effectiveness-NTU method is used to analyze each sub heat exchanger:

```
"!Applying effectiveness-NTU method"
duplicate j=1,N
    eff[j]=q_dot/(N*C_dot_H[j]*(T_H[j]-T_c))
    NTU[j]=HX('counterflow', eff[j],c_dot_H[j], C_dot_c, 'NTU')
    UA[j]=NTU[j]*C_dot_H[j]
end
```

The convection coefficient for each sub heat exchanger is computed in EES in a similar fashion to the solution shown in the modeling of the first stage heat exchanger. The length of each sub heat exchanger is computed:

```
D=1[in]/16*convert(in,m)                                    "ID of tube"
epsilon_d=1.5e-6[m]
RelRough=epsilon_d/D                                        "Relative roughness"
x[1]=0[m]                                                   "Location of first node"

duplicate j=1,N
    call PipeFlow_local('Helium',T_avg[j],P_h,m_dot,D,x_avg[j],RelRough:h_T_x[j], h_H_x[j], dPdx[j])
    x_avg[j]=(x[j]+x[j+1])/2                                "Location of each sub-HX"
    h_local[j]=h_T_x[j]                                     "Local convection coefficient in each sub-HX"
    T_avg[j]=(T_H[j]+T_H[j+1])/2                            "Temperature within each sub-HX"
    dx[j]=UA[j]/(h_local[j]*pi#*D)                          "Finding length of each sub-HX"
    x [j+1]=x[j]+dx[j]                                      "Accumilating length"
    dP[j]=dPdx[j]*dx[j]
end
```

The required length for the Pre-HX is found to be 39 cm. The total pressure loss in the Pre-HX is found by summing all the pressure losses in the sub heat exchangers. The total pressure loss is found to be only 10 Pascal.

3.4.2 Condensation stage in second stage heat exchanger

After being precooled to the saturation temperature in the precooler stage of the second stage heat exchanger, helium starts to condense in the Cond-HX. Helium enters the Cond-HX at the saturation temperature and stays at this temperature throughout this stage. The analysis for the Cond-HX is the same as the Pre-HX. The only difference is that the quality, the ratio of vapor to liquid, of helium in each sub heat exchanger must be found through EES internal routines given

the pressure and enthalpy of helium in each sub heat exchanger. Also note that helium's enthalpy significantly changes at a constant temperature during condensation therefore the capacitance rate of the hot stream during condensation remains a large constant value. In EES, Procedure *Cond_HorizontalTube* calculates the heat transfer coefficient for condensation of saturated vapor of quality, *x*, inside a circular tube (Nellis and Klein 2009):

```
$if condition$='condensation'
"!Known information"
T_c=3.9[K]
T_H_in=T_sat('Helium', P=p_H)+0.0001[K]                "Inlet temperature"
T_H_out=T_sat('Helium', P=p_H)-0.0001[K]               "Outlet temperature"
m_dot=7e-6[kg/s]                                       "Mass flow rate"
p_H=2[atm]*convert(atm,Pa)                             "Pressure within HX"

"!Finding the total heat transferred in HX1"
i_H_in=enthalpy('Helium', T=T_H_in, P=P_H)             "Inlet enthalpy"
i_H_out=enthalpy('Helium', T=T_H_out, P=P_H)           "Outlet enthalpy"
q_dot=m_dot*(i_H_in-i_H_out)                           "Total heat transfer during precooling at 1st
stage"

N=250                                                  "Number of sub-HX"
"!Equal heat for all sub-HX"
duplicate j=1,N
    q_dot[j]=j*q_dot/N
end

T_H[1]=T_H_in                                          "Temperature of first node"
i_H[1]=i_H_in                                          "Enthalpy of first node"

"!Finding enthalpy of each node"
duplicate j=2,(N+1)
    i_H[j]=i_H[j-1]-q_dot/(N*m_dot)
end

"!Finding the quality for each node"
duplicate j=1,N
    quality_H[j]=Quality(Helium,T=T_sat('Helium', P=p_H),h=(i_H[j]+i_H[j+1])/2)
end

"!Capacitance rates"
C_dot_H=100
C_dot_c=100

"!Applying effectiveness-NTU method"
duplicate j=1,N
    eff[j]=q_dot/(N*MIN(C_dot_H,C_dot_C)*(T_sat('Helium', P=p_H)-T_c))
    NTU[j]=HX('counterflow', eff[j],c_dot_H, C_dot_c, 'NTU')
    UA[j]=NTU[j]*MIN(C_dot_H,C_dot_c)
end
```

```
D=1[in]/16*convert(in,m)                                   "ID of tube"
RelRough=1.5e-6[m]/D                                       "Relative roughness"
x[1]=0[m]                                                  "Location of first node"

duplicate j=1,N
    Call Cond_HorizontalTube('Helium', m_dot,  quality_H[j], T_sat('Helium',P=P_H), T_c, D : h_x[j], F$[j])
    x_avg[j]=(x[j]+x[j+1])/2                               "Location of each sub-HX"
    h_local[j]=h_x[j]                                      "Convection coefficient of each sub-HX"
    T_avg[j]=T_sat('Helium', P=p_H)                        "Temperature of each sub-HX"
    x[j+1]=x[j]+dx[j]                                      "Accumilating length"
    dx[j]=UA[j]/(h_local[j]*pi#*D)                         "Finding length of eac sub-HX"
end
```

The required length of tube for the Cond-HX is found to be 3.3 cm. Unfortunately the calculation for the pressure loss in this stage is not straightforward due its two-phase flow nature.

3.4.3 Subcooling stage in the second stage heat exchanger

After being completely liquefied in the Cond-HX, helium enters the third and final section of the second stage heat exchanger the SC-HX. Helium enters the SC-HX at saturation temperature and the approach temperature difference is 0.1 K. The approach temperature difference is constrained to be a small value because as discussed later, sub-cooling helium to lower temperatures will enhance the cooling capacity of the 1 K facility. The analysis for the SC-HC is exactly identical to the one presented for the Pre-HX. The model for this section is entered in EES:

```
$else if

"!Known information"
T_c=3.9[K]
T_H_in=T_sat('Helium', p=p_H)-0.1[K]                       "Inlet temperature"
T_H_out=4[K]                                               "Outlet temperature"
m_dot=7e-6[kg/s]                                           "Mass flow rate"
p_H=2[atm]*convert(atm,Pa)                                 "Pressure within HX"

"!Finding the total heat transferred in HX1"
i_H_in=enthalpy('Helium', T=T_H_in, P=P_H)                 "Inlet enthalpy"
i_H_out=enthalpy('Helium', T=T_H_out, P=P_H)               "Outlet enthalpy"
q_dot=m_dot*(i_H_in-i_H_out)                               "Total heat transfer during precooling at 1st
stage"
```

```
N=250                                                    "Number of sub - HX"
"!Equal heat transfer rate for all sub-HX"
duplicate j=1,N
    q_dot[j]=j*q_dot/N
end

T_H[1]=T_H_in                                            "Temperature of first node"
i_H[1]=i_H_in                                            "Enthalpy of first node"

"!Finding temperature of each node"
duplicate j=2,(N+1)
    i_H[j]=i_H[j-1]-q_dot/(N*m_dot)
    T_H[j]=temperature('Helium',h=i_H[j],p=p_H)
end

"! Finding capacitance rate for each sub-HX"
duplicate j=1,N
    C_dot_H[j]=m_dot*(i_H[j]-i_H[j+1])/(T_H[j]-T_H[j+1])
end

C_dot_c=100

"!Applying effectiveness-NTU method"
duplicate j=1,N
    eff[j]=q_dot/(N*C_dot_H[j]*(T_H[j]-T_c))
    NTU[j]=HX('counterflow', eff[j],c_dot_H[j], C_dot_c, 'NTU')
    UA[j]=NTU[j]*C_dot_H[j]
end

D=1[in]/16*convert(in,m)                                 "ID of tube"
epsilon_d=1.5e-6[m]
RelRough=epsilon_d/D                                     "Relative roughness"
x[1]=0[m]                                                "Location of first node"

duplicate j=1,N
    call PipeFlow_local('Helium',T_avg[j],P_h,m_dot,D,x_avg[j],RelRough:h_T_x[j], h_H_x[j], dPdx[j])
    x_avg[j]=(x[j]+x[j+1])/2                             "Location of each sub-HX"
    h_local[j]=h_T_x[j]                                  "Local convection coefficient in each sub-HX"
    T_avg[j]=(T_H[j]+T_H[j+1])/2                         "Temperature within each sub-HX"
    dx[j]=UA[j]/(h_local[j]*pi#*D)                       "Finding length of each sub-HX"
    x[j+1]=x[j]+dx[j]                                    "Accumilating length"
end

Total_length=SUM(dx[j],j=1,N)
```

The required length of tube for the SC-HX is found to be 31 cm. The total pressure loss in the SC-HX is found to be only 0.5 Pascal. The combined result of the three sections of the second stage heat exchanger is shown in Figure 3-12 where temperature as a function of position is shown along the heat exchanger tube.

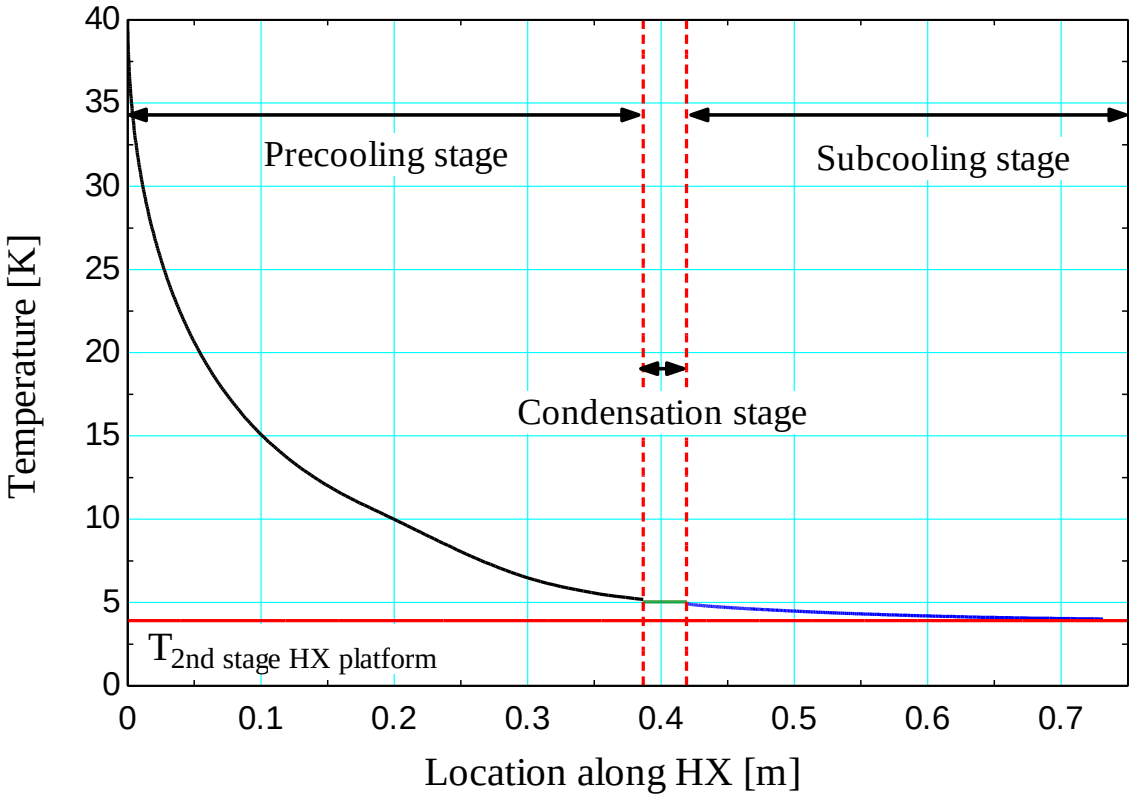

Figure 3-12 Temperature as a function of position for the second stage heat exchanger

3.5 Modeling of the second stage recuperator

Helium enters the second stage recuperator after being precooled, condensed and subcooled in the second stage heat exchanger. The second stage recuperator has the same configuration as the first stage recuperator; a 1/16 inch stainless steel tube with an internal diameter of 0.03 inch is shaped in a coil and used to carry the hot stream of helium. The cold stream of helium vapor rises up from the 1 K pot and flows over the coil to cool the incoming helium. Thus the modeling of the second stage recuperator is exactly identical to the modeling shown for the first stage recuperator. There is only one difference; unfortunately EES cannot return the thermodynamic properties of helium at temperatures lower than 2.17 K. Since the inlet temperature of the cold stream is below this temperature, 1.3 K, another source must be used to determine the

thermodynamic properties of helium for the first stage recuperator. HePak (Horizon Technologies 1999), a program utilized for calculating the thermodynamic properties of helium, is used in order to extract these properties at various temperatures and constant pressures. The data is then copied and pasted into a lookup table in EES. Thermodynamic properties are then evaluated in EES by cubic interpolation of this lookup table. The objective of this model is to find the required length of tube needed to subcool the helium. Because of the large heat transport properties of superfluid helium it is not practical for the outlet temperature of the second stage recuperator to be less than the lambda point, 2.17 K (Pfotenhauer 1992). Thus the hot stream of helium entering the second stage recuperator at a temperature equal to the outlet of the second stage heat exchanger, 4 K, is constrained to leave at a temperature slightly higher than the lambda point, 2.2 K:

```
p_H=2[atm]*convert(atm,Pa)                          "Pressure in hot stream"
p_C=150[Pa]                                         "Pressure in cold stream"
T_H_in=4[K]                                         "Inlet hot stream temperature"
T_C_in=1.3[K]                                       "Inlet cold stream temperature"
T_H_out=2.2[K]                                      "Outlet hot stream temperature"

i_H_in=INTERPOLATE('HX_h','T','i_h',T=T_H_in)       "Inlet cold stream enthalpy"
i_H_out=INTERPOLATE('HX_h','T','i_h',T=T_H_out)     "Outlet hot stream enthalpy"


m_dot=7e-6[kg/s]                                    "Mass flow rate"
q_dot=m_dot*(i_H_in-i_H_out)                        "Finding total heat transfer between cold and hot
stream"

i_C_in=INTERPOLATE('HX_c','T','i_c',T=T_C_in)       "Inlet cold stream enthalpy"
i_c_out=i_C_in+q_dot/m_dot                          "Outlet cold stream enthalpy"
T_C_out=INTERPOLATE('HX_c','T','i_c',i_c=i_c_out)   "Outlet cold stream temperature"


N=100[-]                                            "Number of sub-HX"
duplicate j=1,N
    q_dot[j]=j*q_dot/N                              "Equal heat for each sub-HX"
end

T_H[1]=T_H_in                                       "Temperature of first node in hot stream"
T_c[1]=T_c_out                                      "Temperature of first node in cold stream"

i_H[1]=i_H_in                                       "Enthalpy of first node in hot stream"
i_C[1]=i_C_out                                      "Enthalpy of first node in cold stream"
```

```
"Finding the temperature for each node in hot stream"
duplicate j=2,(N+1)
    i_H[j]=i_H[j-1]-q_dot/(N*m_dot)
    T_H[j]=INTERPOLATE('HX_h','i_h','T',i_h=i_H[j])
end

"Finding the temperature for each node in cold stream"
duplicate j=2,(N+1)
    i_C[j]=i_C[j-1]-q_dot/(N*m_dot)
    T_C[j]=INTERPOLATE('HX_c','T','i_c',i_c=i_C[j])
end

"Calculating capacitance rates for hot and cold stream"
duplicate j=1,N
    C_dot_H[j]=m_dot*(i_H[j]-i_H[j+1])/(T_H[j]-T_H[j+1])
    C_dot_C[j]=m_dot*(i_C[j]-i_C[j+1])/(T_C[j]-T_C[j+1])
end

"Applying effectiveness NTU method"
duplicate j=1,N
    eff[j]=q_dot/(N*MIN(C_dot_H[j],C_dot_C[j])*(T_H[j]-T_C[j+1]))
    NTU[j]=HX('crossflow_one_unmixed', eff[j], C_dot_H[j], C_dot_C[j], 'NTU')
    UA[j]=NTU[j]*MIN(C_dot_H[j],C_dot_C[j])
end


D_c=1[in]*convert(in,m)                                  "ID of cold stream tube"
A_c=pi#*D_c^2/4                                          "Cross sectional area in cold stream tube"

D=0.03*convert(in,m)                                     "ID of hot stream tube"
A_h=pi#*D^2/4                                            "Cross sectional area in hot stream tube"
epsilon_d=0.015e-3[m]                                    "Dispersions in SS tube wall - hot stream tube"
RelRough=epsilon_d/D                                     "Relative roughness of hot stream tube"

x[1]=0[m]                                                "Location of first node"

Duplicate j=1,N
    "Hot stream"
    call PipeFlow_N_local(Re_H[j],Pr_H[j],xoverD[j],RelRough: Nusselt_T_x[j],Nusselt_H_x[j],f_x[j])
        Re_H[j]=m_dot*D/(A_h*mu_H[j])                    "Reynolds number - hot stream"
            mu_H[j]= Prandtl('Helium', T=T_H[i], p=p_H)  "Viscosity - hot stream"
        Pr_H[j]=INTERPOLATE('HX_h','T','Pr',T=T_H[j])
        xoverD[j]=x[j]/D                                 "Length to diameter ratio"
    Nusselt_H_x[j]=h_conv_1[j]*D/k_H[j]                  "Nusselt number - hot stream"
        k_H[j]= Conductivity('Helium', T=T_H[i],p=p_H)   "Conductivity - hot stream"
end

Duplicate j=1,N
"Cold stream"
    Call External_Flow_Cylinder_ND(Re_c[i],Pr_c[j]: Nusselt[j],C_d[j])
        Re_c[j]=m_dot*(D_c)/(A_c*mu_He_c[j])             "Reynolds number - cold stream"
            mu_He_c[j]=INTERPOLATE('HX_c','T','mu',T=T_C[j])  "Viscosity - cold stream"
        Pr_c[j]=INTERPOLATE('HX_c','T','Pr',T=T_C[j])    "PRandtl number - cold stream"
     Nusselt[j]=h_conv_2[j]*D/k_c[j]                     "Nusselt number - cold stream"
        k_c[j]=INTERPOLATE('HX_c','T','k',T=T_C[j])      "Conductivity - cold stream"
```

```
end

Duplicate j=1,N
    "Pressure loss for hot stream"
    f_x[j]=d_P[j]/dx[j]*2*D/(INTERPOLATE('HX_h', 'T','rho', T=T_H[j])*u_m[j]^2)
          m_dot=INTERPOLATE('HX_h', 'T','rho', T=T_H[j])*u_m[j]*A_h
end


Duplicate j=1,N
    "!Finding the length of each sub-HX"
    dx[j]=UA[j]/(pi#)*(1/(h_conv_1[j]*D)+1/(h_conv_2[j]*D))
    x[j+1]=x[j]+dx[j]
end

P_loss=SUM(d_P[j],j=1,N)                                    "Calculating pressure loss in hot stream"
Total_length=x[N+1]      "Finding total length needed for hot stream tube"
```

The total length of tube needed for the second stage recuperator is found to be 20 cm. The total pressure loss in the hot stream is found to be only 13 Pa. The temperature of the hot and cold streams in the second stage recuperator as a function of position is shown in Figure 3-13.

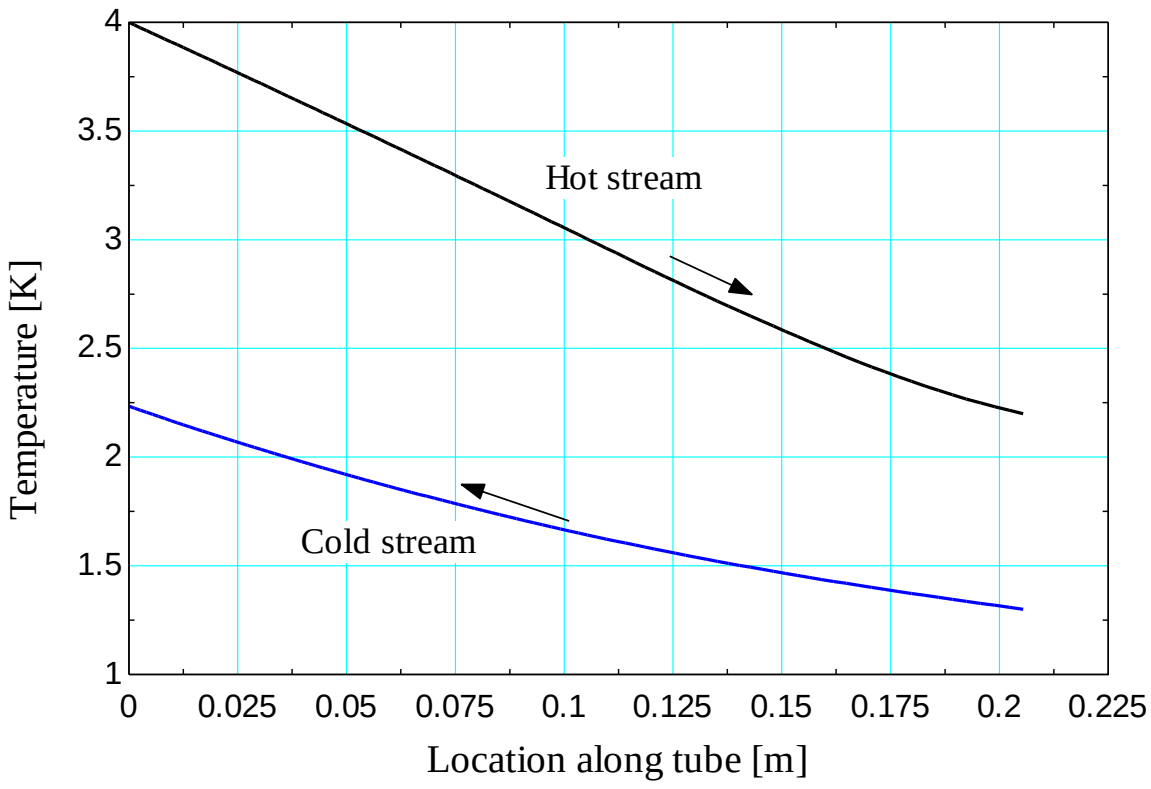

Figure 3-13 Temperature as a function of position along the hot stream tube in the second stage recuperator

3.6 Modeling of the Joule-Thompson restrictor

The helium leaving the second stage recuperator is slightly higher than the lambda point. The temperature of helium must be further reduced before entering the 1 K pot. The Joule-Thompson (J-T) effect can be used for this purpose. An isenthalpic expansion causes the fluid temperature to decrease provided that the temperature of the fluid entering the throttling process is below the J-T inversion temperature. The J-T inversion temperature for helium is 39 K over a wide pressure range (for pressures up to 600 kPa).

Helium enters a J-T restrictor, a flow restriction device used to create a pressure difference between its inlet and outlet, at a known temperature and pressure as shown in Figure 3-14 and is discharged to a vessel at a low pressure. If no heat transfer occurs during this expansion the relationship between the inlet and outlet enthalpy is:

$$i_{inlet} = i_{outlet} \tag{3.31}$$

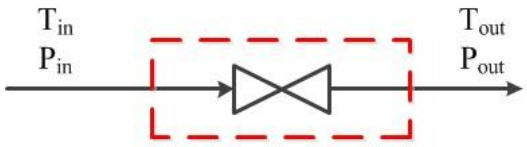

Figure 3-14 J-T restrictor

The outlet temperature can be determined since the enthalpy and pressure are known. Depending on the inlet and outlet conditions, the temperature of the helium can either be reduced or increased as a result of the J-T effect. Figure 3-15 shows helium's pressure as a function of enthalpy at various constant temperatures. Line 1 in this figure shows that if helium enters a J-T restrictor at 200 kPa and 4 K and is discharged to a vessel maintained at 15 Pa then the outlet

temperature must be 1 K; therefore, helium cools during this process. Also it can be seen that during the expansion process, helium enters a two phase region of liquid and vapor after it crosses the saturated liquid line. Line 2 shows an expansion process over the same pressure range shown for line 1 but starting from a lower temperature (2 K). These two lines suggest that the quality of the two phase mixture at the outlet will be lower for a lower J-T restrictor inlet temperature at same inlet pressure. Higher liquid fraction exiting the J-T restrictor means higher cooling power in the 1 K pot because cooling is a result of liquid helium evaporation in the pot. Therefore, the use of a recuperator is advantageous.

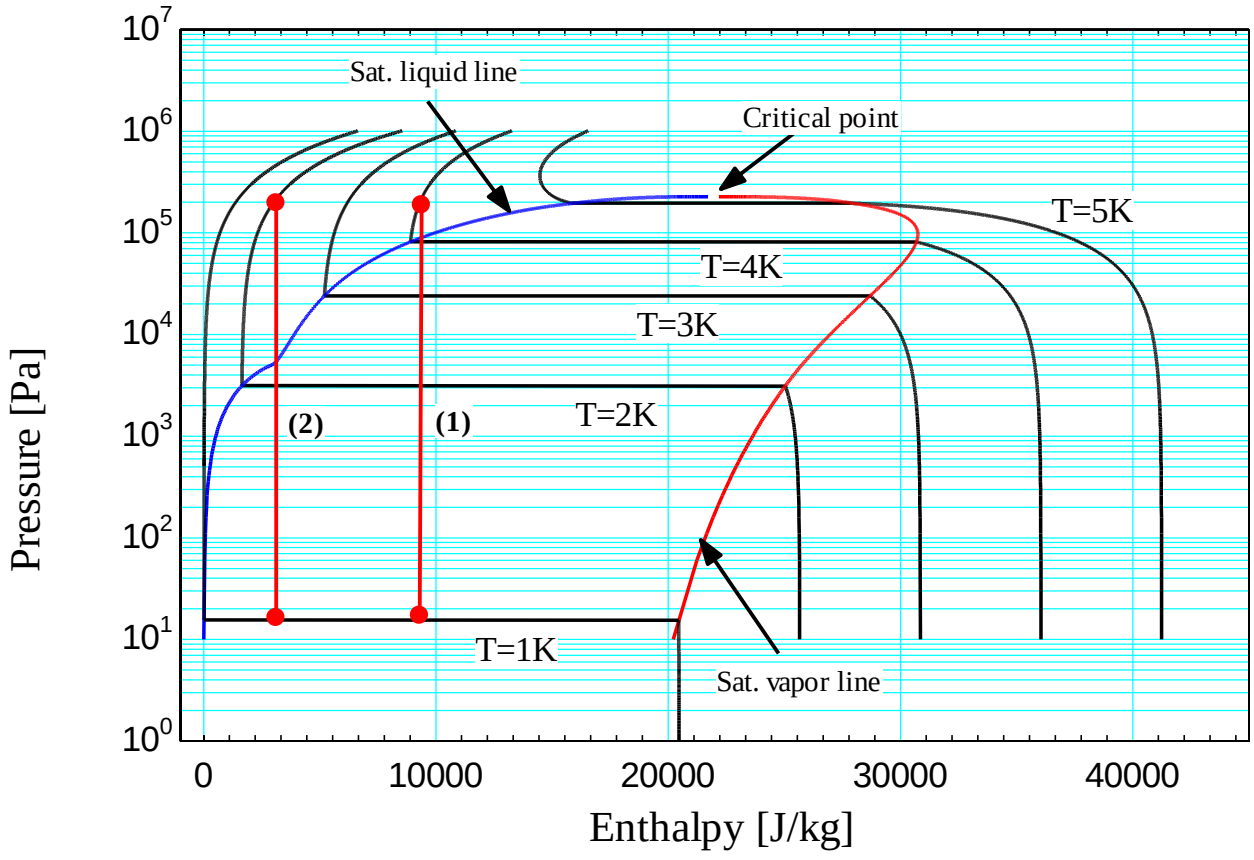

Figure 3-15 Pressure as a function of enthalpy for various constant temperatures

The J-T restrictor's yield, the liquid to vapor ratio of helium exiting the J-T restrictor and entering the 1 K pot, can be calculated by noting that the J-T restrictor's inlet enthalpy must be equal to the outlet enthalpy; the enthalpy of the liquid state plus the enthalpy of the gaseous state of helium entering the 1 K pot as shown in the system in Figure 3-16:

$$i_1 = i_2 = (1-y)i_{2,g} + yi_{2,l} \tag{3.32}$$

where y is the yield, i_1 and i_2 are the inlet and outlet specific enthalpy of the J-T restrictor, respectively, and subscripts g and l denote gaseous and liquid states. Eq. (3.32) can be rearranged to give an explicit relation for the yield:

$$y = \frac{i_1 - i_{2,g}}{i_{2,l} - i_{2,g}} = \frac{i_2 - i_{2,g}}{i_{2,l} - i_{2,g}} \tag{3.33}$$

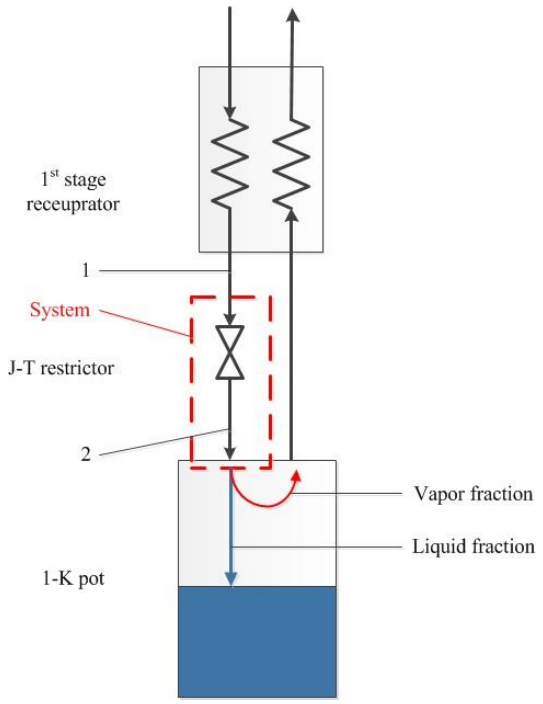

Figure 3-16 J-T restrictor configuration and system setup

Figure 3-17 shows the yield as a function of J-T restrictor's inlet temperature for a 1 K pot operating with liquid helium at 1 and 2 K. The usefulness of incorporating a second stage recuperator can be seen in the same figure; the lower the J-T restrictor's inlet temperature the higher the yield.

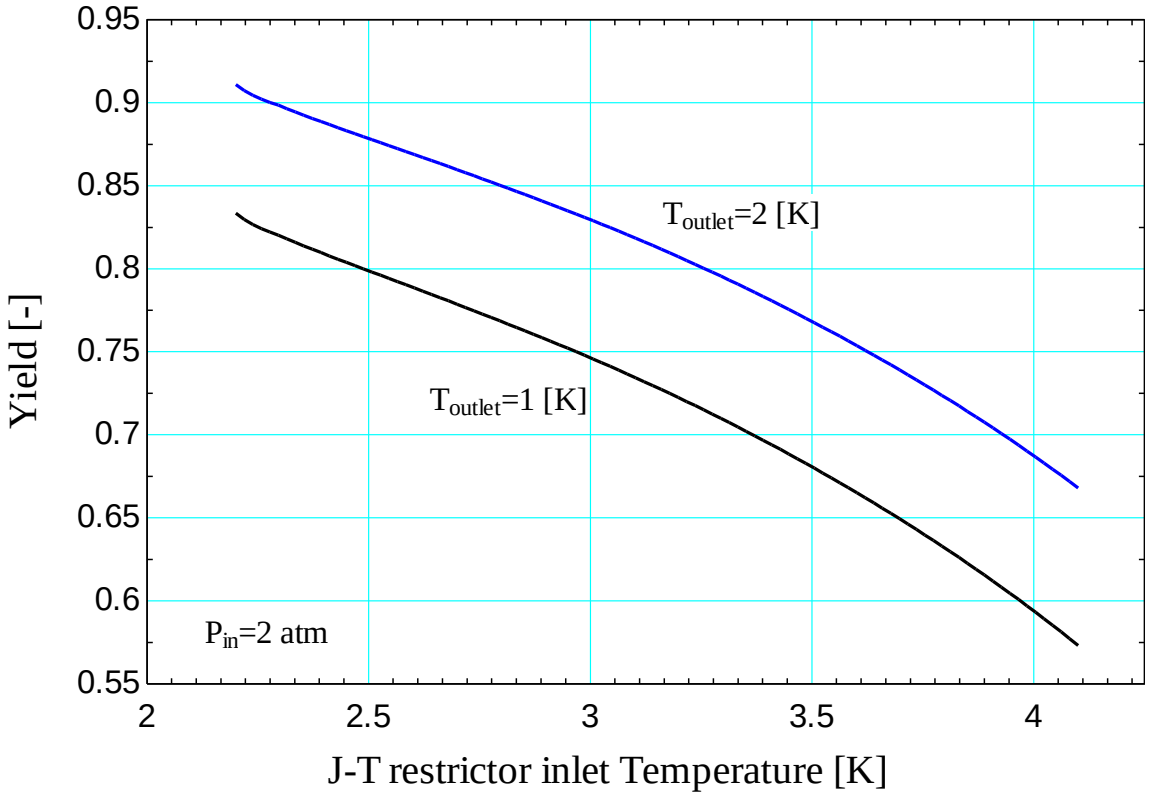

Figure 3-17 Yield as a function of J-T restrictor inlet temperature for pot temperatures of 1 and 2 K

Ideally, the mass flow rate entering the 1 K pot can be controlled by using a needle valve as a J-T restrictor. However, a capillary is used as a J-T restrictor for this work due to the Dewar's vacuum space inaccessibility during its operation. When helium flows through the capillary, the pressure drops from 2 atm to a lower pressure in the pot, which is defined by the rotary vane

pump. By inspecting Figure 3-15, it is obvious that partial vaporization is expected within the capillary.

Due to the two phase flow nature of the helium flow in the restrictor, the capillary design is not straightforward. The capillary is characterized by a quantity *Z*, called the impedance factor, which is calculated from measurements at room temperature using the following equation (Wheatley et al. 1970):

$$Z = \left(\frac{1}{\mu}\right)\frac{\Delta P}{\dot{V}} \tag{3.34}$$

where ΔP is the pressure drop required to cause the volume flow rate of laminar flow V of a gas of viscosity μ. The actual flow of helium in the capillary during the operation of the 1 K facility is quite complicated due to its gradual two phase composition change along the J-T process. Therefore, the capillary size is determined purely by empirical methods. Wheatley et al. (1970) provide several values for the impedance factor at different critical powers; critical power is the power at which the 1 K pot's temperature starts departing from its minimum equilibrium value. The empirical data were plotted and a curve was fitted to the data. Impedance factor as a function of critical power is shown in Figure 3-18.

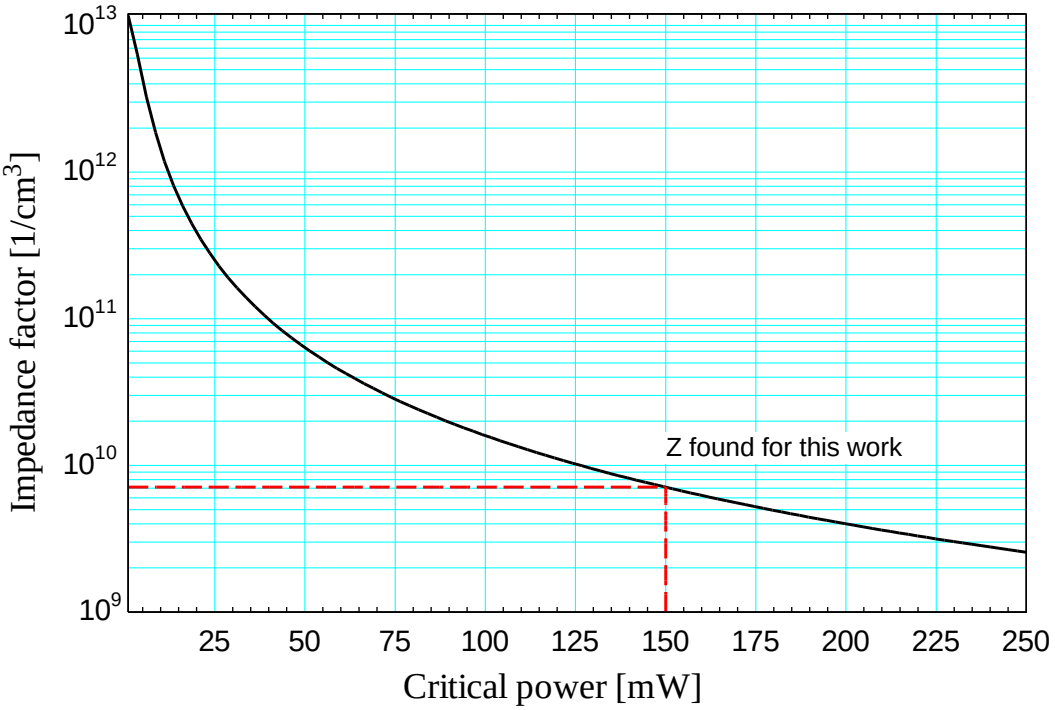

Figure 3-18 Empirical data; Capillary impedance factor as a function of critical power

The impedance factor of the capillary is found to be 7.103 x 10^{-9} ($1/cm^3$) for this work. The experimental procedure for the sizing of the capillary will be discussed in chapter 4. The helium pressure is reduced from 2 atm at the capillary inlet to the pressure within the 1 K pot upon leaving the capillary. If the pressure in the pot is maintained at 158 Pascal, the temperature of liquid helium in the pot must be at 1.3 K. Changing the inlet pressure of the 1 K facility will change the mass flow rate through the capillary, thus changing the cooling power provided by the facility.

3.7 1 K pot and 1 K heat exchange platform design

Once helium is discharged from the capillary, it enters the 1 K pot. As discussed in earlier sections, the 1 K pot holds liquid helium at a nominal temperature of 1 K. A flat surface must be

thermally linked to the 1 K pot in order to utilize the cooling power provided by the 1 K pot. This flat surface will be referred to as the 1 K heat exchange platform. The most influential factor in the design of the 1 K pot and its heat exchange platform is its ability to conduct heat within itself at such a cold temperature range. For this purpose these two components are made out of OFHC copper due to its excellent thermal transport properties at low temperatures.

During an experiment studying heat flow around a copper block immersed in He II in 1941, Kapitsa observed negligible temperature gradients within the liquid helium. However in the same experiment he discovered that there is a sizable temperature difference between the copper block and He II. The temperature difference between a solid surface and He II is a result of what is now known as the Kapitsa conductance. Van Sciver (1986) suggests a correlation for Kapitsa conductance between a copper surface and He II as:

$$h_{k,Cu} = 4.4\left[\frac{kW}{m^2 - K^4}\right]T^3 \tag{3.35}$$

where T is the temperature of the He II. Note that the dimension of the Kapitsa conductance matches the convection coefficient (W/m^2-K). Thus heat transfer due to Kapitsa conductance from a copper surface (T_{cu}) to He II ($T_{HE\,II}$) can be expressed as:

$$\dot{q}_k = h_{k,Cu} A_s \left(T_{cu} - T_{He\,II}\right) \tag{3.36}$$

where A_s is the contact surface area between copper and He II. Kapitsa resistance is the only considerable resistance between the liquid helium contained in the 1 K pot and its surrounding surface. Hence, the objective of the design is to size the pot such that the temperature gradient between the copper and liquid helium is small. In this case, the definition of small is a case of engineering judgment. For this work, a temperature difference of 1 mK between the pot and the

helium is considered sufficient. Therefore a heat transfer rate of 150 mW (the power of the 1 K pot) to the helium within the pot requires a minimum internal surface area of 158 cm^2. A pot 10 cm tall with 5 cm internal diameter is sufficient for this work. Surface area as a function of temperature for various constant heat loads is shown in Figure 3-19.

The 1 K heat exchange platform must be joined to the 1 K pot in order for the two to thermally communicate with each other. A thin 6 inch square OFHC copper block is selected to be used as the 1 K heat exchange platform. The response time of the 1 K heat exchange platform to a heat pulse is an important factor when conducting experiments with the 1 K pot. The time required for a thermal wave to penetrate through a material in the 1 K heat exchange platform can be expressed as:

$$t_{diffuse} = \frac{\rho c L^2}{4k} \tag{3.37}$$

where ρ is the density, c the specific heat capacity, L the length scale of the platform and k the conductivity of the material. The time required to diffuse across the 1 K heat exchange platform is found to be only 2 ms.

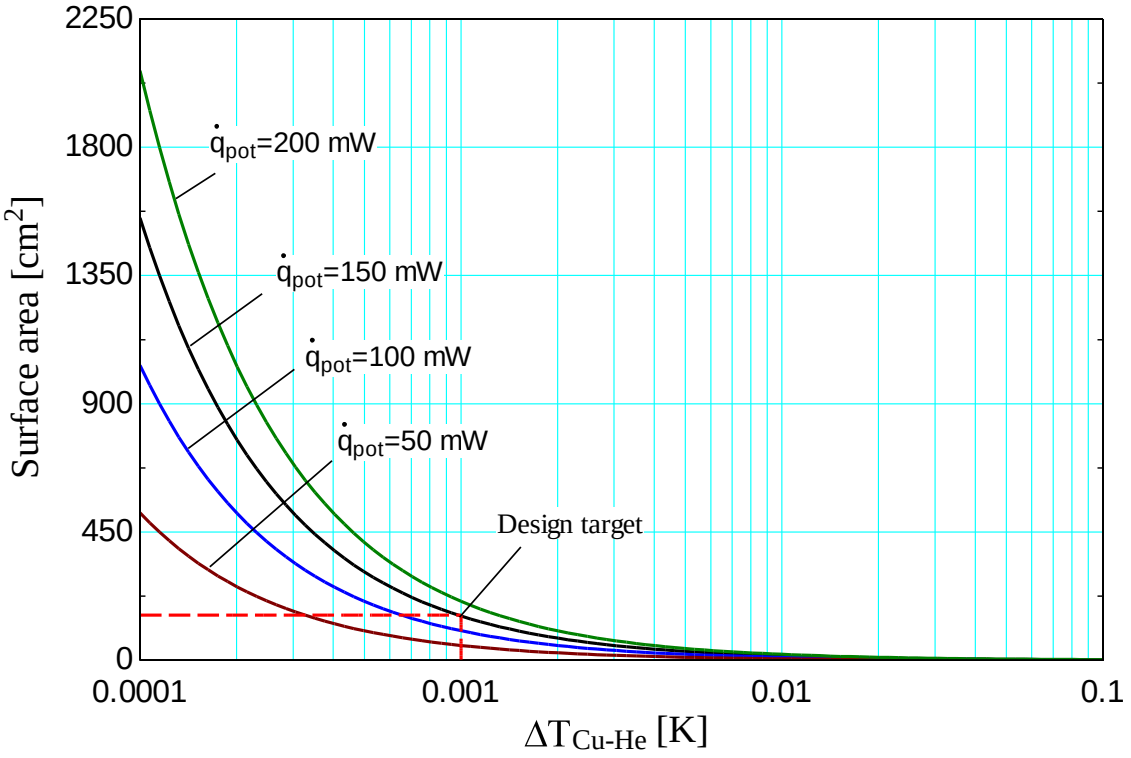

Figure 3-19 Surface area as a function of temperature difference between a copper surface and He II at various constant heat loads

3.8 Designing the superfluid film killer

During an experiment in 1922, Kammerlingh Onnes discovered a flow of He II on surfaces above the liquid helium level. He interpreted this flow in terms of an evaporation and condensation mechanism. This interpretation was later found invalid. In 1937, Simon and Rollin were able to interpret this film flow phenomenon based on the He II theory. Superfluid helium forms a mobile multi layer film above its liquid surface and it spontaneously creeps up the walls of a container holding helium II. This phenomenon is known as the Rollin film theory. The objective of this section is to provide a solution to minimize the film flow of superfluid helium and its escape from the 1 K pot.

Empirical relationships have been established that relate the film thickness f_{th} to the height H above the helium surface (Van Sciver 1986):

$$f_{th} = \frac{K_R}{H^n}[cm] \tag{3.38}$$

where K_R = 3x10^{-6} [cm^{n+1}] and n is a number between 0.3 and 0.45. Therefore, for a height of 1 cm above the liquid helium II level in the 1 K pot, the film thickness would be 30 nm or 80 atomic layers. The thickness of the film can be reduced by introducing a restriction in the path of the flow by reducing the diameter of the pot at the top. This restriction is called the superfluid film killer. A schematic of the superfluid film killer and its configuration with respect to the pot is shown in Figure 3-20.

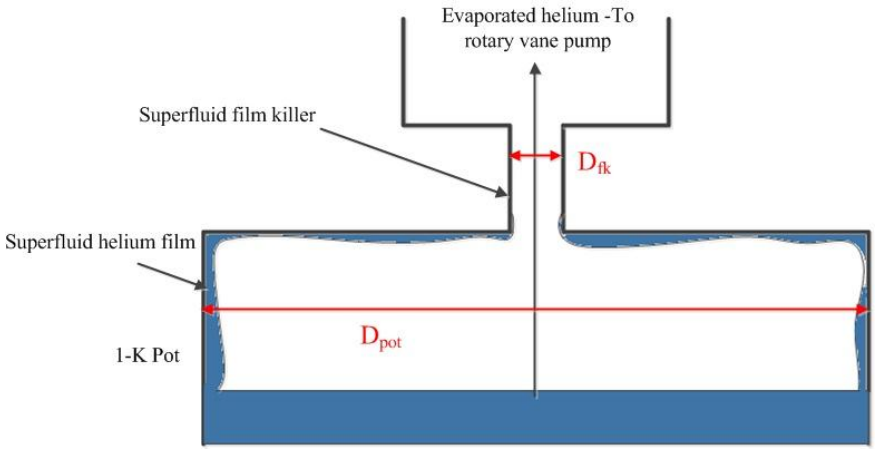

Figure 3-20 Superfluid film killer

Van Sciver (1986) suggests that the film flow in a restriction is directly proportional to the ratio of the smaller to bigger diameter:

$$f_{th,fk} = f_{th,pot}\frac{d_{fk}}{d_{pot}} \tag{3.39}$$

where subscripts *fk* and *pot* refer to the film killer and the 1 K pot respectively. Assuming a 3.17 mm diameter film killer, the film thickness on the film killer's surface is found to be only 1.87 nm or about 5 atomic layers. It is possible to estimate the fraction of film flow in the pot making its way through the superfluid film killer by applying:

$$f_{th,\,fraction} = \left(\frac{\#\ of\ \ atomic\ layers\ in\ \ fk}{\#\ of\ \ atomic\ layers\ in\ \ pot} \right) \frac{d_{fk}}{d_{pot}} \tag{3.40}$$

The fraction is found to be 0.003 or 0.3%. Thus a superfluid film killer with an internal diameter of 3.17 mm will be used for this work. This concludes the modeling of the 1 K facility.

3.9 Summary of the modeling results of the 1 K facility

The cryocooler provides the cooling necessary to precool the incoming helium by exchanging heat with the first stage and second stage heat exchange platforms. Two recuperators are to be integrated with the 1 K facility; a first stage recuperator is necessary to decrease the heat load on the second stage of the cryocooler and a second stage recuperator is incorporated to increase the yield of helium entering the 1 K pot thus increasing the cooling capacity of the 1 K pot compared to a case where no second stage recuperator is integrated. A J-T restrictor in the form of a capillary is used to achieve the final temperature of helium as it enters the 1 K pot. The 1 K pot is designed such that the temperature gradient between the liquid helium in the pot and the pot surface is minimized. The 1 K heat exchange platform is verified to have a high response time to a heat pulse within itself. A superfluid film killer will be integrated in the 1 K facility to decrease the escape of superfluid helium from the 1 K pot. A summary of the modeling results is presented in Table 3-1.

Parameter/component	Modeling result	Description of structure
Power	150 mW	-
Mass flow rate	7×10^{-6} kg/s	-
1st stage HX	30 cm	1/8 inch copper tubing
1st stage recuperator	58 cm	1/16 inch stainless steel tubing
2nd stage HX	73 cm	1/8 inch copper tubing
2nd stage recuperator	20 cm	1/16 inch stainless steel tubing
J-T restrictor (capillary)	Will be determined by empirical relationships in Ch. 4	0.007 inch internal diameter capillary
1 K pot	Area: 158 cm^2	OFHC - cylinder 2 inch ID
1 K HX platform	6 inch x 6 inch	OFHC - thin copper block
Superfluid film killer	Diameter: 3.17 mm	Stainless steel tubing

Table 3-1 Summary of the modeling results for the 1 K facility

3.10 References

Binder, R.C. , Fluid mechanics, Prentice Hall, 1973

Horizon technologies, HePak, Cryodata Inc. , Ver 3.4, 1999

Klein, S.A. , Engineering Equation Solver, F-Chart software, 2011

Nellis, G.F., Klein, S.A., Heat transfer, Cambridge, New York, 2009

Pfotenhauer, J.M., "Design issues for a superfluid helium subcooler", Heat transfer and superconducting magnetic energy storage-ASME, Vol. 211 (1992)

Van Sciver, S.W., Helium cryogenics, Plenum Press, New York, 1986

Wheatley, J.C., DeLong, L.E., Symko, O.G., "Continuously operating ^{4}He evaporation refrigerator", The review of scientific instruments, Vol. 41 (1970) No.1

4 Experimental setup and assembly of the 1 K facility

4.1 A review of the 1 K facility

Each of the components of the 1K facility listed below was discussed in chapter 3.

- First and second stage heat exchangers
- First and second stage recuperators
- A capillary (the J-T restrictor)
- 1 K pot
- 1 K heat exchange platform
- Superfluid film killer
- Pump out line
- Rotary vane pump

The first and second stage heat exchangers are thermally linked to the first and second stage heat exchange platforms, respectively. The first and second stage recuperators are made of 1/16 inch outer diameter stainless steel tubing that is shaped into a coil and inserted in a 1 inch tube (the pump out line). The helium evaporated from the pot flows over the coil. The capillary has an internal diameter of 0.007 inch and a length that is estimated using empirical relationships from the literature. The 1 K pot, with a 2 inch internal diameter and 5 inch length, is made out of OFHC copper. The heat exchanger, a 6 inch by 6 inch thin square block, is made out of OFHC copper. The superfluid film killer is a 1/8 inch diameter restriction installed at the top of the pot. The objective of this chapter is to review the methods and techniques used to fabricate and install each part of the 1 K pot.

4.2 First and second stage heat exchanger construction and assembly

Both heat exchangers, the first and second stage, were modeled based on a 1/8 inch copper tube. Helium flows through this tube and exchanges heat with the heat exchange platforms. The tube must be thermally linked to the corresponding heat exchange platforms. It is undesirable to directly and permanently solder the tubes to the heat exchange platforms because the platforms will be reused for other experiments. Thus, the tubes are first soldered to a thin OFHC copper plate and then the plate and tube subassemblies are bolted to the heat exchange platforms. Indium or thermal grease must be used between the copper plate and the heat exchange platforms in order to reduce thermal contact resistance between the two mating surfaces.

The approach temperature difference in the heat exchangers is decreased by using a longer tube. The goal is to ensure that the helium is precooled and leaves the heat exchanger at a temperature close to the temperature of the first stage heat exchange platform. The model of the first stage heat exchanger showed that the minimum required length of the 1/8 inch copper tube must be 30 cm for the specified conditions. The length of the heat exchangers are chosen such that higher mass flow rates (up to 1 $x10^{-4}$ kg/s) and higher inlet pressures (up to 4 atm) could be handled therefore the predicted tube length is multiplied by a factor of safety of 4. The only disadvantage of using a longer tube instead of a shorter one is the increase in the thermal mass of the system. Higher thermal mass means a longer time to cool the heat exchange platforms from room temperature to the ultimate low temperature upon cryocooler activation. However longer cool down time is not a primary concern for this work therefore the actual length of tube used in the first stage heat exchanger is chosen to be 120 cm.

Figure 4-1 shows an image of the first stage heat exchanger after its assembly. A 1/16 inch thick OFHC copper plate is cut into four arcs. In order to be able to mount these plates, several holes were drilled into the arcs to be matched with the threaded hole pattern on the first stage heat exchange platform. A 50/50 Pb-Sn solder was used to join the 1/8 inch copper tube to each arc shaped plate. The tube was bent upwards between each plate to provide a leeway in the tube in order to make the sub assembly (the tube and the copper plates) flexible so that the holes in the plates could be more easily matched with the threaded hole pattern in the first stage heat exchange platform. Thermal grease, Apiezon-N, is used between the mating surfaces to reduce thermal resistance before bolting down the first stage heat exchanger sub assembly to the first stage heat exchange platform. It should be noted that Indium is preferred to be used to fill gaps between solid contacts at low temperatures however due to the high price of indium Apiezon-N was used as a comparable alternative.

Figure 4-1 An assembled view of the first stage heat exchanger

For the second stage heat exchanger, the model predicted the minimum required length of the 1/8 inch copper tube to be 73 cm. A factor of safety of 4 was used and thus the actual length of tube in the second stage heat exchanger is rounded up to 3 m.

Figure 4-2 shows an assembled view of the second stage heat exchanger. A 1/16 inch thick OFHC copper plate is cut into four rectangles, 6 inch by 2 inch each, with a 1 inch by 1 inch hole grid pattern drilled into the plates in order to be able to match the holes with the threaded hole pattern in the second stage heat exchange platform. A 50/50 Pb-Sn solder was used to join the copper tube to the copper plates and the leeway in the tube between each plate provides flexibility to the tube and plate sub assembly for proper positioning. The sub assembly is then bolted to the second stage heat exchange platform. A thin layer of indium was used between the joints in order to reduce the thermal resistance between the two mating surfaces.

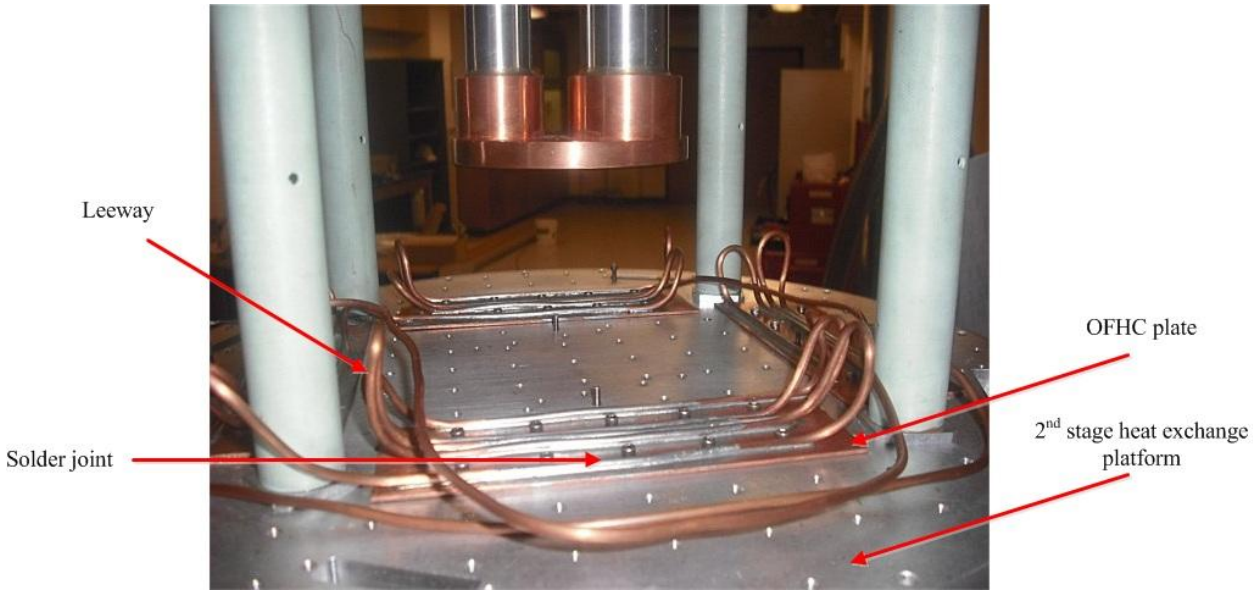

Figure 4-2 An assembled view of the second stage heat exchanger

4.3 First and second stage recuperator construction and assembly

Both recuperators, the first and second stage, were modeled based on a 1/16 inch outer diameter (0.03 inch inner diameter) stainless steel tube. The hot stream of helium flows through these coil shaped tubes and exchanges heat with the vapor helium that flows through the pump out line and over the coil. The pump out line is a 1 inch stainless steel tube that is extended from the pot to the rotary vane pump. The construction and assembly of the first and second stage recuperator is described in this section.

The minimum required length of tube for the first and second stage recuperators were predicted to be 58 and 20 cm respectively. The factor of safety does not need to be as high as the one used for the heat exchangers because there is no interfacial contact resistance between the cold and hot streams (the 1/16 inch stainless steel tube is directly exposed to the hot and cold streams). A factor of safety of 2.5 is used for the recuperators, therefore 147 and 50 cm lengths of tube are used for the first and second stage recuperator respectively.

An assembled view of the first and second stage recuperator is shown in Figure 4-3. The annealed soft stainless steel tube can be shaped into a coil by winding the tube around a solid shaft that is held in place by a lathe. The coil is then inserted into a section of the 1 inch pump out line and the two ends of the 1/16 inch tubes are pulled out from two pre drilled holes on the side of the 1 inch tube wall. The two ends of the coil are affixed to the 1 inch tube by brazing the joints. An example of the brazed joints is also shown in Figure 4-3.

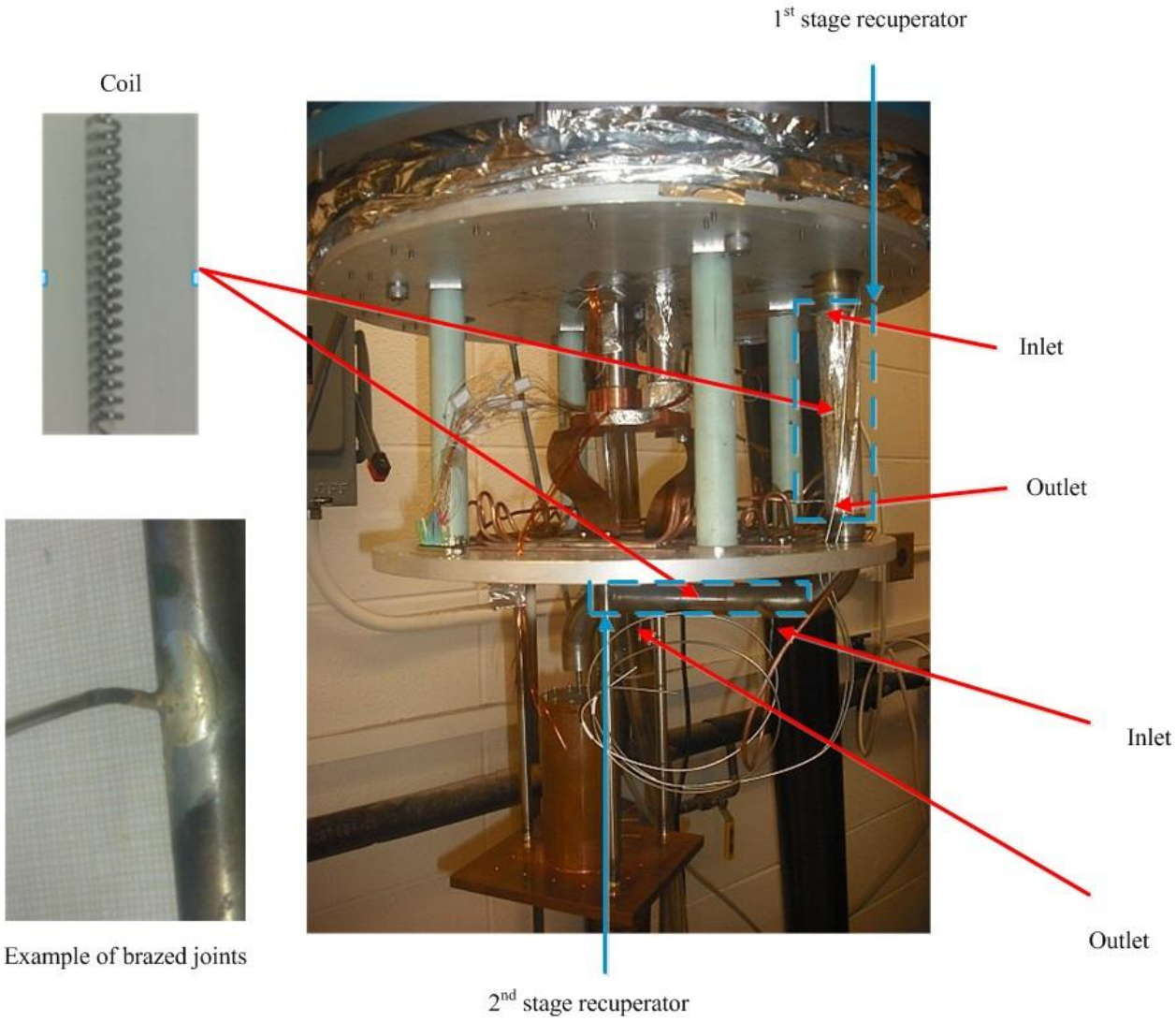

Figure 4-3 An assembled view of the first and second stage recuperators

4.4 Capillary – empirical sizing and installation

The design of the capillary via theoretical methods is not straightforward because of helium's two phase flow through the capillary at low temperatures. Therefore measurements at room temperature and empirical relations found in the literature are used to determine the appropriate size of the capillary: The impedance required for the capillary was found to be 7.103×10^{-9} ($1/cm^3$) in chapter 3. Equation (3.34) is used to find the corresponding required volumetric flow

rate through the capillary with a specified pressure difference across the capillary at room temperature. Hypodermic stainless steel tubing with an internal diameter of 0.007 inch is selected for this work. The objective of this section is to find the required length of the capillary.

Figure 4-4 shows the experimental setup that is used to make the measurements required to size the capillary. A regulator is attached to the helium tank allowing the user to control the pressure of helium exiting the reservoir. A monometer, a "U" shaped tube which is filled by a fluid with a known density (such as water), must be used to precisely measure the relative pressure of the helium before it enters the capillary. Once helium flows through the capillary it will exit into an inverted calibrated cylinder in order to measure the volumetric flow rate of helium through the capillary.

If helium enters one side of the monometer and the other side of the monometer is open to ambient then the relative pressure (pressure difference between the helium going to the capillary and ambient) is found by:

$$\Delta P = \rho g \Delta h \tag{4.1}$$

where ρ is the density of the fluid in the monometer, g is the gravitational acceleration (9.8 m/s^2), and Δh is the height difference between the two columns of fluid. The height difference between the two columns of the monometer is chosen to be 14 inches in order to allow easy and accurate measurement. The information is entered into EES in order to find the required volumetric flow rate through the capillary (corresponding to the impedance found in chapter 3):

```
"!known information"
Z=7.103e9                                   "Impedance corresponding to 150 mW power in 1 K pot"
Z_SI=Z*convert(1/cm^3,1/m^3)                "Impedance in SI Units"
p_atm=1[atm]*convert(atm,Pa)                "Atmospheric pressure"
T_room=298[K]                               "Room temperature"
```

```
"!Calculating volumetric flow rate through the capillary"
Z_SI=1/mu_He*delta_P/V_dot                                  "Wheatley et al. correlation-1970"
mu_He=Viscosity('Helium', T=T_room,p=p_atm)                 "Viscosity of helium"
delta_P=rho_water*g#*delta_h                                "Relative pressure measured by monometer"
    delta_h=14[in]*convert(in,m)                            "Height different in the monometer column"
    rho_water=Density('Water', T=T_room, P=1[atm]*convert(atm,Pa))      "Density of water"
```

The required volumetric flow rate at room temperature is found to be 2.468×10^{-8} m^3/s. The experimental procedure requires determining the appropriate length of the capillary by trial and error; the volumetric flow rate through the capillary found by the experiment must match with the calculated value found by Eq. (3.34). As helium exits the capillary, bubbles will float to the top of the water in the inverted calibrated cylinder. The water level goes down as the bubbles are released at the surface. Thus the volumetric flow rate is experimentally determined by dividing the water column displacement in the calibrated inverted cylinder by the time during the measurement. A lower experimental volumetric flow rate than the one found by the empirical relationship indicates that the tube is too long and vice versa. The required length of capillary for the 1 K facility is found to be 13.5 cm using this method.

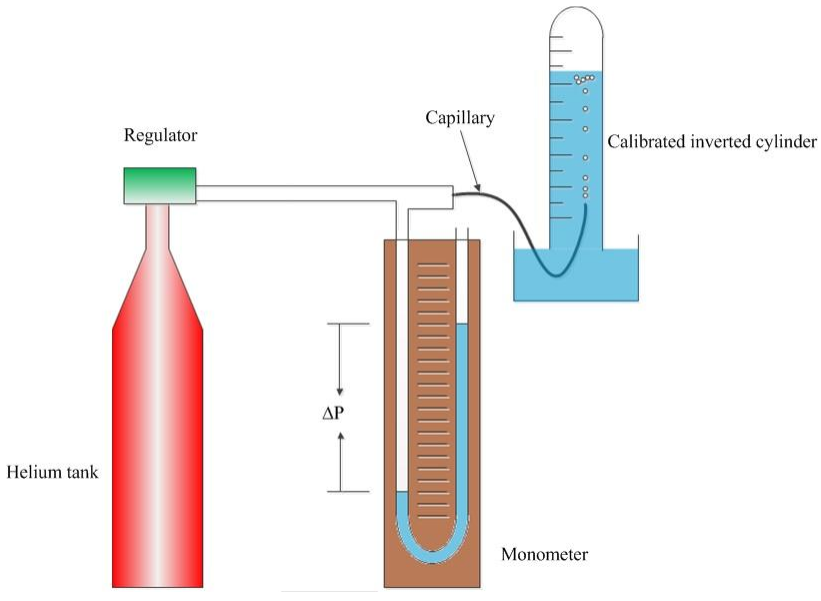

Figure 4-4 Experimental setup used to size the capillary

An adapter must be used in order to connect the capillary to the outlet of the second stage recuperator due to the small size of the capillary. The other end of the capillary must be connected to the pot; a 1/16 inch stainless steel tubing is fed through the lid and soldered in place for this purpose. Thus the same adapter that is used to connect the 1/16 inch tube and the capillary can be used to join the capillary to the feedthrough than runs to the pot. The joint between each part and the adapter is soldered using a 60/40 Sn-Pb solder. Figure 4-5 shows an assembled view of the capillary.

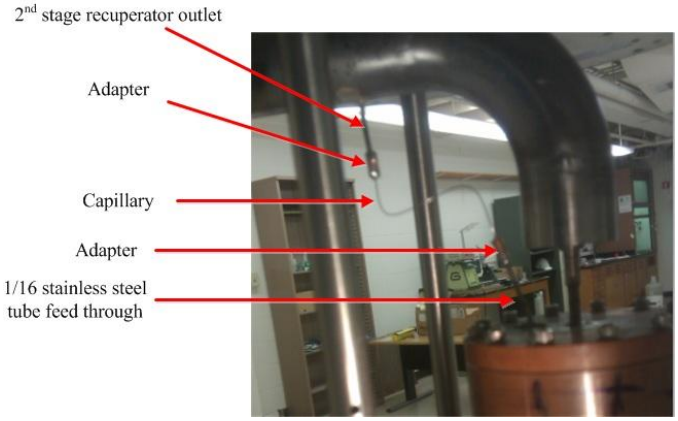

Figure 4-5 An assembled view of the capillary

4.5 1 K pot, 1 K heat exchange platform and stand offs

The 1 K pot is made out of an OFHC copper cylinder. It is 5 inches long, has an internal diameter of 2 inches and the wall thickness is 1/4 inch. The 1 K heat exchange platform is made out of an OFHC copper block, 6 inch by 6 inch with a thickness of 0.375 inch. A 1 inch by 1 inch hole grid pattern of size 4-40 is drilled into the heat exchange platform in order to be able to mount experimental components to the platform. The bottom of the 1 K pot is joined to the surface of the 1 K heat exchange platform by eight uniformly distributed circular pattern bolts. Indium is used between the two mating surfaces in order to reduce interfacial thermal contact

resistance. The 1 K heat exchange platform and the pot are then suspended from the second stage heat exchange platform by three stand offs. The heat transfer between the second stage heat exchange platform and the 1 K heat exchange platform must be minimized. For this reason the stand offs are made out of the thinnest available wall (0.01 inch) stainless steel tube with a 0.375 inch diameter. Figure 4-6 shows an assembled view of the 1 K pot, heat exchange platform and the stand off's.

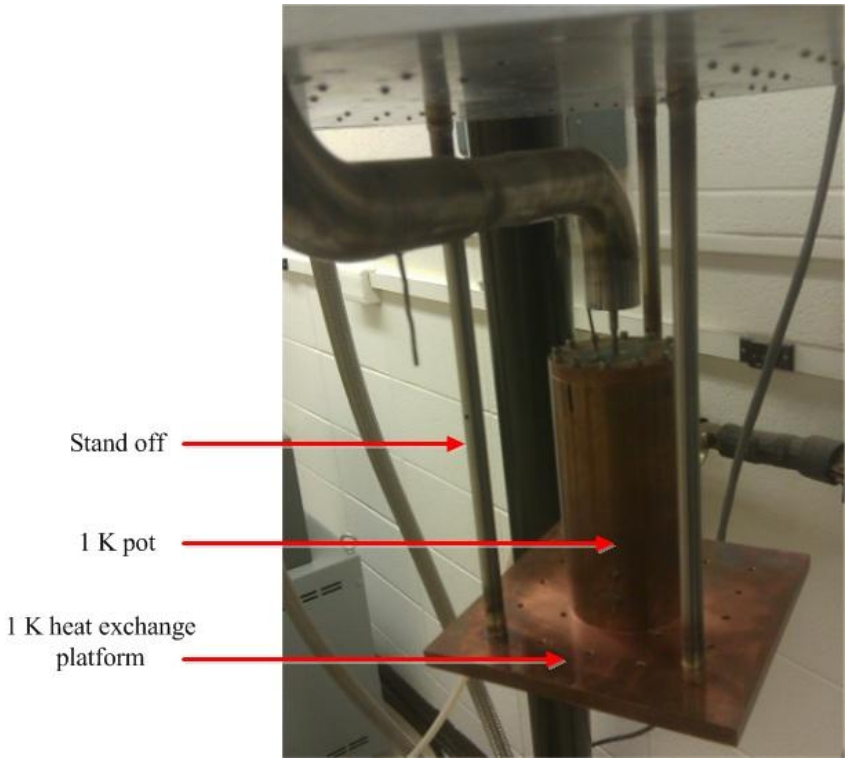

Figure 4-6 1 K pot, heat exchange platform and stand offs

4.6 Sealing the 1 K pot

Superfluid helium can escape from holes as small as 10 nm in diameter; therefore, the 1 K pot must be tightly sealed in order to prevent the escape of superfluid helium. For this reason indium is selected to be used as a sealant between the pot and its lid because indium is a soft metal that can be used to fill gaps between two solid surfaces. Twelve uniformly distributed bolts are used to pinch an indium o-ring between the lid and the pot, as shown in Figure 4-7 . Belleville washers must be used before bolting the lid to the pot because once the bolts are tightened and the assembly is cold the washers will push against the lid in order to keep the joint leak tight and counteract any motion caused by thermal contractions in the materials (Copper contracts more than stainless steel bolts when temperature is decreased).

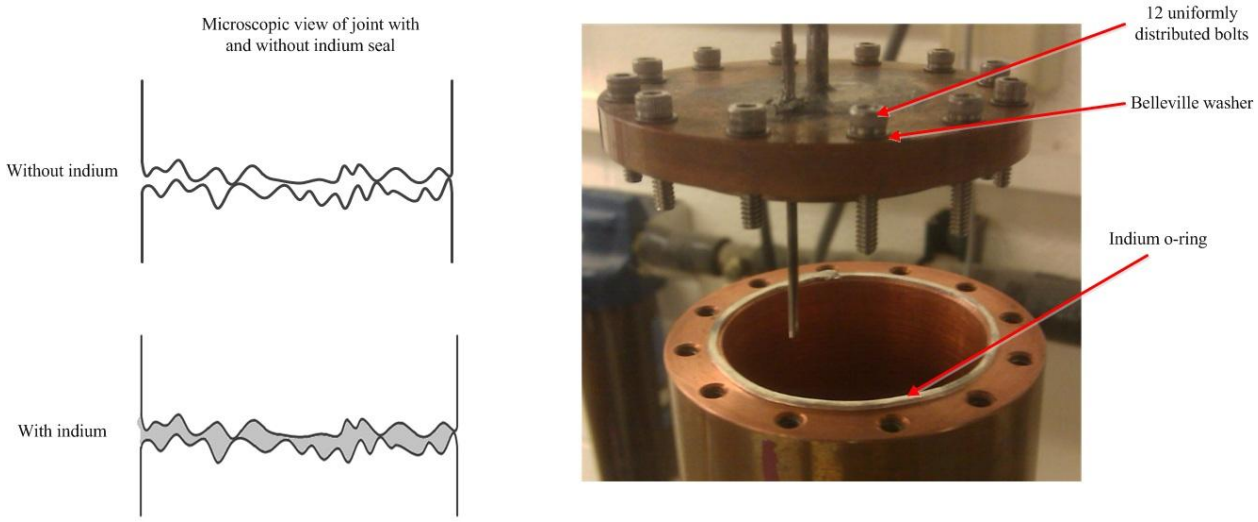

Figure 4-7 A view of indium seal between the lid and the pot

4.7 Superfluid film killer fabrication and installation

According to the Rollin film theory (Van Sciver 1986), superfluid helium can spontaneously climb up the walls and escape from the top of an open container. Thus a superfluid film killer is

incorporated to minimize the escape of superfluid helium from the 1 K pot. The film killer, a 1/8 inch stainless steel tube, is soldered to the lid as shown in Figure 4-8. A stainless steel adapter must be fabricated to join the 1/8 inch tube to the 1 inch pump out line. The 1/8 inch tube is brazed to the bottom of the adapter and the top of the adapter is welded to the pump out line.

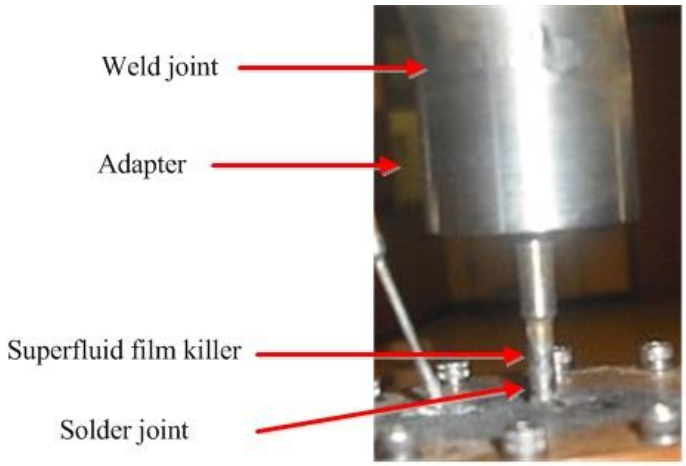

Figure 4-8 Superlfuid film killer

4.8 Sizing the rotary vane pump

Any heat transferred to the 1 K pot will directly evaporate the liquid helium in the pot. In order to maintain the liquid helium at low temperatures, the pressure must be kept at low levels. To do this, a rotary vane pump is used to remove the helium vapor from the pot. The speed of the pump, the volume of gas which the pump can remove in unit time, determines the temperature of liquid helium in the pot. If the pump cannot remove as much helium as it is introduced to the pot then the temperature of liquid helium in the pot will start to rise because the vapor pressure is increasing as shown in Figure 3-1. The pump must be sized correctly in order to ensure proper steady state operation of the 1 K facility. The rotary vane pump used in this work was purchased

during the early stages of the design and therefore this section provides an analysis of this existing pump performance in conjunction with the 1 K pot.

Helium vapor's temperature increases along the pump out line as it moves away from the 1 K pot. When helium vapor reaches the end of the pump out line, its temperature has increased to near room temperature because the low density helium exchanges heat with the section of the pump out line that is exposed to room temperature outside of the Dewar, as shown in Figure 4-9. The helium vapor entering the rotary vane pump will be at or very near room temperature. The volumetric flow rate of helium going to the pump is calculated according to:

$$\dot{V}_{1K} = \frac{\dot{m}_{1K}}{\rho_g} \tag{4.2}$$

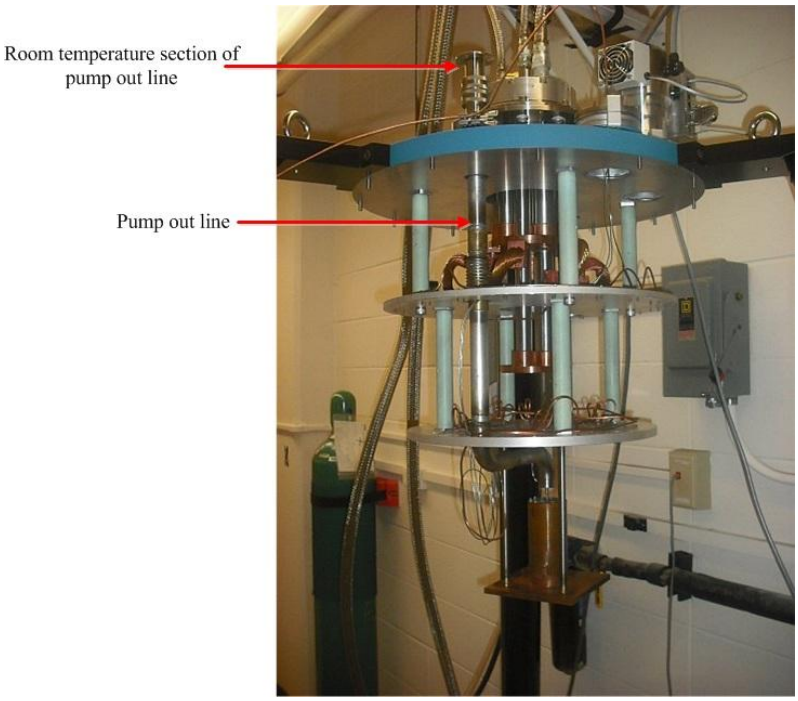

Figure 4-9 Pump out line in respect to the system

The rotary vane pump used in this work is a SogeVac SV-25B. The ultimate pressure (P_u) and maximum speed (S_{max}) of this pump are 50 Pascal and 25 m^3/hr (27.5 m^3/hr for helium)

respectively. The speed of the pump at various pressures can be determined from (O'Hanlon 2003):

$$S = S_{\max}\left(1 - \frac{P_u}{P}\right) \tag{4.3}$$

The speed as a function of pressure is shown in Figure 4-10. Also, the volumetric flow rate of helium vapor traveling to the pump at various pressures is shown for different mass flow rates. The intersection of each line with the pump curve is the pressure that will exist in the 1 K pot for the corresponding mass flow rate. For instance, if the mass flow rate is $1x10^{-6}$ kg/s throughout the 1 K facility, then the pressure in the pot must be at 131 Pascal. According to Figure 3-1, this vapor pressure corresponds to a temperature of 1.27 K for liquid helium in the 1 K pot.

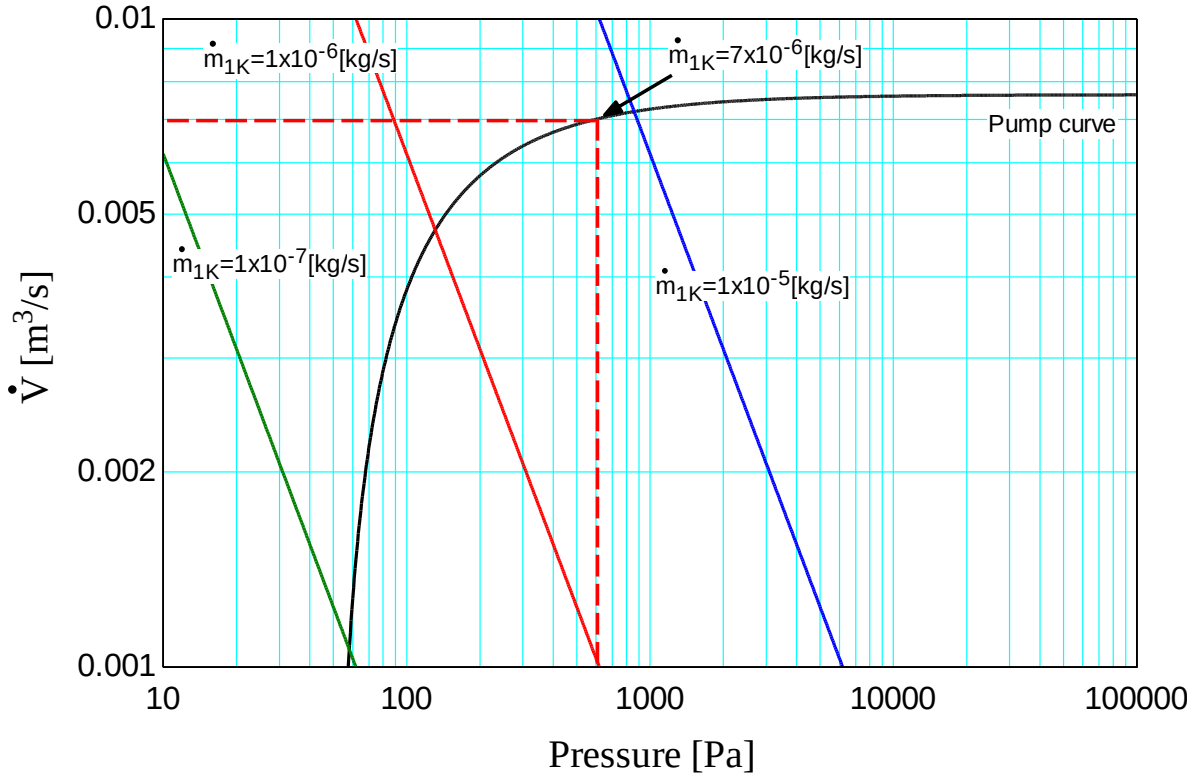

Figure 4-10 Pump speed vs. pressure and helium vapor volumetric flow rate as a function of pressure for various constant mass flow rates through the 1 K facility

4.9 Heat switch

The 1 K pot must be thermally isolated from its surroundings and the heat load on the pot must be minimized in order maximize the cooling power of the 1 K facility; there is no convective heat transfer between the pot and the surroundings because of the vacuum in the Dewar, and conductive heat transfer is minimized by using very thin stainless steel tubes (standoffs) and a thin stainless steel tube at the top of the pot (film killer). The rate of radiation heat transfer is high at higher temperatures and quickly diminishes at lower temperatures. The only disadvantage of the 1 K pot's thermal isolation is now apparent; precooling the 1 K pot assembly from room temperature to low temperatures will take a substantially long time (in the order of months). To address this issue, some type of heat switch must be used to precool the 1 K pot assembly.

A heat switch is a device that allows thermal communication between two objects upon activating the switch and isolates the objects when it is deactivated. One form of heat switch is a heat exchanger (similar to the first and second stage heat exchangers): the heat switch can be turned on by sending fluid through the heat exchanger and turned off by evacuating the heat exchanger. Figure 4-11 shows the schematic of the heat switch used to precool the 1 K pot assembly.

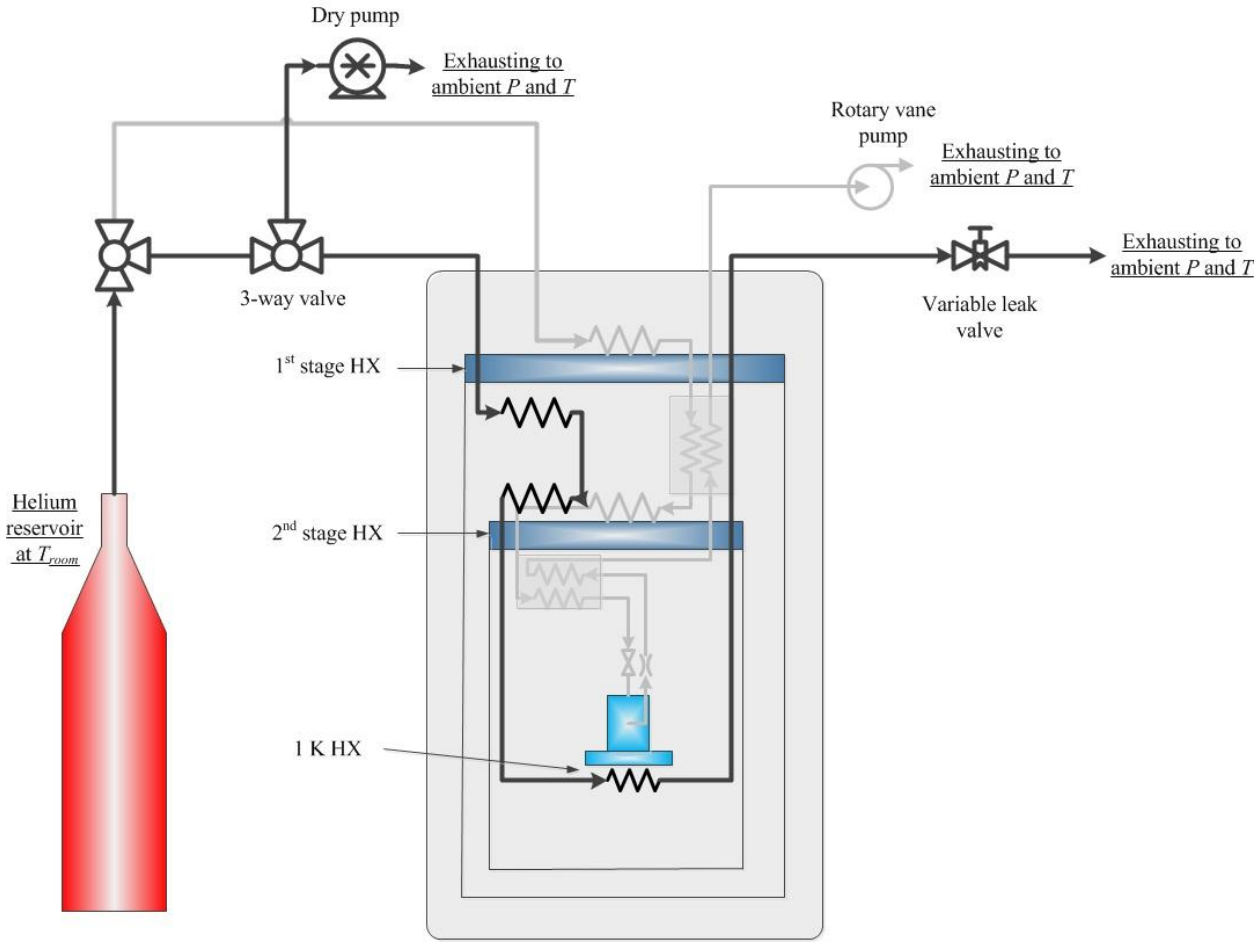

Figure 4-11 Heat switch for the 1 K pot

Helium is is pulled from the helium reservoir at room temperature and atmospheric pressure. After entering the Dewar, helium exchanges heat with the first and second stage heat exchange platforms. These two heat exchangers are identical in design to the first and second stage heat exchangers. After being cooled to the ultimate low temperature (the temperature of the second stage heat exchange platform), helium enters the 1 K heat exchanger (identical to the structure of the first and second stage heat exchangers) thus cooling the 1 K pot assembly by exchanging heat with the 1 K heat exchange platform. Helium is then discharged to the ambient. Two valves are used in the heat switch system: a three way valve before helium enters the Dewar that can be used to either send helium to or evacuate the heat switch line, and a variable leak valve at the

outlet of the heat switch is used to control the mass flow rate of helium through the heat switch system. The objective is to find how long it will take to cool the 1 K pot assembly at a specified mass flow rate and inlet conditions.

Helium enters the 1 K heat exchanger at a temperature that is nearly equal to the second stage heat exchange platform and leaves at nominally the temperature of the 1 K pot assembly. The amount of energy leaving the 1 K pot assembly must be equal to the heat transfer rate between the helium and the 1 K pot assembly:

$$m_{pot\ assembly}\ c(T)\frac{dT}{dt} = \dot{q}_{1K\ HX} = \dot{m}_{heat\ switch}\left(i_{1K\ HX,in} - i_{1K\ HX,out}\right) \tag{4.4}$$

where $\dot{m}_{pot\ assembly}$ is the mass of the 1 K pot and the 1 K heat exchange platform, *c(T)* is the heat capacity of the pot assembly as a function of its temperature, *dT* is the differential temperature difference, *dt* is the differential time difference, and $\dot{m}_{heat\ switch}$ is the mass flow rate of helium in the heat switch system. Eq. (4.4) is separable and can be rearranged to solve for the time required to cool the 1 K pot assembly from initial temperature (T_{ini}) to final temperature (T_{final}):

$$t = \int_{T_{ini}}^{T_{final}} \frac{m_{pot\ assembly}\ c(T)}{\dot{m}_{heat\ switch}\left(i_{1K\ HX,in} - i_{1K\ HX,out}\right)}\ dT \tag{4.5}$$

The mass of the pot assembly is 3.6 kg. The heat capacity of copper as a function of temperature is provided by NIST (2011). The temperature of helium entering the 1 K heat exchanger is 4 K. The time required to cool the 1 K pot assembly from room temperature to 5 K is found in EES:

```
"!Copper heat capacity (NIST 2011)"
Function copper_c(T)
    a=-1.91844
    b=-0.15973
    c=8.61013
```

```
    d=-18.996
    e=21.9661
    f=-12.7328
    g=3.54322
    h=-0.3797
    i=0
    copper_c=10^(a+b*(log10(T))+c*(log10(T)^2)+d*(log10(T)^3)+e*(log10(T)^4)+f*(log10(T)^5)+g*(log10(T)^6)+h*(log10(T)^7)+i*(log10(T)^8))
end

"!Known information"
mass=3.6[kg]                                   "Mass of the pot assembly"
p_HX=1[atm]*convert(atm,Pa)                    "1 K HX presssure"
T_in=4[K]                                      "Inlet temperature"
T_ini=300[K]                                   "Initial temperature of 1 K pot assembly"
T_final=5[K]                                   "Final temperature of 1 K pot assembly"

"!Solving for time"
h_in=Enthalpy('Helium', T=T_in, P=P_HX)        "Inlet enthalpy"
h_out=Enthalpy('Helium', T=T_int, P=P_HX)      "Outlet enthalpy"
time=INTEGRAL(mass*copper_c(T_int)/(m_dot*(h_in-h_out)), T_int, T_ini,T_final)   "Time"
```

The mass flow rate as a function of cooldown time is shown in Figure 4-12. As can be seen from this figure if the mass flow rate of helium in the heat switch is 2×10^{-6} kg/s, it will take the 1 K pot assembly 100 hours to cool from room temperature to 5 K.

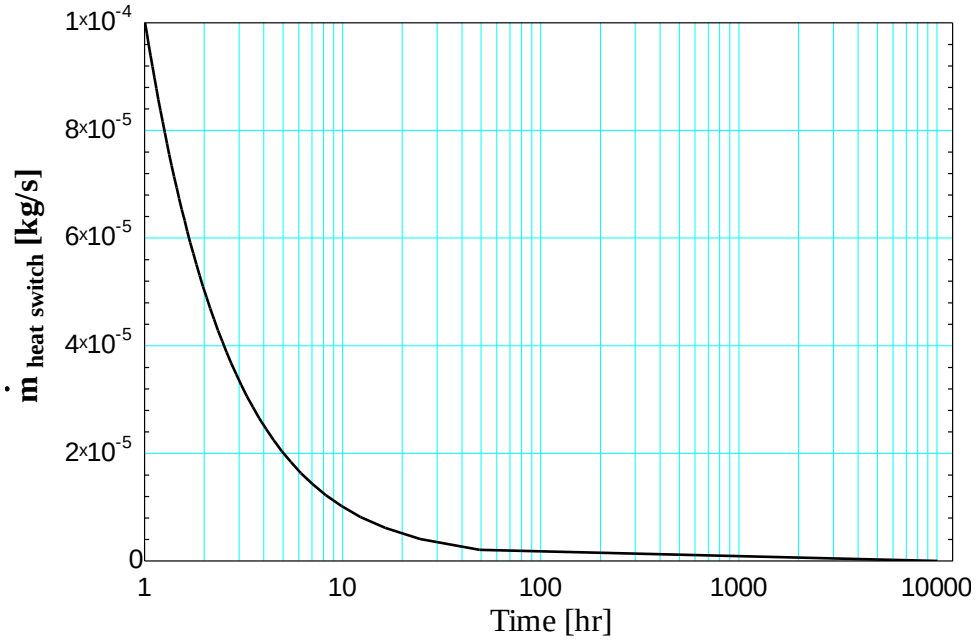

Figure 4-12 Mass flow rate of helium through heat switch as a function of time

4.10 Heat load estimation on the 1 K pot

The design of the 1 K facility was done based on the required cooling power of the 1 K pot. Part of the cooling power provided by the 1 K facility compensates for the heat leaks to the 1 K pot and the rest of the power is used for the SMP experiment. The heat leaks to the 1 K pot are either a result of conductive or radiative heat transfer. Note that there is no convective heat transfer to the 1 K pot due to the vacuum inside the Dewar. The objective of this section is to estimate the amount of heat leak to the 1 K pot system.

The major source of heat leak to the 1 K pot is heat transfers from the top of the pump out line at room temperature. Heat transfer due to radiation from the second stage shield to the 1 K pot is very small (~10's of nW) and can be safely ignored. Figure 4-13 shows a schematic of the 1 K pot and the pump out line. The cross sectional area of the tube used in the pump out line varies. The dimensions of each section of the pump out line are given in Table 4-1.

Section	Internal tube diameter (inch)	Outer tube diameter (inch)	Length (inch)
1	0.96	1	15
2	0.875	1	7
3	1/8	0.135	1

Table 4-1 Dimensions of each section of the pump out line

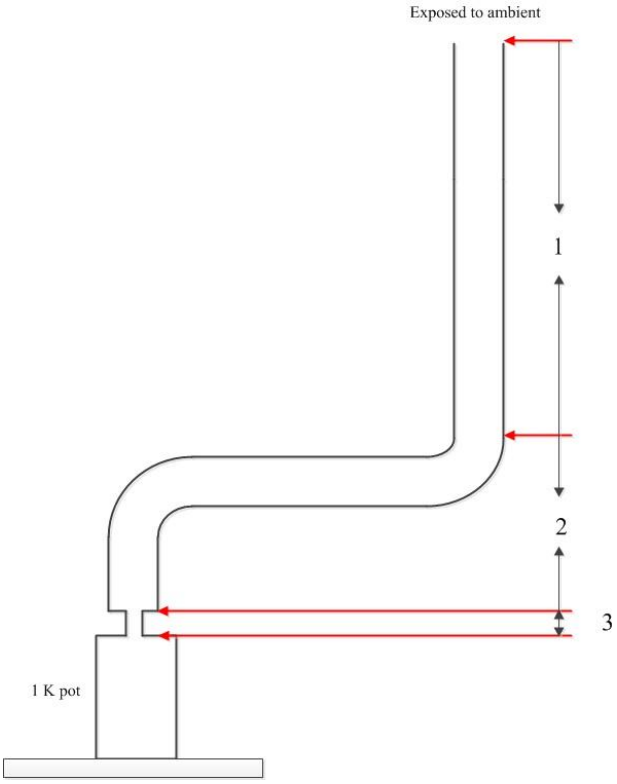

Figure 4-13 Schematic of the pump out line

The dimensions of each section are entered in EES:

```
"!Known information"
L[1]=15[in]*convert(in,m)                    "Length of first section"
L[2]=7[in]*convert(in,m)                     "Length of second section"
L[3]=1[in]*convert(in,m)                     "Length of third section"

D_in[1]=0.96[in]*convert(in,m)               "Inner diameter of first section"
D_in[2]=0.875[in]*convert(in,m)              "Inner diameter of second section"
D_in[3]=0.125[in]*convert(in,m)              "Inner diameter of third section"

D_out[1]=1[in]*convert(in,m)                 "Outer diameter of first section"
D_out[2]=1[in]*convert(in,m)                 "Outer diameter of second section"
D_out[3]=0.135[in]*convert(in,m)             "Outer diameter of third section"
```

The cross sectional area of each section is calculated according to:

$$A_{c,i} = \pi \frac{\left(d_{out}^2 - d_{in}^2\right)}{4} \quad for\ i = 1\ to\ 3 \tag{4.6}$$

```
"Cross sectional area of each section"
Duplicate i=1,3
    A_c[i]=pi#*(D_out[i]^2-D_in[i]^2)/4
```

```
end
```

The temperature at the top most part of the pump out line assembly (T_{room}) and the pot ($T_{1K\ pot}$) are known therefore the total heat transfer rate can be calculated according to:

$$\dot{q}_{leaks\,1K} = \frac{T_{room} - T_{1K\ pot}}{\sum_{i=1}^{3} R_i} = \frac{T_{room} - T_{1K\ pot}}{\sum_{i=1}^{3} \frac{L_i}{k_{ss} A_{c,i}}} \tag{4.7}$$

where R_i is thermal resistance of each section, L_i is the length of each section and k_{ss} is the average integral thermal conductivity of stainless steel between T_{room} and $T_{1K\,pot}$. The heat leak to the 1 K pot is calculated in EES:

```
k=10.23[W/m-K]                    "Average integral thermal conductivity between 300[K] and 1.3[K]"

"Thermal resistance"
Duplicate i=1,3
    R[i]=L[i]/(k*A_c[i])
end

T_room=300[K]                                   "Temperature at top of pump out line"
T_1K_pot=1.3[K]                                 "Temperature of the 1 K pot"
q_dot=(T_room-T_1K_pot)/(SUM(R[i],i=1,3))       "Heat transfer rate - leak to the 1 K pot"
```

The heat leak to the 1 K pot is found to be 100 mW. This heat leak was considered as part of the cooling power needed for the 1 K pot during the early stages of the design. However later during the actual operation of the 1 K pot, two points of the pump out line were thermally linked to the first and second stage heat exchange platforms in order to reduce the amount of heat leak to the 1 K pot.

4.11 Summary of techniques used in the 1 K facility

The heat exchangers, first and second stage, were made by soldering a copper tube to a thin OFHC copper sheet and bolting down this subassembly to the corresponding heat exchange platforms. The first and second stage recuperators were made by shaping a stainless steel tube

into a coil and inserting the coil into a section of the pump out line. Both ends of the coil were brazed to the pump out line tube wall. The capillary was sized based on empirical relationships and was soldered to the outlet of the second stage recuperator and the feed through of the 1 K pot. The 1 K pot and the 1 K heat exchange platform are made out of OFHC copper. The heat leak to the 1 K pot was estimated to be 100 mW.

4.12 References

Marquardt, E.D., Le, J.P., Radebaugh, R. , Cryogenic material properties database, NIST, 2011

Nellis, G.F., Klein, S.A., Heat transfer, Cambridge, New York, 2009

O'Hanlon, J.F. , A user's guide to vacuum technology, John-Wiley, New York, 3 Ed., 2003

Van Sciver, S.W., Helium cryogenics, Plenum Press, New York, 1986

5 Modeling the Superfluid Magnetic Pump (SMP) with no moving parts in support of the sub-Kelvin Pulse tube Superfluid Refrigerator (PSR)

A brief review of the application of the SMP is discussed in the introduction of this chapter. The driving mechanism for the SMP, the magneto-caloric effect, is discussed followed by a qualitative description of the operation of the SMP. A theoretical model of the SMP is presented later in this chapter. The model prediction and outcomes are presented following the theoretical model. The experimental validation of the SMP is not part of this work.

5.1 Introduction to the SMP

A general description of the new PSR proposed by Miller (2008) was presented in chapter 1. As discussed earlier, the new PSR eliminates the only remaining moving parts in the system by replacing the piston bellows assembly with the SMP in the warm end of the system, making this refrigerator completely free of any moving parts as shown in Figure **1-18**. The ultimate purpose of the SMP in the new PSR is to compress and expand ^{3}He solute in an inert background of superfluid ^{4}He in the two refrigerators that operate 180 degrees apart from each other. This research focuses on demonstrating the SMP apart from the refrigeration cycle in order to provide a proof of concept and to validate experimental performance of the SMP against theoretical models. The first prototype of the SMP will be independently tested with pure ^{4}He and not a mixture of ^{3}He-^{4}He because there is no need for using ^{3}He in this proof of concept demonstration. Once proven that the SMP successfully works with pure ^{4}He, it would then be apparent that the SMP will also work with a ^{3}He-^{4}He mixture. In other words, ^{3}He does not affect the performance of the SMP, rather, it affects the whole cycle when integrated in the entire PSR system.

The operation and modeling of the SMP is discussed in detail later in this chapter however it is worth noting the different components of the SMP before delving into the details of the SMP. Figure 5-1 shows a schematic of the SMP used for this work: a cylindrical canister is filled with finely crushed particles of Gadolinium Gallium Garnet (GGG, $Gd_3Ga_5O_{12}$), a paramagnetic salt. A superconducting magnetic coil surrounds this canister. The canister has two ports, an inlet and an outlet, where at one side of the port a vycor glass superleak is installed. During its operation for this work, ^{4}He fills the void volume in the canister and only the superfluid component is allowed to flow back and forth to the canister through the superleak while He II can flow back and forth from the other port. A heat exchanger is used to precool/preheat helium during the operation of the SMP.

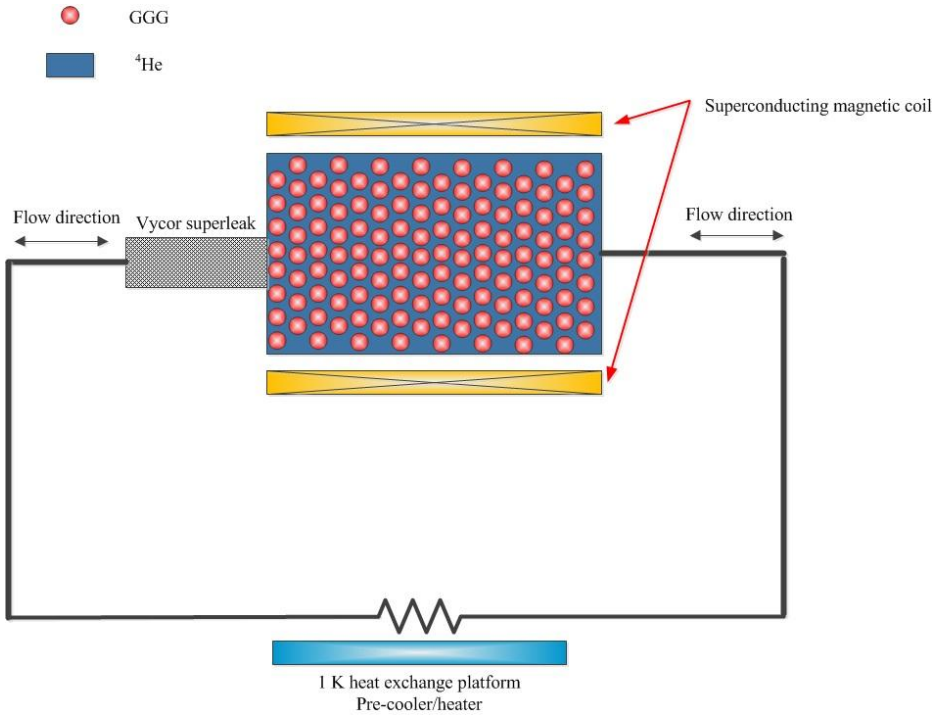

Figure 5-1 A schematic of the SMP used for this work

5.2 Magneto-caloric effect

The magneto-caloric effect or adiabatic temperature change is defined as the heating or cooling of a paramagnetic material due to the application of a magnetic field. The magneto-caloric effect was first discovered by Warburg in 1881. This phenomenon was later explained by Debye and Giauque. They also proposed the first practical application of the magneto-caloric effect: adiabatic magnetization for reaching temperatures lower than that of the boiling point of liquid helium, the lowest achievable temperature at the time.

The magnetic ions in a paramagnetic material can be thought of as springs: work is being done on the ions in a paramagnetic material during the magnetization process, analogous to the work done on a spring in order to compress it. Similarly during the demagnetization process the magnetic ions in a paramagnetic material do work on their surroundings, analogous to a compressed spring that does work once released from the compressed state.

The entropy of a paramagnetic material can be considered as a sum of two contributions: the entropy due to magnetic ordering ($S_{magnetic}$) and the entropy due to the temperature of the material ($S_{thermal}$). Figure 5-2 shows a paramagnetic material under two different conditions. On the left hand side of this figure no external magnetic field is applied on the paramagnetic salt (B=0), thus the magnetic ions are in their natural random orientation. The temperature and total entropy of the subject at state 1 is (T_1) and (S_1) respectively. On the right hand side of the same figure an external magnetic field is applied to the paramagnetic material ($B \neq 0$), thus some of the magnetic ions are aligned to the externally applied magnetic field. The temperature and total entropy of the subject at state 2 is (T_2) and (S_2) respectively. The process between state 1 and state 2 could be either an adiabatic or an isothermal process. Thermodynamics defines entropy as the disorder or

randomness within a system. Entropy is higher for a more disordered system. Thus if the process is adiabatic then the magnetic component of entropy must have decreased at state 2 compared to state 1. In order to preserve the total entropy of the system, the thermal component of entropy must have increased the same amount that the magnetic entropy has decreased. This implies that the temperature of the paramagnetic material at state 2 must be higher than state 1 during an adiabatic process. However the situation is different for an isothermal process: During an isothermal process the magnetic component of entropy decreases but the thermal component of entropy remains the same. This means that the total entropy of the paramagnetic salt must have decreased from state 2 compared to state 1.

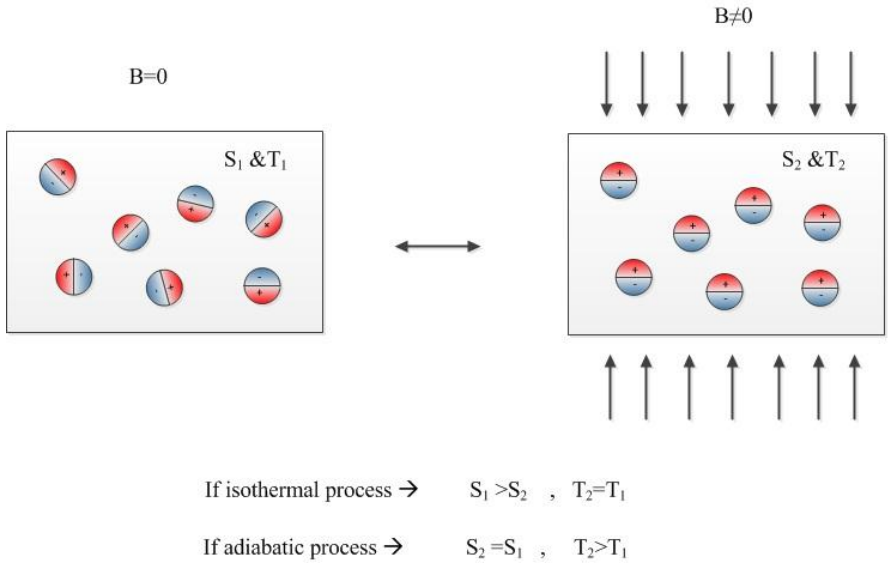

Figure 5-2 A paramagnetic material under two conditions: with applied magnetic field and without magnetic field

The equivalence of this statement to the thermodynamics of an ideal gas is evident: An adiabatic magnetization of a paramagnetic material is analogous to an adiabatic compression of an ideal gas: the pressure increases and because the process is adiabatic the temperature must increase. An isothermal magnetization of a paramagnetic material is analogous to the isothermal

compression of an ideal gas: the pressure is increased and heat must be removed to keep the temperature constant thus the entropy must decrease.

A general equation of state for all paramagnetic salts at low temperatures is expressed by Lounasmaa (1974). Just like any other paramagnetic material GGG's entropy consists of a magnetic and a thermal component. The specific entropy of GGG (J/kg-K) as a function of temperature (T) and externally applied magnetic field (B) is:

$$s(T,B) = \frac{R}{MW_{GGG}} \left[\frac{x}{2J} \coth\left(\frac{x}{2J}\right) - \frac{(2J+1)x}{2J} \coth\left(\frac{(2J+1)x}{2J}\right) + \ln\left(\frac{\sinh\left(\frac{(2J+1)x}{2J}\right)}{\sinh\left(\frac{x}{2J}\right)} \right) \right] \quad (5.1)$$

where R is the gas constant (8.314 J/K-mol), J is a constant (7/2 for GGG), MW_{GGG} is the molar mass of GGG (1.01235 kg/mol), and x is defined as:

$$x = \frac{\beta J g}{k T} \sqrt{b^2 + B^2} \quad (5.2)$$

where β is the Bohr magneton constant (9.274×10^{-24} J/Tesla), g is a constant (2 for GGG), k is the Boltzmann's constant (1.381×10^{-23} J/K), b is the intrinsic internal magnetic field (0.481 Tesla for GGG). Figure 5-3 shows a plot of specific entropy of GGG as a function of temperature at various constant externally applied magnetic fields.

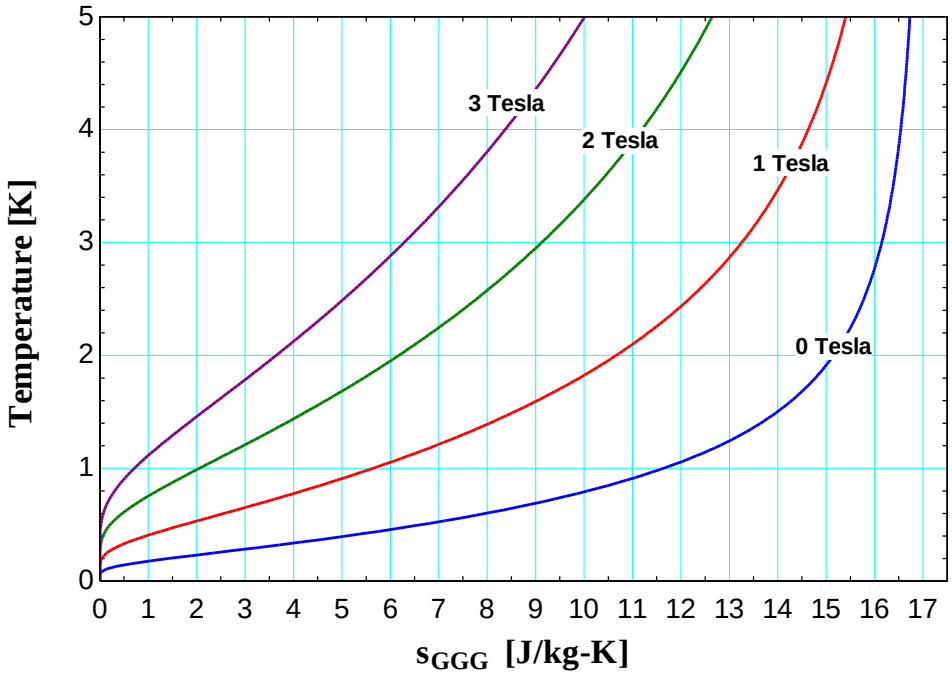

Figure 5-3 Specific entropy of GGG as a function of temperature at various constant external applied magnetic fields

For example, as can be seen from Figure 5-3, the entropy of GGG at 1 K and in the absence of any externally applied magnetic field is 11.65 J/kg-K. If an external magnetic field of 2 Tesla is applied to the GGG during an adiabatic process, then the temperature of the GGG must be at 4.278 K. Therefore the adiabatic temperature change of GGG during this adiabatic magnetization is 3.278 K. Thus the magnetization of GGG has resulted in increasing its temperature during an adiabatic process which matches with the prediction made earlier in this section.

5.3 Qualitative description of the operation of the SMP during one cycle

The objective of this section is to familiarize the reader with the general operation of the SMP during one cycle. The cycle consists of four processes that are analogous to the processes in a piston cylinder system that contains ideal gas as listed in Table 5-1. Note that the liquid helium in the SMP always operates at temperatures lower than the lambda point.

Process	processes for the SMP	processes for the ideal gas system (analogy)
1	Adiabatic magnetization	Adiabatic compression
2	Isothermal magnetization	Isothermal compression
3	Adiabatic demagnetization	Adiabatic expansion
4	Isothermal demagnetization	Isothermal expansion

Table 5-1 Processes involved in the SMP and its analogy to the ideal gas system

Process 1-Adiabatic magnetization

The top portion of Figure 5-4 shows process 1, the adiabatic magnetization, during the operation of the SMP. The constituents of the SMP, the crushed GGG particles and the helium surrounding them, are at (T_{low}) and (B_{low}=0 Tesla) at the beginning of this process. The two fictitious valves shown at each side of the SMP are meant to aid the reader with the visualization of the helium flow to and from the canister. These two valves are "closed" during this process. The real scenario will be discussed at the end of this section. During process 1, no heat is transferred to and from the canister therefore the constituents of the SMP are undergoing an adiabatic process. Electric current is sent through the superconducting magnetic coil, thus increasing the externally applied magnetic field on the canister. By increasing the field, the temperature of the crushed GGG particles must increase during this adiabatic process. Heat transfer between the GGG particles and the surrounding helium causes the helium temperature to rise along with the GGG. The magnetic field is increased until the SMP's constituents reach a new temperature (T_{high}). The magnetic field has increased to an intermediate value at (B_{int1}) by the end of this process. This process is analogous to an ideal gas being compressed during an adiabatic process as shown at the bottom portion of Figure 5-4.

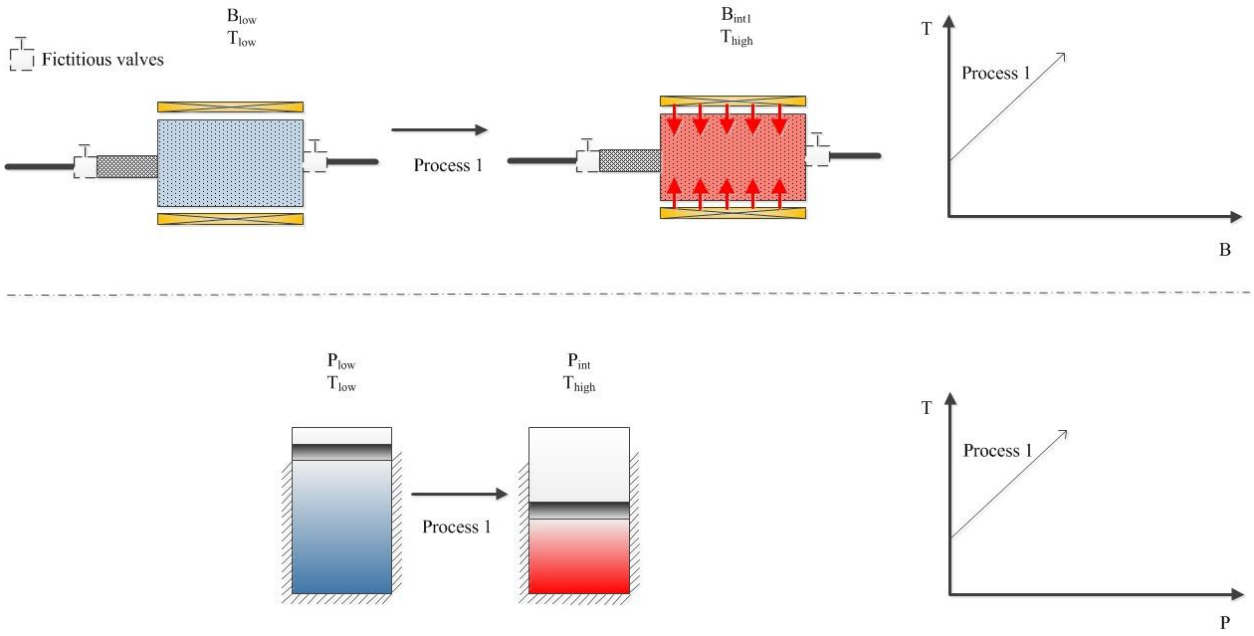

Figure 5-4 Adiabatic magnetization of the SMP analogous to adiabatic compression of an ideal gas

Process 2-Isothermal magnetization

The SMP's constituents are at (T_{high}) and (B_{int1}) at the beginning of the isothermal magnetization process and the two fictitious valves are open. As shown in the top portion of Figure 5-5, the electric current through the superconducting magnetic coil is increased, further increasing the externally applied magnetic field on the canister until it reaches (B_{high}). The additional magnetic field continues to heat the GGG particles. This heat is transferred from the GGG particles to the surrounding helium. Energy is conserved for the helium within canister therefore in order to keep this an isothermal process the additional energy in the helium within the canister must be equal to the net amount of energy (enthalpy) flowing out.. The normal component of helium carries energy out of the canister and only superfluid helium with less energy enters the canister through the vycor glass superleak and replenishes the helium that has left the canister (Note that according to Figure 1-6, below the lambda point the fraction of normal component helium increases as temperature is increased and the fraction of superfluid increases as temperature is

decreased). During this process the 1 K heat exchange platform exchanges heat with the helium inside the closed SMP loop once it exits the canister. Note that the temperature of the 1 K heat exchange platform must be between (T_{high}) and (T_{low}). Process 2 is analogous to the isothermal compression of an ideal gas as shown at the bottom portion of Figure 5-5.

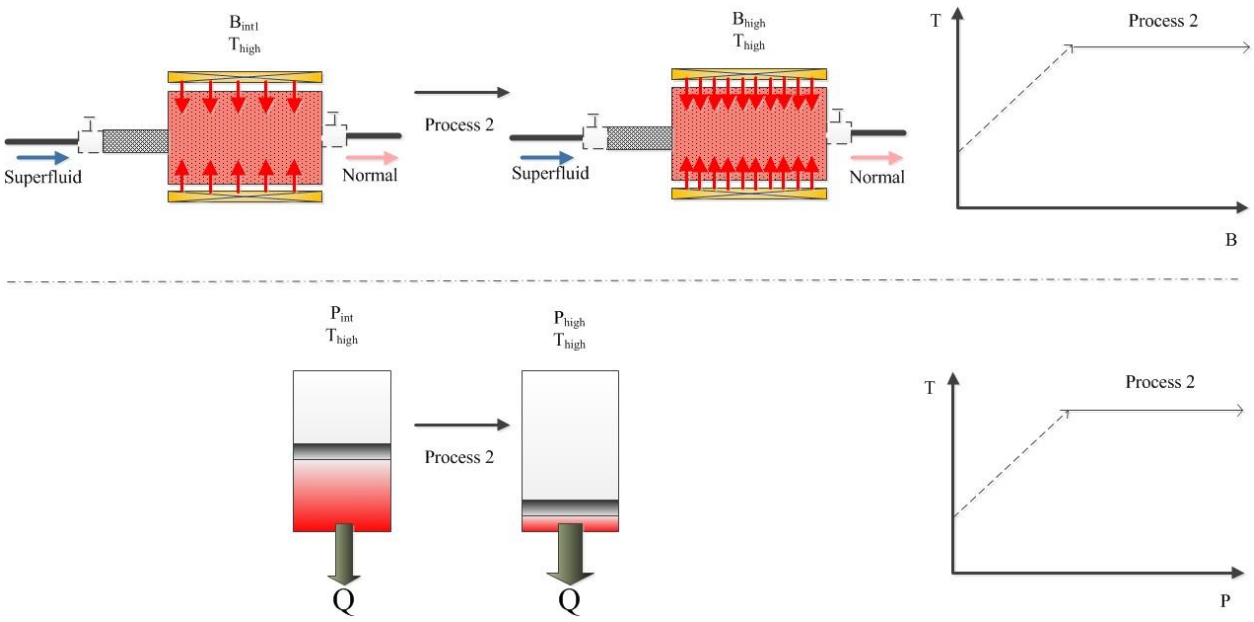

Figure 5-5 Isothermal magnetization of the SMP analogous to isothermal compression of an ideal gas

Process 3-Adiabatic demagnetization

At the beginning of this process the temperature of the SMP's constituents is (T_{high}) and the externally applied magnetic field is (B_{high}). The two fictitious valves are "closed" during the adiabatic demagnetization process. As shown in the top portion of Figure 5-6, the electric current is decreased through the superconducting magnetic coil thus the externally applied magnetic field on the canister is decreased. No heat transfer occurs between the SMP's constituents and its surroundings, therefore the process is adiabatic. By decreasing the magnetic field, the temperature of the GGG decreases. Heat transfer between the GGG and the surrounding helium

causes the helium temperature to fall. The magnetic field is decreased until the temperature of the SMP's constituents' returns to (T_{low}). The magnetic field has decreased to a second intermediate value (B_{int2}) by the end of this process. This process is analogous to the adiabatic expansion of an ideal gas as shown at the bottom portion of Figure 5-6.

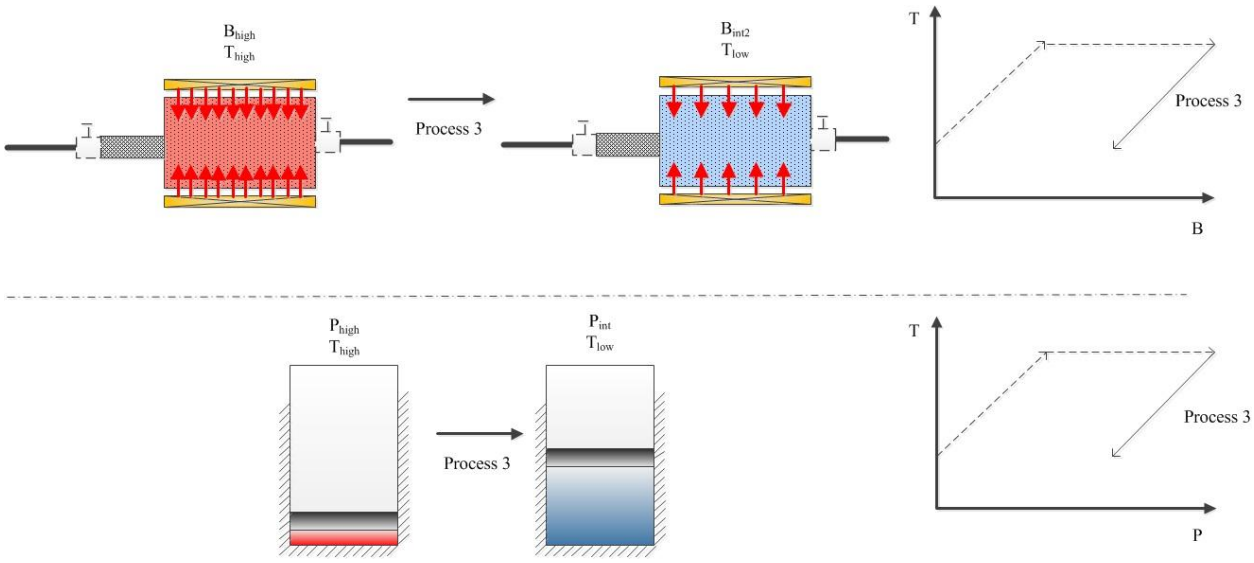

Figure 5-6 Adiabatic demagnetization on the SMP analogous to the adiabatic expansion of an ideal gas

Process 4-Isothermal demagnetization

The SMP's constituents are at (T_{low}) and (B_{int2}) at the beginning of the isothermal demagnetization process and the two fictitious valves are open. As shown in the top portion of Figure 5-7, the electric current through the superconducting magnetic coil is decreased, further decreasing the externally applied magnetic field on the canister until it returns to (B_{low}=0). By decreasing the externally applied magnetic field the GGG particles continue to cool throughout this process. Therefore heat is transferred from the helium to the GGG. During this isothermal process energy is conserved for the helium within the canister. Therefore the amount of energy reduction in the helium within the canister must be equal to the net energy flowing in. The normal component of helium carries energy into the canister and only superfluid helium with less

energy flows out through the vycor glass superleak. The 1 K heat exchange platform exchanges heat with superfluid helium exiting the canister. Note that during this process the 1 K heat exchange platform is preheating the helium that leaves the canister. This process is analogous to the isothermal expansion of an ideal gas as shown in the bottom portion of Figure 5-7. This concludes the qualitative description of the four processes during a one cycle operation of the SMP.

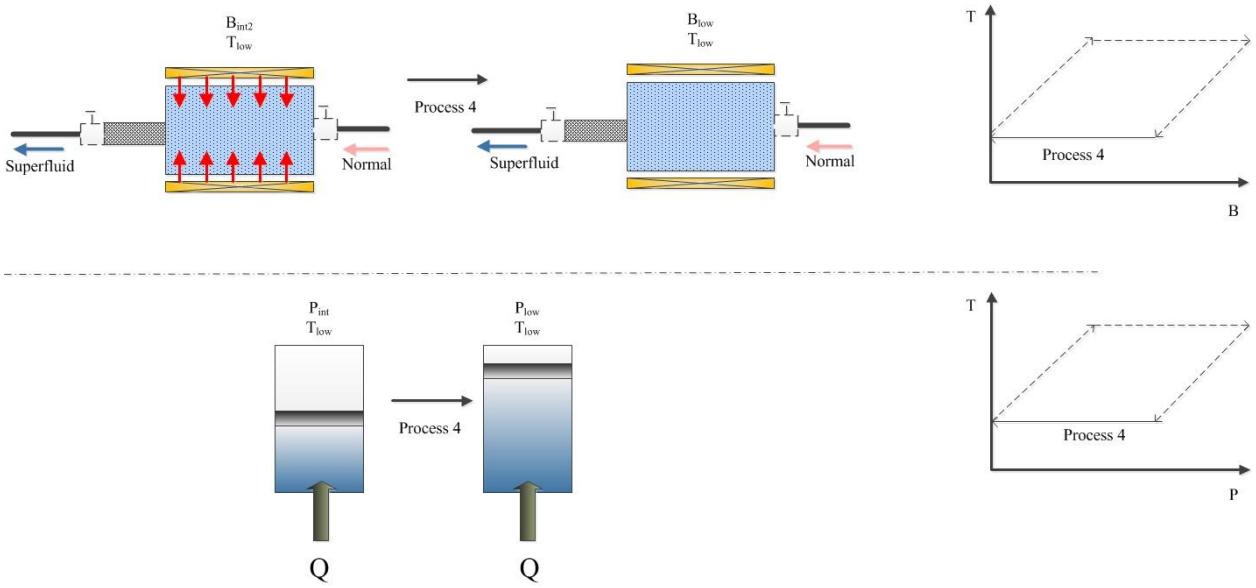

Figure 5-7 Isothermal demagnetization of the SMP analogous to the isothermal expansion of an ideal gas

Two fictitious valves were assumed throughout the qualitative explanation of the SMP's operation. These valves were used to help visualize the helium flow into and out of the canister during the isothermal magnetization and demagnetization. Actually, helium starts flowing out of the canister the moment an external magnetic field is applied to the canister. However the time spent during the adiabatic magnetization process is significantly shorter than the isothermal magnetization process. Thus for simplicity the minimal amount of helium flowing out of the canister during the adiabatic magnetization is ignored. The same approach is used to justify

ignoring the helium flowing in to the canister during the adiabatic demagnetization process. Figure 5-8 shows a qualitative plot of the externally applied magnetic field as a function of time for one cycle operation of the SMP. The next section goes through the theoretical modeling of the SMP.

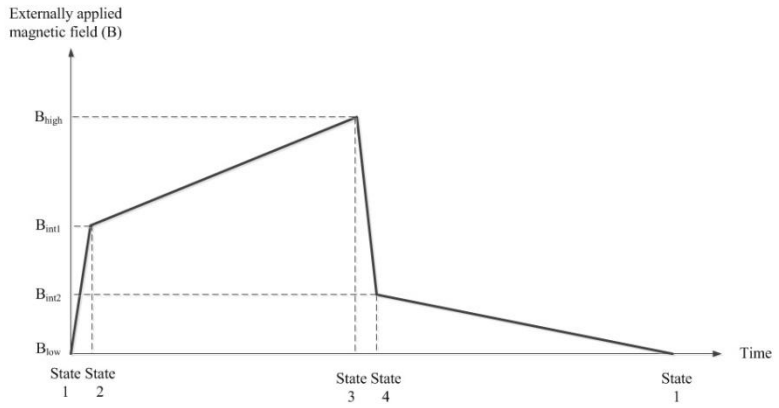

Figure 5-8 Qualitative plot of externally applied magnetic field as a function of time during one cycle operation of the SMP

5.4 Modeling of the SMP

The objectives of the SMP model are: to predict the mass flow rate of helium in and out of the canister during one cycle operation of the SMP and to predict the required temperature of the 1 K heat exchange platform (pre-cooler/heater). In order to provide more clarity, the thermodynamic system for each part of the model is defined and the modeling of each process is divided into two parts when applicable: an entropy balance leads to determining the value of the two intermediate magnetic fields and an energy balance leads to finding the flow conditions and the pre-cooler/heater's temperature.

The diameter ($d_{canister}$) of the cylindrical canister is 4.5 cm and its height ($h_{canister}$) is 7.5cm. The total volume of the canister is calculated according to:

$$V_{canister} = \frac{\pi \, d_{canister}^2}{4} \; h_{canister} \tag{5.3}$$

```
"!SMP dimensions"
V_canister=pi#*d_canister^2*h_canister/4        "Volume of the SMP canister"
d_canister=4.5[cm]*convert(cm,m)                "Radius of the SMP canister"
h_canister=7.5[cm]*convert(cm,m)                "Height of the SMP canister"
```

The canister is filled with crushed GGG particles. The porosity (the void volume) of the canister has not been measured but it is estimated to be 0.38 or 38% (Miller 2009). The density of GGG (ρ_{GGG}) is 7080 kg/m^3 (Perry 1995). The mass of the GGG in the canister is calculated according to:

$$m_{GGG} = V_{canister} \; \rho_{GGG} \left(1 - porosity\right) \tag{5.4}$$

Liquid helium is assumed to be incompressible (its density does not change significantly over a low temperature span). Since liquid helium's temperature in the SMP varies between 1.5 K and 1.9 K the density of liquid helium is determined at an average temperature of 1.7 K. The density of liquid helium (ρ_{He}) at this temperature is 147.11 kg/m^3. Thus the mass of liquid helium in the canister at any point of time during the cycle is:

$$m_{He} = \rho_{He} \, V_{canister} \; porosity \tag{5.5}$$

```
"!Calculating mass of helium and GGG in the canister"
Porosity=0.38                                   "Porosity - estimated"
m_GGG=rho_GGG*V_canister*(1-porosity)           "Calculating mass of GGG in canister"
    rho_GGG=7.08[g/cm^3]*convert(g/cm^3,kg/m^3) "Density of GGG"
m_He=rho_He*V_canister*porosity                 "Calculating mass of helium in
canister"
rho_He=147.11[kg/m^3]"Density of helium"
```

The minimum and maximum values for the externally applied magnetic field on the canister are constrained to 0 and 2 Tesla respectively. The minimum and maximum temperature of the constituents of the SMP during the cycle is constrained to 1.5 and 1.9 K respectively.

```
"!Constrained thermodynamic states"
B_min=0[Tesla]                    "Minimum applied magnetic field"
B_max=2[Tesla]                    "Maximum applied magnetic field"
T_low=1.5[K]                      "Minimum temperature of SMP constituents"
T_high=1.9[K]                     "Maximum temperature of SMP constituents"
```

The thermodynamic state functions (entropy and enthalpy) of helium must be defined in order to be able to carry the energy and entropy balance through the model. For temperatures between 0.5 K and the lambda point, Miller (2001) suggests the following equation for the specific entropy:

$$s_{He} = \frac{1}{MW_{He}}\left[4\,B\,T^3 + A\left(\frac{\Delta_1}{T}+\frac{3}{2}\right)\sqrt{T}\,\exp\left(-\frac{\Delta_1}{T}\right)+C\,\frac{\Delta_2}{T^2}\exp\left(-\frac{\Delta_2}{T}\right)\right] \tag{5.6}$$

where T is the temperature of helium, MW_{He} is the molar mass of helium (kg/mol), A is 23.2 (J/mol-K$^{1.5}$), B is 0.00675 (J/mol-K^4), C is 500 (J/mol), Δ_1 and Δ_2 are 8.65 and 15.7 K respectively. The specific internal energy is given by:

$$u_{He} = \frac{1}{MW_{He}}\left[3\,B\,T^4 + A\left(\frac{\Delta_1}{T}+\frac{1}{2}\right)T^{3/2}\,\exp\left(-\frac{\Delta_1}{T}\right)+C\left(\frac{\Delta_2}{T}-1\right)\exp\left(-\frac{\Delta_2}{T}\right)\right] \tag{5.7}$$

and the specific enthalpy of helium is:

$$i_{He} = u_{He} + P\,v \tag{5.8}$$

where P is pressure (Pa), and v is the specific volume (m^3/kg). Eq's. (5.1), (5.6), (5.7), and (5.8) are programmed in EES:

```
"!Specific entropy of GGG (Lounasmaa 1974)"
Function S_GGG(T,B)
```

```
    B_int:=0.481[Tesla]                                   "Internal magnetic field"
    J:=7/2                                                "constant"
    beta:=9.274e-24[J/Tesla]                              "Bohr Magneton constant"
    g:=2[-]                                               "Lande-g factor"
    BB:=sqrt(B_int^2+B^2)                                 "B resultant"
    k:=1.381e-23[J/K]                                     "Boltzmann's constant"
    X=beta*g*J*BB/(k*T)                                   "Magnetic susceptibility"
    S_GGG=R*(x/(2*J)*(COSH(x/(2*J))/SINH(x/(2*J)))-
(2*J+1)*x/(2*J)*(COSH((2*J+1)*x/(2*J))/SINH((2*J+1)*x/(2*J)))+LN(SINH((2*J+1)*x/(2*J))/SINH(x/(2*J))))
"Specific entropy"
        MW_GGG=1.01235[kg/mol]                            "Molar mass of GGG"
        R=R#/MW_GGG                                       "Specific gas constant for GGG"
END


"!Specific entropy for Helium (Miller, Brisson 2001)"
Function S_He(T)
    MW_He4=MolarMass(Helium)                              "MW of helium"
    A=23.2[J/mol-K^1.5]                                   "Coefficient"
    B=6.75e-3[J/mol-K^4]                                  "Coefficient"
    C=500[J/mol]                                          "Coefficient"
    d1=8.65[K]                                            "Constant"
    d2=15.7[K]                                            "Constant"
    S_He=(4*B*T^3+A*(d1/T+3/2)*sqrt(T)*exp(-d1/T)+C*(d2/T^2)*exp(-d2/T))/(MW_He4*convert(g,kg))
"Specific entropy"
END

"!Specific internal energy for helium (Miller, Brisson 2001)"
Function u_He(T)
    MW_He4=MolarMass(Helium)                              "MW of helium"
    A=23.2[J/mol-K^1.5]                                   "Coefficient"
    B=6.75e-3[J/mol-K^4]                                  "Coefficient"
    C=500[J/mol]                                          "Coefficient"
    d1=8.65[K]                                            "Constant"
    d2=15.7[K]                                            "Constant"
    u_HE=(3*B*T^4+A*(d1/T+1/2)*(T^(3/2))*exp(-d1/T)+C*(d2/T-1)*exp(-d2/T))/(MW_He4*convert(g,kg))
"Specific int. energy"
end

"!Specific enthalpy for Helium (Miller, Brisson 2001)"
Function i_He(T)
    nu=1/147.11[kg/m^3]                                   "Specific volume of He"
    P=101325[Pa]                                          "Pressure inside the SMP loop"
    i_He=u_He(T)+P*nu                                     "Specific enthalpy"
END
```

Process 1- Adiabatic magnetization

The constituents of the canister, the GGG, and the helium surrounding it are at state 1 at the beginning of this process. The temperature of state 1 is (T_{low}) and the applied magnetic field is (B_{min}). The magnetization begins and continues until the constituents of the canister reach (T_{high}) at state 2. The thermodynamic states for this process are listed in Table 5-2.

Thermodynamic state	B (Tesla)	T (K)
1	0	1.5
2	To be determined	1.9

Table 5-2 Thermodynamic states 1 and 2

- Entropy balance for process 1:

The thermodynamic system for this part is the constituents of the canister. The applied external magnetic field at state 2 is unknown and must be found though applying an entropy balance on the constituents of the canister. There is no heat transfer to and from the canister with the surroundings therefore the process is adiabatic. During process 1, the entropy of the helium in the canister changes according to:

$$\Delta S_{He,1-2} = m_{He}\left(s_{He}\left(T_2\right) - s_{He}\left(T_1\right)\right) \tag{5.9}$$

The entropy of GGG during this process changes according to:

$$\Delta S_{GGG,1-2} = m_{GGG}\left(s_{GGG}\left(T_2, B_2\right) - s_{GGG}\left(T_1, B_1\right)\right) \tag{5.10}$$

Assuming a reversible process, an entropy balance during this adiabatic process yields:

$$\Delta S_{GGG,1-2} + \Delta S_{He,1-2} = 0 \tag{5.11}$$

```
"!Adiabatic magnetization"
"Entropy balance"
T[1]=T_low                                   "Temperature at state 1"
```

```
B[1]=B_min                                          "Applied magnetic field at state 1"
T[2]=T_high                                         "Temperature at state 2"
DS_He_12=m_He*(S_He(T[2])-S_He(T[1]))               "Entropy change of helium during
process 1"
DS_GGG_12=m_GGG*(S_GGG(T[2],B[2])-S_GGG(T[1],B[1])) "Entropy change of GGG during
process 1"
DS_He_12+DS_GGG_12=0                                "Entropy balance for process 1"
```

➢ Energy balance for process 1:

The thermodynamic system for this part is the helium within the canister as shown in Figure 5-9. The heat transfer from the GGG must be equal to the heat transfer into the surrounding helium within the canister therefore the heat transfer to the helium during process 1 is:

$$Q_{1-2,He} = m_{He}\left(u_{He}\left(T_2\right) - u_{He}\left(T_1\right)\right) = -Q_{1-2,GGG} \tag{5.12}$$

```
"Energy balance"
Q_12_He=m_He*(u_He(T[2])-u_He(T[1]))   "Heat transfer to the helium"
Q_12_He=-Q_12_GGG                      "Heat transfer  to the GGG"
```

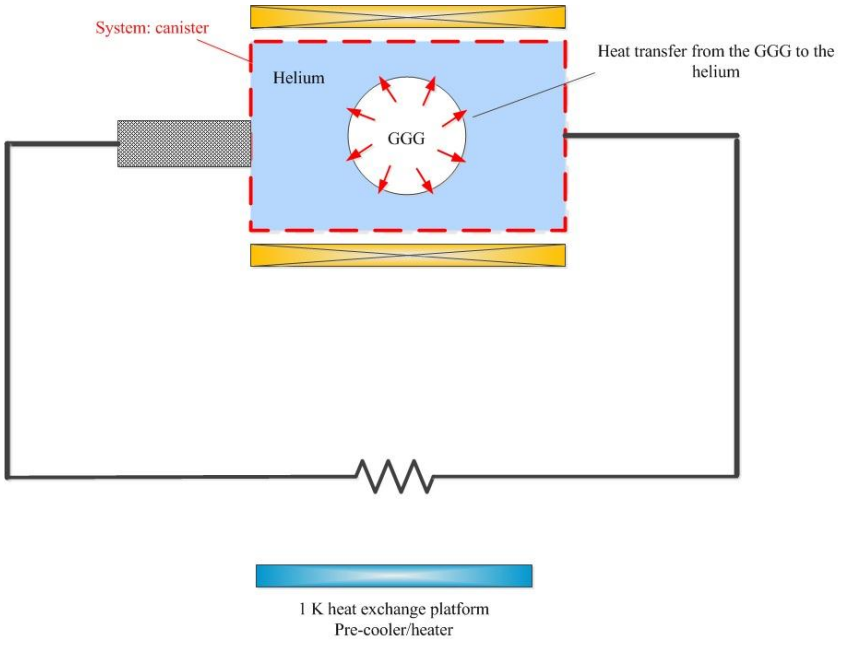

Figure 5-9 Heat transfer during process 1

Process 2-Isothermal magnetization

The temperature of the constituents of the canister remains constant throughout the isothermal magnetization process. The applied external magnetic field is increased from state 2 to state 3, where the magnetic field has reached (B_{max}). The temperature and applied magnetic field for state 3 are listed in Table 5-3. The additional magnetic field during the isothermal magnetization has two effects on the process: some energy leaves the canister (He II flowing out), and heat is transferred from the GGG to the incoming superfluid helium. Therefore the temperature of superfluid helium entering the canister is raised to the temperature of state 3.

Thermodynamic state	B (Tesla)	T (K)
3	2	1.9

Table 5-3 Thermodynamic state 3

- Energy balance for process 2:

The thermodynamic system for this part is the helium within the canister as shown in Figure 5-10. Since this process is isothermal the heat transfer from the GGG is calculated according to:

$$Q_{2-3,GGG} = \int_2^3 T\, ds = m_{GGG}\, T_2 \left(s_{GGG}\left(T_3, B_3\right) - s_{GGG}\left(T_2, B_2\right)\right) \tag{5.13}$$

The heat transfer from the GGG is equal to the heat transfer to the surrounding helium:

$$Q_{2-3,He} = -Q_{2-3,GGG} \tag{5.14}$$

Only superfluid helium can flow through the vycor glass superleak port. Therefore when considering the enthalpy of helium flowing into the canister only the enthalpy of superfluid must be considered. The reference value for the enthalpy of helium in Eq. (5.8) is equal to the enthalpy

of superfluid helium ($i_{superfluid}$=689 J/kg). An energy balance on the helium within the canister is done according to:

$$m_{2-3,in}\ \ i_{superfluid} - m_{2-3,out}\ \ i_{He}\left(T_3\right) + Q_{2-3,He} = 0 \tag{5.15}$$

Mass conservation for the helium within the canister during the isothermal magnetization process implies:

$$m_{2-3} = m_{2-3,in} = m_{2-3,out} \tag{5.16}$$

```
"!Isothermal magnetization"
T[3]=T_high                                                    "Temperature at state 3"
B[3]=B_max                                                     "Applied magnetic field at state 3"

"Energy balance"
Q_23_GGG=m_GGG*T[2]*(S_GGG(T[3],B[3])-S_GGG(T[2],B[2]))  "Heat from the GGG during isothermal magnetization"
Q_23_He=-Q_23_GGG                                              "Heat transfer to the helium"
i_superfluid=689[J/kg]                                         "Enthalpy of superfluid helium using reference value"
m_23_in*(i_superfluid)-m_23_out*(i_He(T[3]))+Q_23_He=0         "Finding mass of helium leaving the canister"
m_23=m_23_out                                                  "Mass conservation"
m_23=m_23_in                                                   "Mass conservation"
```

The 1 K heat exchange platform must cool the helium that leaves the canister. The heat transfer from the helium in the SMP loop to the 1 K heat exchange platform is expressed as:

$$Q_{2-3,p\_ch} = m_{2-3}\left(i_{He}\left(T_{p\_ch}\right) - i_{He}\left(T_3\right)\right) \tag{5.17}$$

where T_{p_ch} is the required temperature of the 1 K heat exchange platform (pre cooler/heater).

```
Q_23_p_ch=m_23*(i_He(T_p_ch)-i_He(T[3]))    "Heat needed during the precooling process"
```

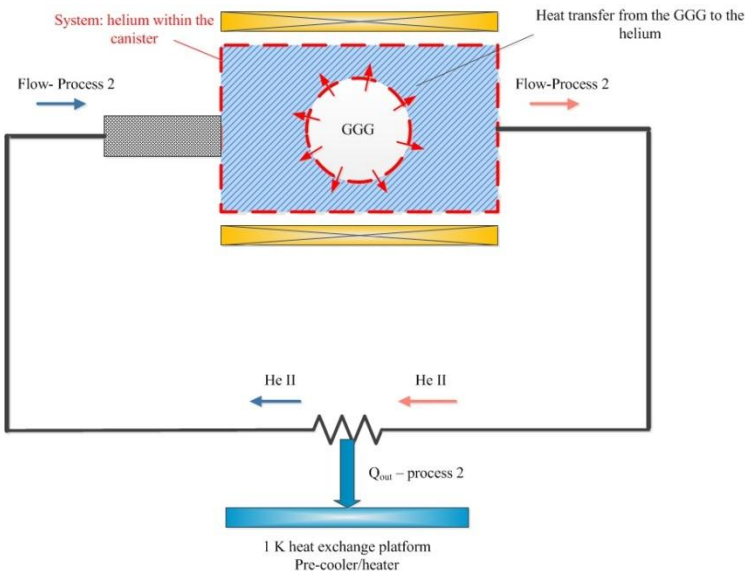

Figure 5-10 Heat transfer during process 2

Process 3-Adiabatic demagnetization

The externally applied magnetic field on the canister starts to decrease from state 3 to an unknown intermediate value (different from the first intermediate value) during the adiabatic demagnetization process. There is no heat transfer to or from the constituents of the SMP during this process, therefore the process is adiabatic. Demagnetization of the GGG particles causes their temperature to drop during this adiabatic process, which in turn causes the surrounding helium to cool. The demagnetization continues until the constituents of the SMP reach (T_{low}) at state 4. Thermodynamic values of state 4 are listed in Table 5-4.

Thermodynamic state	B (Tesla)	T (K)
4	To be determined	1.5

Table 5-4 Thermodynamic state 4

➢ Entropy balance for process 3:

The thermodynamic system for this part is the constituents of the canister. During the adiabatic demagnetization the entropy of helium in the canister changes according to:

$$\Delta S_{He,3-4} = m_{He}\left(s_{He}\left(T_4\right) - s_{He}\left(T_3\right)\right) \tag{5.18}$$

And the entropy of the GGG particles changes according to:

$$\Delta S_{GGG,3-4} = m_{GGG}\left(s_{GGG}\left(T_4, B_4\right) - s_{GGG}\left(T_3, B_3\right)\right) \tag{5.19}$$

Assuming reversible, an entropy balance on the constituents of the SMP yields:

$$\Delta S_{GGG,3-4} + \Delta S_{He,3-4} = 0 \tag{5.20}$$

```
"!Adiabatic demagnetization"
"Entropy balance"
T[4]=T_low                                                  "Temperature at state 4"
DS_He_34=m_He*(S_He(T[4])-S_He(T[3]))                       "Entropy change of helium in process 3"
DS_GGG_34=m_GGG*(S_GGG(T[4],B[4])-S_GGG(T[3],B[3]))         "Entropy change of GGG in process 3"
DS_He_34+DS_GGG_34=0                                        "Entropy balance for process 3"
```

➢ Energy balance for process 3:

The thermodynamic system for this part is the helium within the canister as shown in Figure 5-11. The heat transfer from the helium within the canister must be equal to the heat transfer to the GGG particles therefore the heat transfer to the helium is calculated according to:

$$Q_{3-4,He} = m_{He}\left(u_{He}\left(T_4\right) - u_{He}\left(T_3\right)\right) = -Q_{3-4,GGG} \tag{5.21}$$

```
"Energy balance"
Q_34_He=m_He*(u_He(T[4])-u_He(T[3]))                        "Heat transfer from the helium"
Q_34_He=-Q_34_GGG                                           "Heat transfer to the GGG"
```

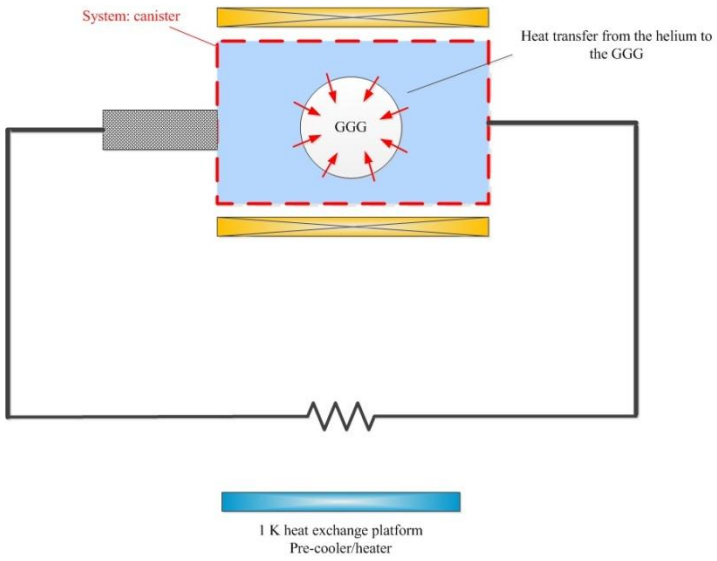

Figure 5-11 Heat transfer during process 3

Process 4-Isothermal demagnetization

The temperature of the constituents of the SMP is kept constant during the isothermal demagnetization process. The externally applied magnetic field decreases from state 4 and returns to state 1 (B_{min}). The demagnetization has two effects during this process: it brings in some energy into the canister (He II flowing in), and cools the incoming helium to (T_{low}). Thus the temperature returns to the original state (T_{low}).

- Energy balance for process 4:

The thermodynamic state for this part is the helium within the canister as shown in Figure 5-12. This process is isothermal therefore the heat transfer to the GGG is calculated according to:

$$Q_{4-1,GGG} = \int_4^1 T\, ds = m_{GGG}\, T_1 \left(s_{GGG}\left(T_1, B_1\right) - s_{GGG}\left(T_4, B_4\right) \right) \tag{5.22}$$

The heat transfer to the GGG must be equal to the heat transfer from the surrounding helium:

$$Q_{4-1,He} = -Q_{4-1,GGG} \tag{5.23}$$

An energy balance on the helium within the canister is done according to:

$$m_{4-1,in} \;\; i(T_1) - m_{4-1,out} \;\; i_{superfluid} + Q_{4-1,He} = 0 \tag{5.24}$$

Mass conservation for the isothermal demagnetization process implies:

$$m_{4\_1} = m_{4\_1,in} = m_{4\_1,out} \tag{5.25}$$

```
"!Isothermal demagnetization"

"Energy balance"
Q_41_GGG=m_GGG*T[1]*(S_GGG(T[1],B[1])-S_GGG(T[4],B[4])) "Heat transfer from the GGG during isothermal demagnetization"
Q_41_He=-Q_41_GGG                                       "Heat transfer to the helium"
m_41_in*(i_He(T_p_ch))-m_41_out*(i_superfluid)+Q_41_He=0 "Finding mass of helium entering the canister"
m_41=m_41_out                                           "Mass conservation"
m_41=m_41_in                                            "Mass conservation"
```

The 1 K heat exchange platform must heat the superfluid helium that leaves the canister. The heat transfer from the superfluid helium in the SMP loop to the 1 K heat exchange platform is expressed as:

$$Q_{4-1,p\_ch} = m_{4-1}\left(i_{He}\left(T_{p\_ch}\right) - i_{superfluid}\right) \tag{5.26}$$

```
Q_41_p_ch=m_41*(i_He(T_p_ch)-i_superfluid)   "Heat needed during the preheating process"
```

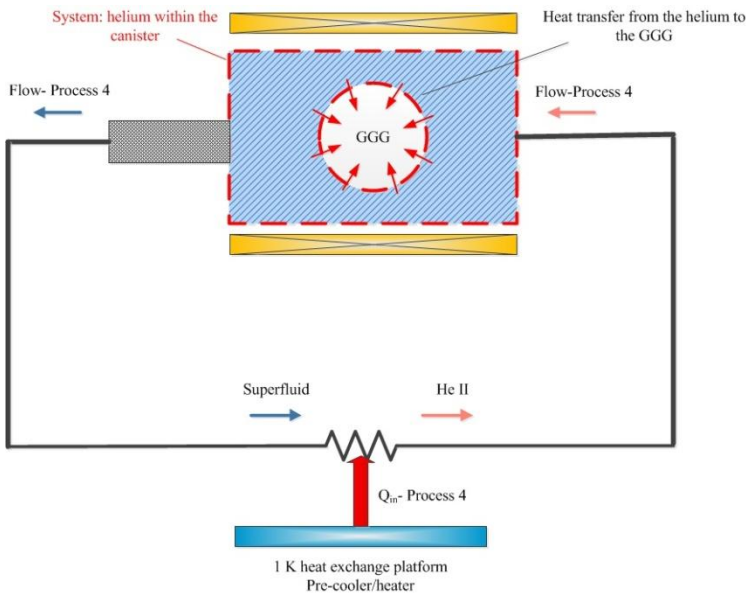

Figure 5-12 Heat transfer during process 4

This concludes the analysis of each process during the operation of the SMP. The total heat transferred to the helium in the canister during the entire cycle is (note that the first two terms on the right hand side are calculated to be positive and the second two terms are negative):

$$Q_{canister} = Q_{1-2,He} + Q_{2-3,He} + Q_{3-4,He} + Q_{4-1,He} \tag{5.27}$$

The total heat transfer to the helium in the SMP loop during the pre-cooling/heating stage with the 1 K heat exchange platform is (note that the first term on the right hand side is calculated to be negative and the second term to be positive):

$$Q_{p\_ch} = Q_{2-3,p\_ch} + Q_{4-1,p\_ch} \tag{5.28}$$

The cycle must be thermodynamically closed for the SMP. This means that the total heat transfer to the helium within the canister during the entire cycle must be equal to the heat transfer to the helium in the SMP loop during the pre-cooling/heating with the 1 K heat exchange platform, therefore the precooler/heater temperature (1 K heat exchange platform) is found by applying:

$$Q_{p\_ch} = Q_{canister} \tag{5.29}$$

```
"!Closing the cycle for the energy balance"
Q_canister=Q_12_He+Q_23_He+Q_34_He+Q_41_He  "Heat transfer in the canister"
Q_p_ch=Q_23_p_ch+Q_41_p_ch                  "Heat transfer during pre-cooling/heating stage"
Q_p_ch=Q_canister                           "Closing cycle"
```

5.5 Model predictions

The four processes during one cycle operation of the SMP were modeled in the previous section. A plot of the temperature of the constituents of the canister as a function of the externally applied magnetic field is shown in Figure 5-13. The model predicts the temperature of the 1 K heat exchange platform to be at 1.638 K. The intermediate applied magnetic field required for state 2 and 4 are found to be 1.486 and 0.482 Tesla respectively. The model predicts 1.769 g and 3.317 g of helium being pumped out of the canister during the isothermal magnetization and demagnetization process respectively. The mismatch between the two mass flows during the two separate isothermal processes is due to the fact that the pre-cooler/heater temperature is closer to (T_{low}) than (T_{high}): more energy is spent to heat the incoming superfluid helium to the canister during the isothermal magnetization than the energy spent to cool the incoming He II to the canister during the isothermal demagnetization process. As a result of this, more helium is pushed out during the isothermal demagnetization compared to the isothermal magnetization process. As discussed earlier the time spent during the adiabatic magnetization and adiabatic demagnetization is significantly shorter compared to the isothermal magnetization and demagnetization. The period of one cycle will be set to 100 s by controlling the externally applied magnetic field during one cycle so the mass flow rate during the two isothermal processes can be estimated according to:

$$\dot{m}_{2-3} = \frac{m_{2-3}}{\frac{\tau}{2}} = \frac{m_{2-3}}{\tau_{hc}}$$
$$\dot{m}_{4-1} = \frac{m_{4-1}}{\frac{\tau}{2}} = \frac{m_{4-1}}{\tau_{hc}} \quad (5.30)$$

where τ is the period for one cycle, and τ_{hc} is the half cycle period (The period for either the isothermal magnetization or demagnetization). Thus the mass flow rate of helium during the isothermal magnetization and isothermal demagnetization are found to be 35.3 and 66.3 mg/s respectively. Similarly the heat transfer rate to the helium in the SMP loop for the precooling/heating stage during the two isothermal processes is calculated according to:

$$\dot{Q}_{2-3,p\_ch} = \frac{Q_{2-3,p\_ch}}{\tau_{hc}}$$
$$\dot{Q}_{4-1,p\_ch} = \frac{Q_{4-1,p\_ch}}{\tau_{hc}} \quad (5.31)$$

```
"!Estimating heat transfer rate needed from/to the 1 K heat exchange platform"
tau=100[s]                                          "Period of one cycle"
tau_hc=tau/2                                        "Time duration for process 2 and 4"
Q_dot_23_p_ch=Q_23_p_ch/tau_hc                      "Heat transfer rate during process 2"
Q_dot_41_p_ch=Q_41_p_ch/tau_hc                      "Heat transfer rate during process 4"

"!Estimating the mass flow rate in and out of the canister"
m_in_mg=m_in*convert(kg,mg)                         "Helium entering in milligrams"
m_out_mg=m_out*convert(kg,mg)                       "Helium exiting in milligrams"
m_dot_in=m_in_mg/tau_hc                             "In-Mass flow rate in mg/s"
m_dot_out=m_out_mg/tau_hc                          "Out-Mass flow rate in mg/s"
```

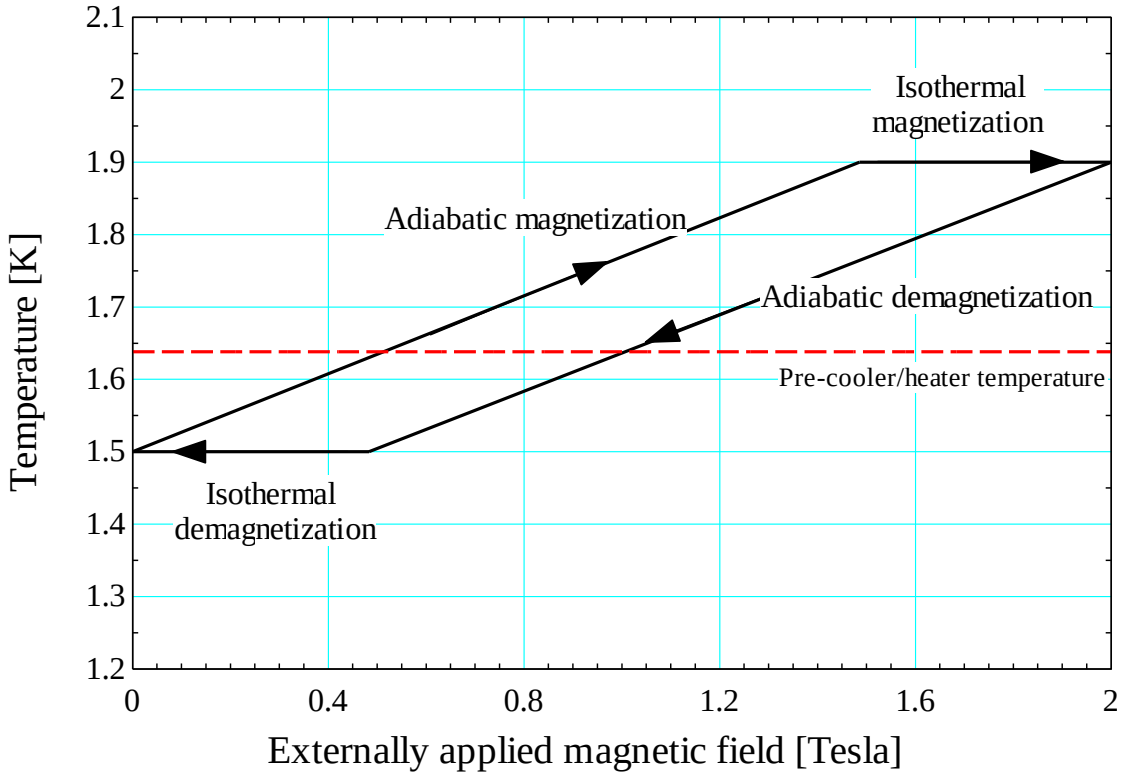

Figure 5-13 The temperature of the constituents of the SMP as a function of the externally applied magnetic field during one cycle operation of the SMP

The design of the 1 K facility was done based on the required cooling power of the 1 K pot. Part of the cooling power provided by the 1 K facility compensates for the heat leaks to the 1 K pot, which was calculated in chapter 4, and the rest of the power is used for the SMP experiment. The cooling power needed for the SMP experiment is:

$$\dot{q}_{SMP} = \dot{Q}_{2-3,p\_ch} \tag{5.32}$$

Therefore the cooling power needed for the SMP experiment is found to be 23 mW. The heat transfer rate for pre heating the helium during the isothermal demagnetization is estimated to be 31 mW. The temperature of the 1 K heat exchange platform will be kept at 1.638 K by the temperature controller that was discussed earlier in chapter 2.

5.6 Summary of the SMP model and results

The SMP is a new pump with no moving parts that can be integrated with the PSR in order to make it the first sub Kelvin refrigerator with no moving parts. The SMP will be demonstrated as a proof of concept independent from the refrigeration system. A qualitative description of the operation of the SMP during one cycle was presented followed by a theoretical model which predicted the behavior of the SMP during the proof of concept demonstration. A list of important predictions and outcomes of the model are listed in Table 5-5. According to the theoretical model the SMP only produces a net flow meaning that all the work or heat produced in the SMP are extracted without any mechanical or thermal use of the cycle. However it should be noted that the SMP's role in the PSR is to compress and expand ^{3}He in a ^{3}He-^{4}He mixture as discussed earlier in chapter 1. ^{3}He solute acts as an ideal gas in the inert background of superfluid ^{4}He. Therefore the usefulness of the SMP is evident once it is integrated in the PSR system.

Parameter	Value
Temperature of 1 K HX platform	1.638 K
Helium pumped out	1.769 g
Helium pulled in	3.317 g
Period of 1 cycle	100 s
Mass flow rate of helium – pumped out	35.3 mg/s
Mass flow rate of helium – pulled in	66.3 mg/s
Heat transfer rate - cooling	23 mW
Heat transfer rate - heating	31 mW
Intermediate magnetic field-state 2	1.486 Tesla
Intermediate magnetic field-state 4	0.482 Tesla

Table 5-5 Predictions and outcomes of the model

5.7 References

Lounasmaa, O.V. , Experimental principles and methods below 1 K, Academic Press, New York, 1974

Miller, F.K. , "A simple method for the analysis of sub-Kelvin refrigerators that use a dilute superfluid ^{3}He-^{4}He mixture as the working fluid", Journal: Cryogenics (Elsevier), Vol. 41 (2001) pg. 311-318

Miller, F.K. , "Sub-Kelvin space cryocooling without moving parts", Proposal: NASA, 2008

Miller, F.K. , Brisson, J.G. , "A superfluid pulse tube driven by a thermodynamically reversible magnetic pump", Conference: CEC, 2009

Perry, D.L. , Phillips, S.L, Handbook of inorganic compounds, CRC Press, Boca Raton, FL, 1995

6 Results and Discussions

An experiment was carried out in order to demonstrate the performance of the 1 K facility. The location of each thermometer and the heater used in the experiment is shown in Figure 6-1. Three Lakeshore silicon diode thermometers (DT-470) were used to monitor the temperature of the first and second stage heat exchange platforms, and the pump out line at the pot's exhaust. These silicon diode thermometers follow a standard curve. Five Cernox thermometers (CX-1030-CU): one calibrated by Lakeshore, and four "to be calibrated" were mounted on one corner of the 1 K heat exchange platform. A heater was mounted on the 1 K heat exchange platform (on the opposite corner of the thermometers) and was used to heat the 1 K pot sub assembly for calibration purposes and to obtain the cooling power of the 1 K pot.

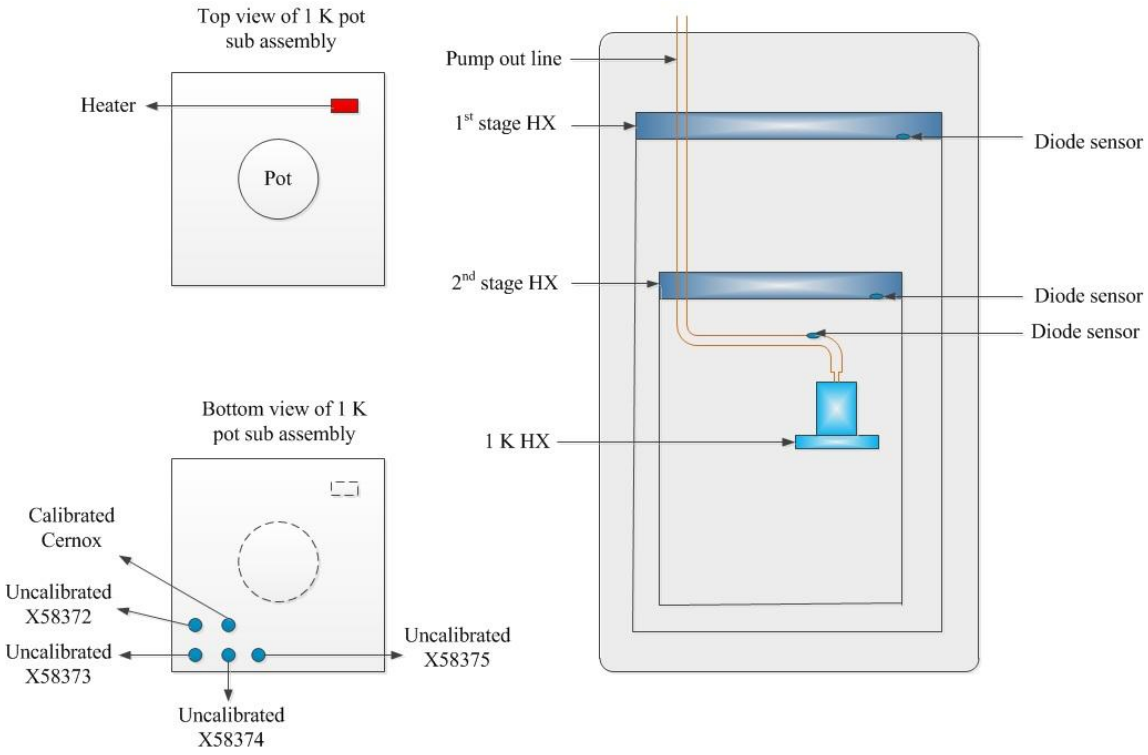

Figure 6-1 Experimental setup for the 1 K facility

6.1 Uncertainty analysis

The inherent uncertainty in the thermometers is published by the manufacturer and is listed in Table 6-1.

Silicon Diode (DT-470) accuracy-Band 13	
2 to100 K	± 1 K
100 to 305K	± 1% of Temp. reading
Cernox – Calibrated accuracy (CX-1030-CU)	
1.4 K	± 5 mK
4.2 K	± 5 mK
10 K	± 6 mK
20 K	± 9 mK
30 K	± 10 mK
50 K	±13 mK
77 K	±16 mK
300 K	±40 mK

Table 6-1 Thermometer accuracy

The Cryocon temperature controllers were used to monitor the temperatures. The manufacturer reports an inherent uncertainty in the temperature measurement by these controllers and suggests using the following equation to calculate the uncertainty for temperature readings with silicon diode thermometers (Cryocon 2005):

$$MAV = 60\times10^{-6} + 5\times10^{-5} SenRdg \tag{6.1}$$

where *MAV* is the electronic measurement accuracy in Volts, and *SenRdg* is the sensor reading in volts at the desired temperature. The *MAT* (Measurement Accuracy Temperature) in Kelvin is calculated according to:

$$MAT = \frac{MAV}{Sensen} \tag{6.2}$$

where *Sensen* is the sensor sensitivity in Volts/Kelvin at the desired temperature. The manufacturer provides a table with the different values of *SenRdg* and *Sensen* for DT-470 silicon diode thermometers. The uncertainty is listed in Table 6-2 for various temperature readings with DT-470.

Temperature	Uncertainty (μV)	Uncertainty (mK)
1.4	±144.9	±11.06
4.2	±141.3	±4.205
10	±131	±4.565
20	±120.7	±6.859
30	±115.4	±49.29
50	±113.5	±64.87
77.35	±111	±57.82
100	±108.8	±53.32
150	±103.4	±47.23
200	±97.78	±42.33
250	±91.92	±38.78
300	±85.95	±35.81

Table 6-2 Temperature reading uncertainty by Cryocon with DT-470 thermometers

An inherent uncertainty with temperature measurements with Cernox thermometers is also reported. Cryocon (2005) suggests calculating the uncertainty of the temperature readings with these thermometers according to:

$$MAR = 5\times10^{-5}\,SenVal + 5\times10^{-5}\,Range \tag{6.3}$$

where *MAR* is electronic measurement accuracy in ohms, *SenVal* is temperature in Kelvin, and *Range* is the resistance range in ohms. The measurement uncertainty of temperature in K is computed according to:

$$MAT = \frac{MAR}{Sensen} \tag{6.4}$$

Cryocon provides a table with the values of *Range* and *Sensen* for various temperatures. The temperature measurement uncertainties in the Cryocon temperature controllers used with the Cernox (CX-1030-CU) thermometers at various temperatures are listed in Table 6-3.

Temperature (K)	Uncertainty (ohm)	Uncertainty
1	±0.05005	±15.33 μK
1.4	±0.05007	±39.58 μK
2	±0.0501	±98.38 μK
3	±0.00515	±25.87 μK
4.2	±0.00521	±53.52 μK
6	±0.0053	±110 μK
10	±0.0055	±288.8 μK
20	±0.006	±958.8 μK
30	±0.0065	±2 mK
40	±0.007	±3 mK
50	±0.0075	±4 mK
77.35	±0.008868	±10 mK
100	±0.01	±18 mK
150	±0.0125	±42 mK
200	±0.015	±81.522
250	±0.0175	±141 mK
300	±0.02	±227 mK

Table 6-3 Temperature reading uncertainty by Cryocon with CX-1030-CU

6.2 Results

An operation manual for the 1 K facility is available in Appendix D. The performance of the 1 K facility was validated after many trials in the span of several months. Gradual improvements were made to the 1 K facility in order to be able to achieve a nominal temperature of 1 K. The improvements made during the several attempts are described below.

The ultimate low temperature of the 1 K pot during the first run was 150 K. The sub assembly was found to be very well thermally isolated from its surroundings. Radiation from the pot to the second stage shield and heat exchange platform was the only available mode of heat transfer for

cooling the pot. Therefore a “heat switch”, discussed in chapter 4 was integrated with the pot sub assembly in order to pre cool the 1 K pot. During a second trial, the low ultimate temperature of the 1 K pot was 17 K. The J-T effect for helium is weak at this temperature and a colder temperature must be achieved in order to be able to observe the J-T effect. The heat leak model presented in chapter 4 showed a heat leak from room temperature down to the 1 K pot via the pump out line. Therefore the pump out line was thermally linked to the two heat exchange platforms via copper straps. During a third trial, the temperature of the 1 K pot reached an ultimate low temperature of 1.4 K, however shortly after reaching this temperature the pot started to warm up spontaneously. Since the new temperature attained was below the lambda point, the issue was thought to be a superleak through the pot seal. The indium o-ring seal was replaced with a new one before running the facility for the fourth time. During the fourth trial, a low temperature of 2.4 K was achieved (higher than the lambda point), however the pot started to warm up shortly after. Oscillations in temperature were observed to be synchronized between the 1 K pot and the second stage heat exchange platform during this trial. These oscillations remained unexplained and unsolved. The vacuum tubes connecting the Dewar to the rotary vane pump were inspected and leaks were found in the valves and joints. The leak issue was fixed after the inspections. A fifth trial was concluded with baffling results; the ultimate low temperature was 3.2 K and warmed up shortly after. The problem was thought to be the rotary vane pump and the decision was to run with the rotary vane pump one more time, and switch the pump in case a steady low ultimate temperature was not achieved. During a sixth trial, a low steady ultimate temperature of 1.392 K was achieved with the rotary vane pump that was used during previous runs. The problem was solved: a partially blocked capillary had spontaneously

opened during this trial allowing a larger flow of helium through the capillary and ultimately providing the cooling power needed to cool the 1 K pot.

Figure 6-2 shows the temperature as a function of time for the first and second stage heat exchangers, the pump out line at the pot exhaust, and the 1 K heat exchange platform during the last successful trial. This plot contains 4 major parts: the cool down (A to D), the steady state ultimate low temperature operation (F to G), the calibration process (G to H), and the warm up (drift) process (H to I). Each point along with a description is listed in Table 6-4. The low temperature region, between points F and H on Figure 6-2, is shown later in this section.

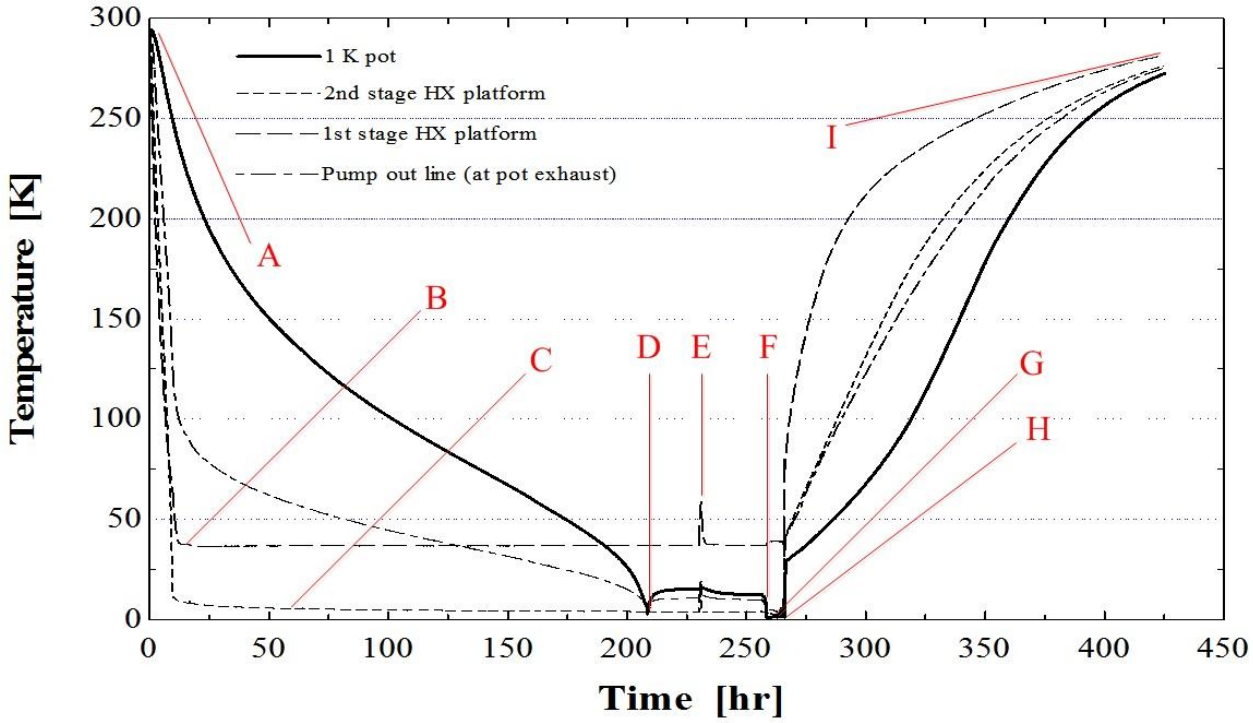

Figure 6-2 Temperature as a function of time for: the first stage and second stage heat exchange platforms, the pump out line at the pot's exhaust and the 1 K heat exchange platform

Point on Figure 6-2	Description
A	Cryocooler is activated
B	1st stage temperature steady at ~36K
C	2nd stage temperature steady ~4K
D	1st low ultimate temp - capillary partially blocked, 1 K HX platform at 2.9 K
E	Cryocooler compressor water filter blocked-automatic shutdown (filter replaced)
F	Successfully achieved steady ultimate low temperature at 1.392 K
G	Calibration process begins
H	Warm up (drift) – Calibrating
I	Last data point before terminating LabView

Table 6-4 various points during the final run

During the last trial an ultimate low temperature was achieved at point (D), however the 1 K pot warmed up shortly after in this run. In order to understand the potential problem, the 1 K pot was left alone, slowly warming up without changing any of the settings (valves, regulator, pump etc.). The system reached a new steady state temperature at about 15 K. After a period of time, the water filter used for filtering the water going in to the cryocooler's compressor was clogged. This caused a pressure drop across the filter, and subsequent automatic shut off of the compressor. Consequently the cryocooler turned off and the system started warming up at point (E). The water filter was replaced soon after and the compressor was turned back on without changing any of the previous settings. It was expected for the 1 K pot assembly to return to the previous steady state temperature at 15 K, however the pot assembly reached a new steady state temperature at 12 K. This clue suggested that the capillary must have been partially blocked and some of the blockage have been removed. At this point the inlet pressure was increased from 1 atm to 2 atm forcing a higher amount of helium through the capillary and to the pot. At point (F) the temperature rapidly dropped from 12 K to 1.392 K and this was the lowest steady state temperature achieved with the 1 K facility.

The Cryocon temperature controllers have the capability to regulate the amount of power in the heater as a percentage of four different settings (50 mW, 500 mW, 5W or 50W). Thus the desired heater power was entered and various steady state temperatures were recorded for each power setting during the 1 K pot's operation. A map of the cooling capacity of the 1 K pot as a function of temperature is shown in Figure 6-3.

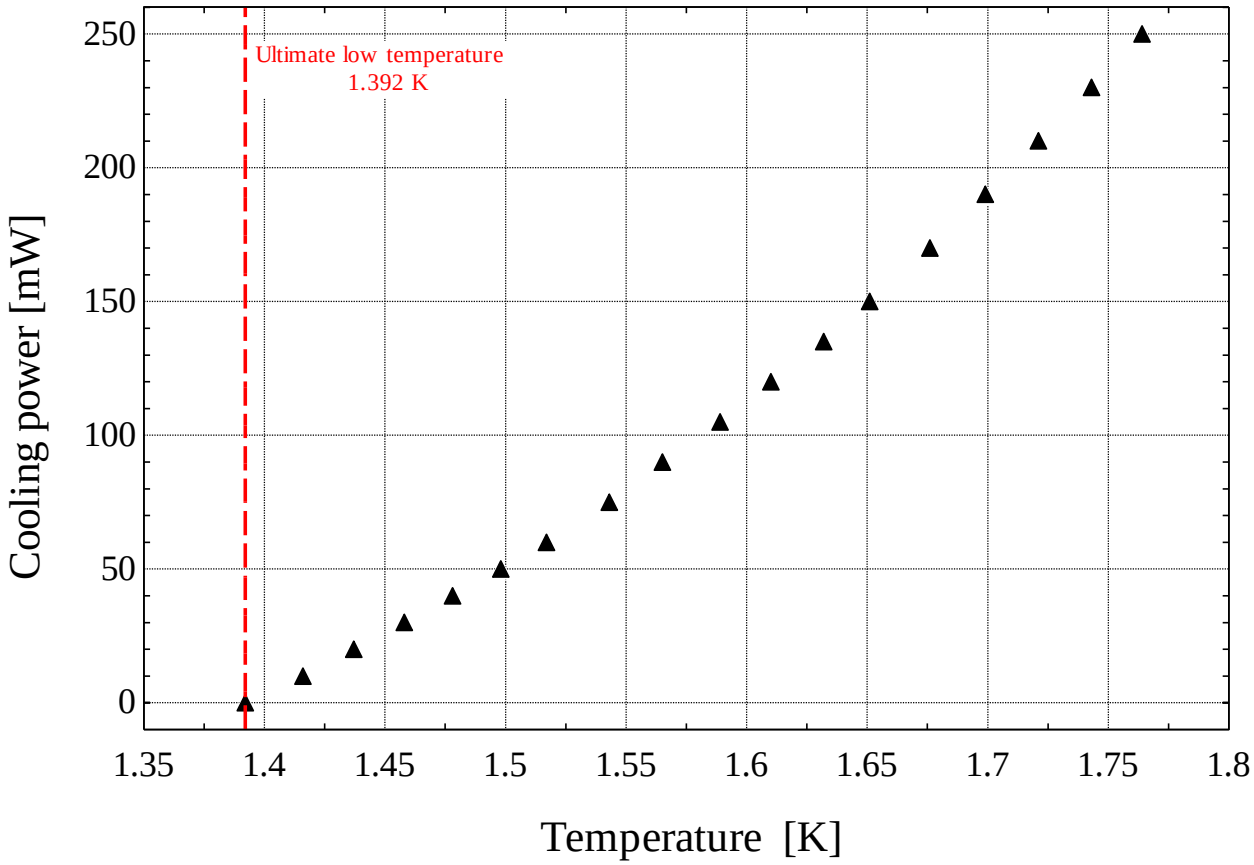

Figure 6-3 Cooling power as a function of temperature for the 1 K pot

6.3 Thermometer calibration

Unfortunately, out of the four uncalibrated Cernox thermometers, one failed to provide an accurate resistance reading therefore only three of them were calibrated against the calibrated

thermometer. The heater was used to control the temperature of the 1 K heat exchange platform by setting the desired temperature on the Cryocon temperature controllers. The calibration process began at the low ultimate temperature of the 1 K pot (1.392 K) and the temperature was increased in a stair case manner until steady state temperature was attained for each step. Figure 6-4 shows the operation of the 1 K pot during the low temperature operation and the calibration process.

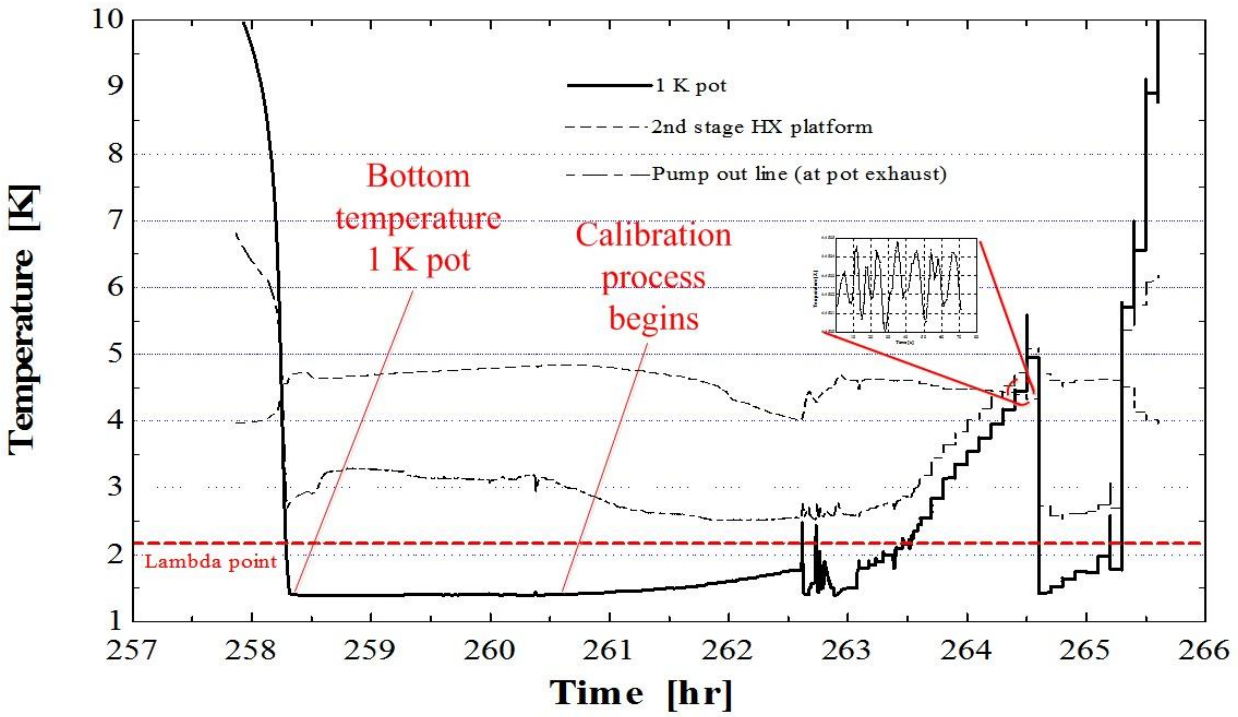

Figure 6-4 Low temperature operation of the 1 K pot along with the calibration process

Small temperature oscillations exist within each steady state temperature recorded for each period of time during the calibration process as shown in Figure 6-4. These will eventually lead to a new uncertainty for each of the calibrated thermometer. The average of these oscillatory temperatures is taken as the temperature for that period. The average of the resistances for each uncalibrated thermometer is also taken for the corresponding period. Therefore each averaged temperature is matched with the corresponding averaged resistance for each individual

uncalibrated thermometer. The accuracy of the thermometers for temperatures below 10 K is critical for future experiments thus the uncertainty analysis is focused for temperatures below 10 K. Standard deviation provides useful information on how scattered the data are from the average or the mean of the data points. The standard deviation of the data points for each quasi-steady temperature is calculated according to:

$$\psi = \sqrt{\frac{1}{N-1}\sum_{i=1}^{N}\left(T_i - \bar{T}\right)^2} \tag{6.5}$$

Where N is the number of samples, T_i is the temperature for each data point, and $\bar{T}$ is the average temperature for all the data points. Thus the standard deviation for each quasi-steady temperature at temperatures below 10 K is calculated and shown in Figure 6-5 (note that the largest value is only 500 μK).

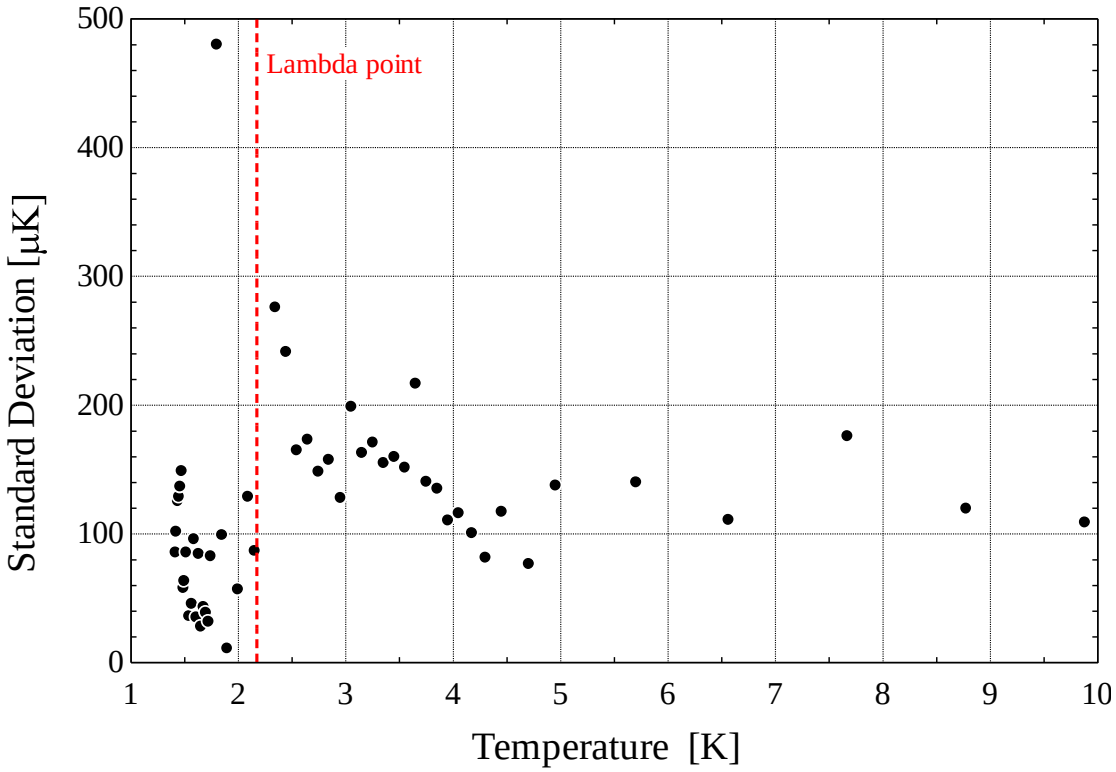

Figure 6-5 Standard deviation for each quasi-steady temperature at temperatures below 10 K

The maximum absolute deviation about a point is the maximum of the absolute deviations of a sample from the average. The uncertainty for each data point is determined by taking the maximum absolute deviation for each quasi-steady temperature calculated according to:

$$Dev = \max\left(\left|T_i - \bar{T}\right|\right) \tag{6.6}$$

Figure 6-6 shows the maximum absolute deviation for each quasi-steady temperature during the calibration process. Therefore the uncertainty for each of the uncalibrated thermometers at temperature below 10 K ranges from 115 μK to 1.25 mK. To be conservative, the new uncertainty for each uncalibrated thermometer is considered to be 1.25 mK for temperatures below 10 K. This uncertainty must be added to the uncertainty of the calibrated thermometer plus the uncertainty resulting from the temperature measurements by the Cryocon in order to provide a new total uncertainty for each of the newly calibrated thermometers.

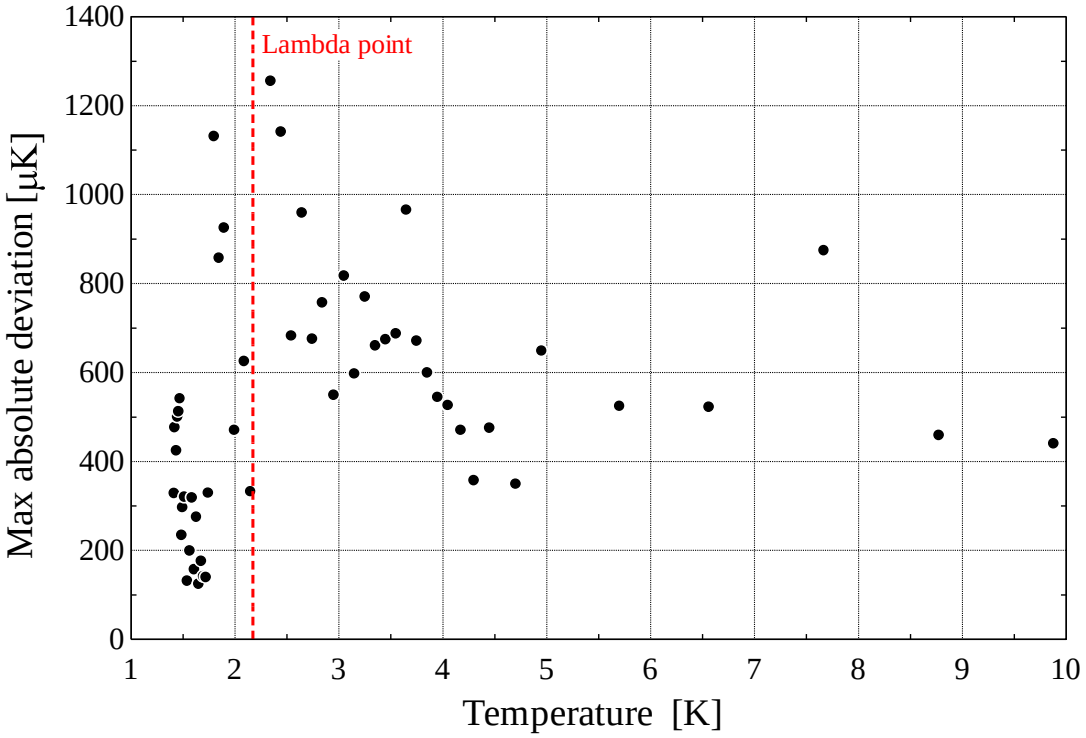

Figure 6-6 Maximum absolute deviation for each quasi-steady temperature during the calibration process

The Cryocon temperature controllers have the capability to interpolate through the calibration points for a thermometer (Electrical resistance as a function of temperature). The calibration result for the Cernox thermometer with serial number X58373 is shown in Figure 6-7. All calibration results are also available as a table in Appendix E.

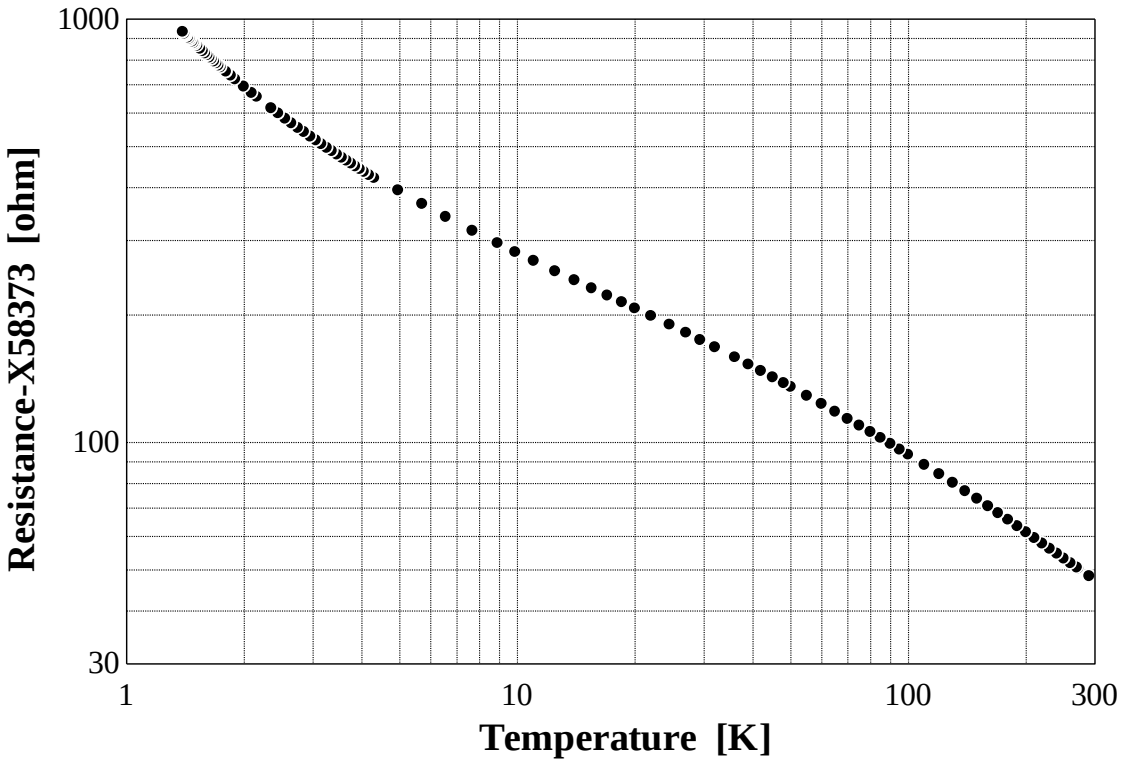

Figure 6-7 Calibration result for thermometer with serial number X58373

The calibration results for the Cernox thermometer with serial number X58374 are shown in Figure 6-8.

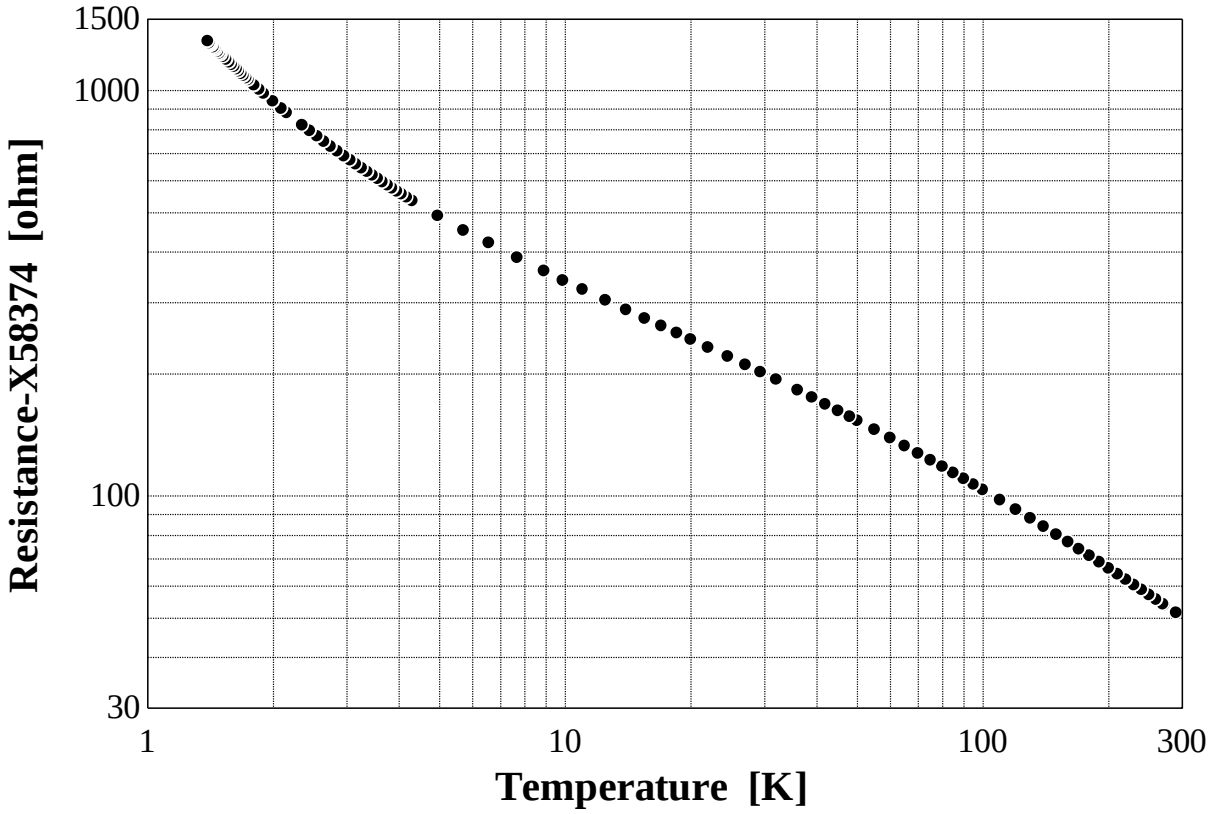

Figure 6-8 Calibration result for the thermometer with serial number X58374

The calibration results for the Cernox thermometer with serial number X58373 are shown in Figure 6-9.

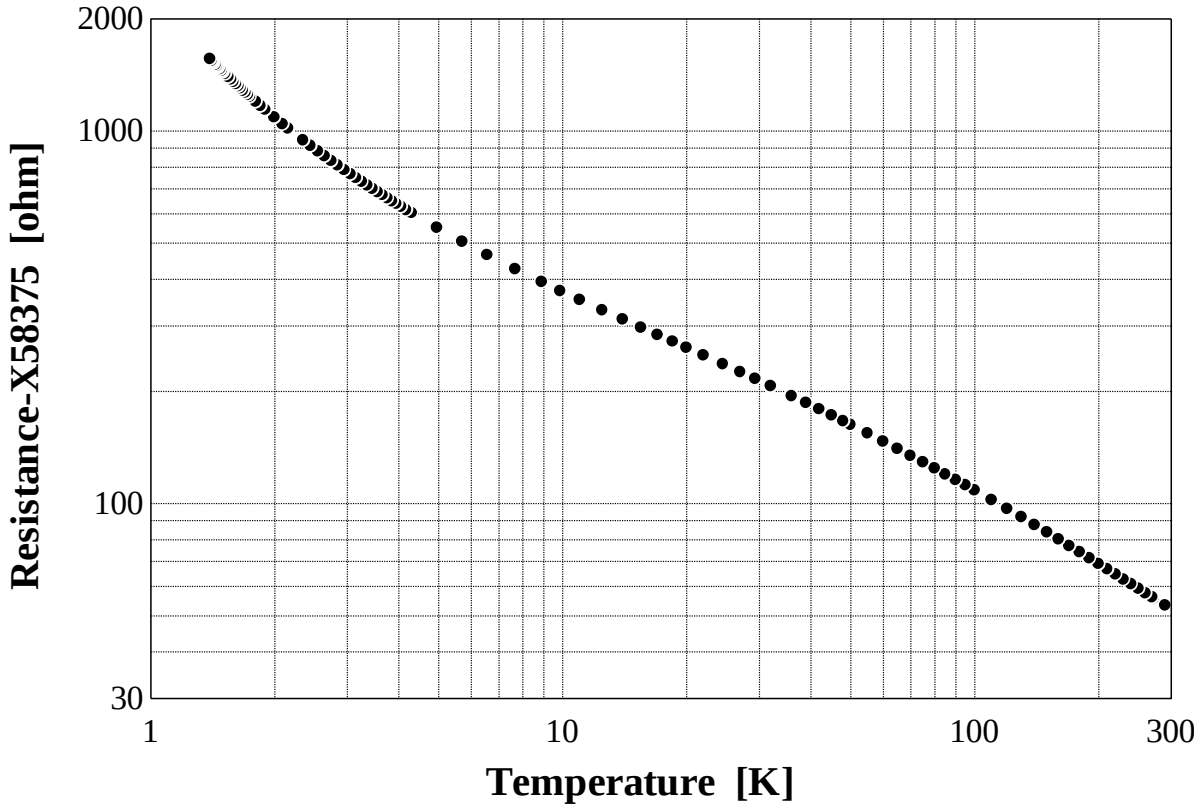

Figure 6-9 Calibration result for the thermometer with serial number X58375

6.4 Conclusions

Unlike traditional 1 K refrigeration systems that work based on evaporative cooling which often requires a liquid helium bath in the vicinity of the 1 K pot, the 1 K facility described in this work uses small amounts of helium to produce the necessary refrigeration. Thus the cost of running such refrigeration system excluding the electricity consumed by the compressor that runs the cryocooler, is minimal. For example, during the last successful run only 200 g of helium was used ($4.25 in 2011). The power provided by the 1 K facility is considered to be sufficient for running the SMP experiment. This experiment validated the performance of the 1 K facility and proved that all the integrated components (Heat exchangers, J-T restrictor, recuperators, etc.), including one of the most critical parts of the facility, the superfluid seal, worked well together.

6.5 Future work and suggestions

The SMP experiment is part of the future continuation of this work. The 1 K pot's cooling power obtained during the experiment is considered to be more than sufficient for running the SMP. Despite this fact, some key enhancements can be made to improve the 1 K facility's performance and to increase the cooling power provided by the 1 K pot:

- The J-T restrictor (capillary) must be free of any blockage for full potential performance of the system. Carefully purging the 1 K facility line with helium several times for long periods of time before turning on the cryocooler can prevent potential blockages in the capillary.

- If the blockage problem in the capillary persists even with the purging process described above, a small heater can be integrated and mounted on the outside of the capillary to "bake out" the blockages when the pot is cold. The helium flow through the capillary must be tested at various times during the cool down process to ensure helium flow and no blockage through the capillary.
- A radiation shield in the form of a baffle can be used in the pump out line in order to limit the amount of radiation that is reflected off the surfaces of the tube from the upper parts down to the pot (Radiation in the interior of the pump out line is similar to light being transmitted in a periscope).
- If more cooling power is desired the capillary can be shortened.
- The rotary vane pump can be switched with a pump that provides a lower ultimate pressure. By doing so the vapor pressure and temperature of liquid helium will be lower in the pot (limited to approximately 1 K).

6.6 References

Cryogenic Control Systems Inc., "Cryogenic temperature controller Model 42 & 44", CryoCon, Rancho Sante Fe, CA, 2005

Appendix A Engineering drawings of cryogenic Dewar

Sectional view of the assembly:

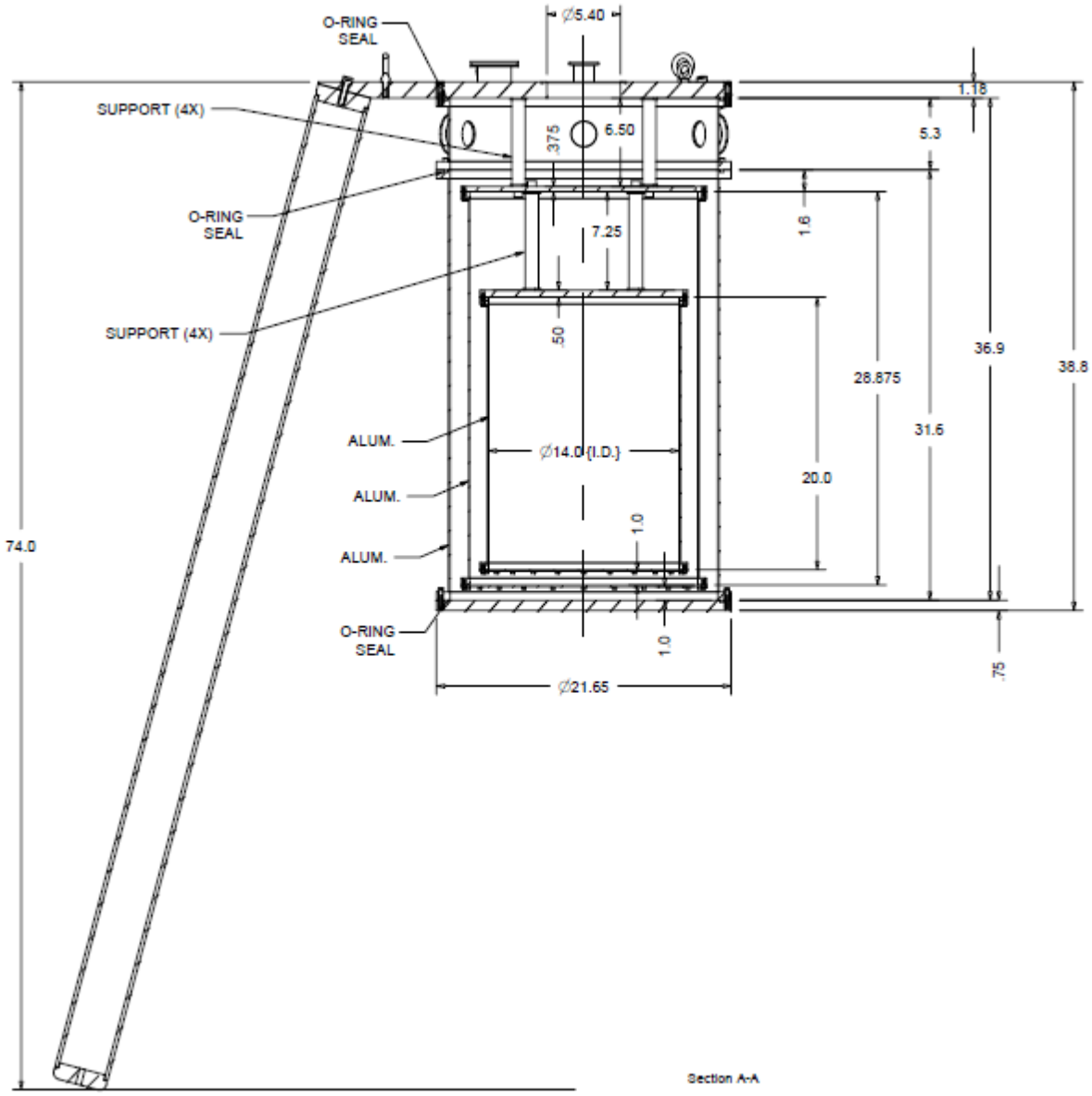

Top view of the assembly:

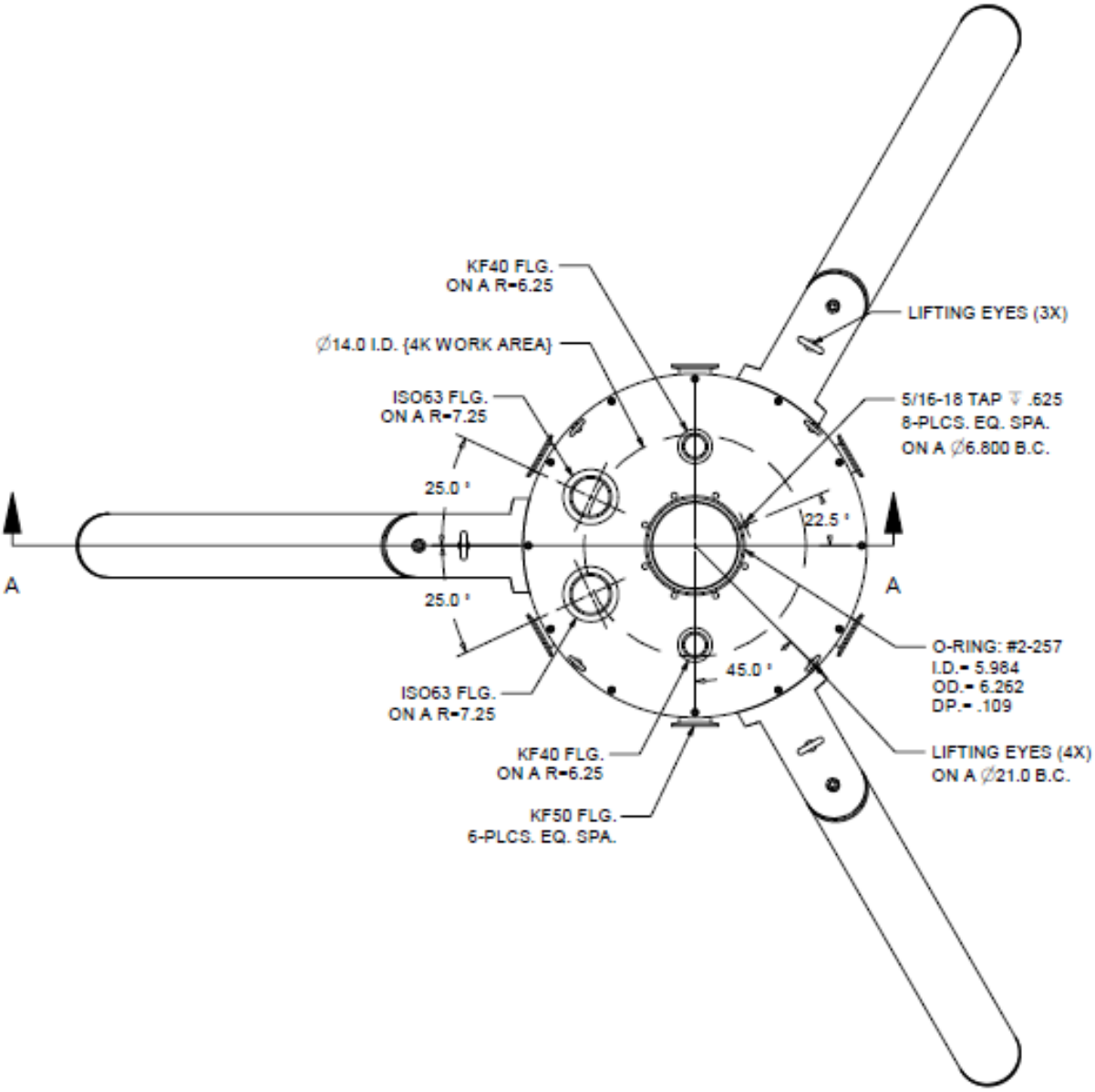

An isometric and front view of the assembly:

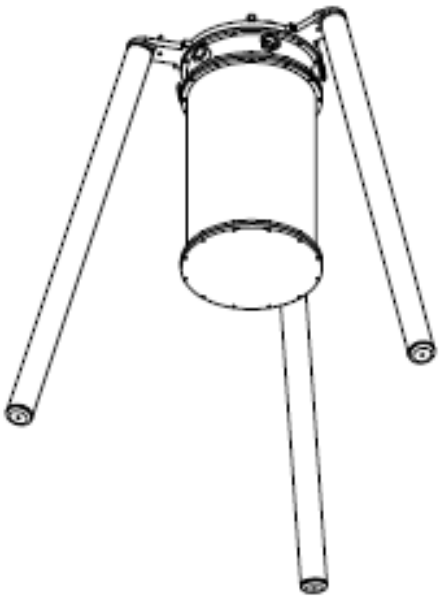

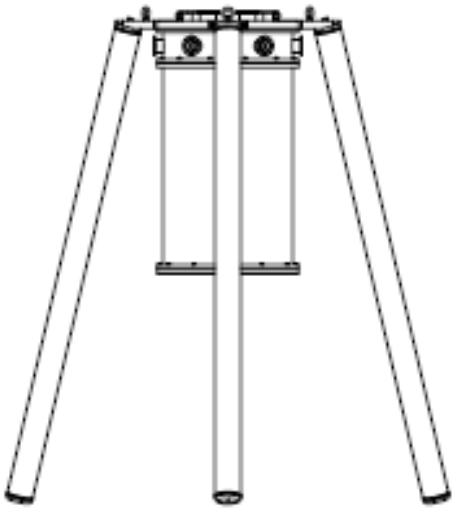

First stage (Before modification):

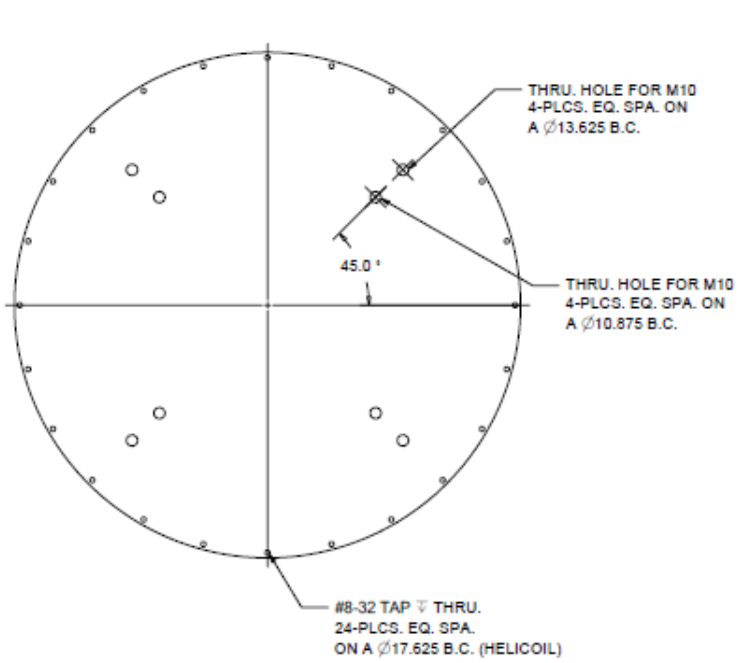

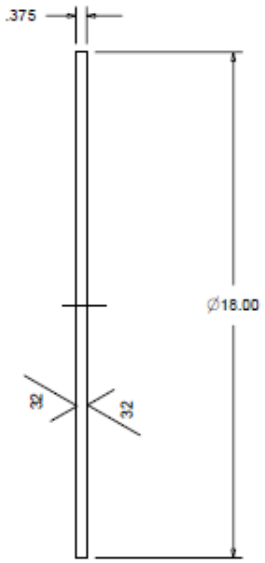

Second stage (Before modification):

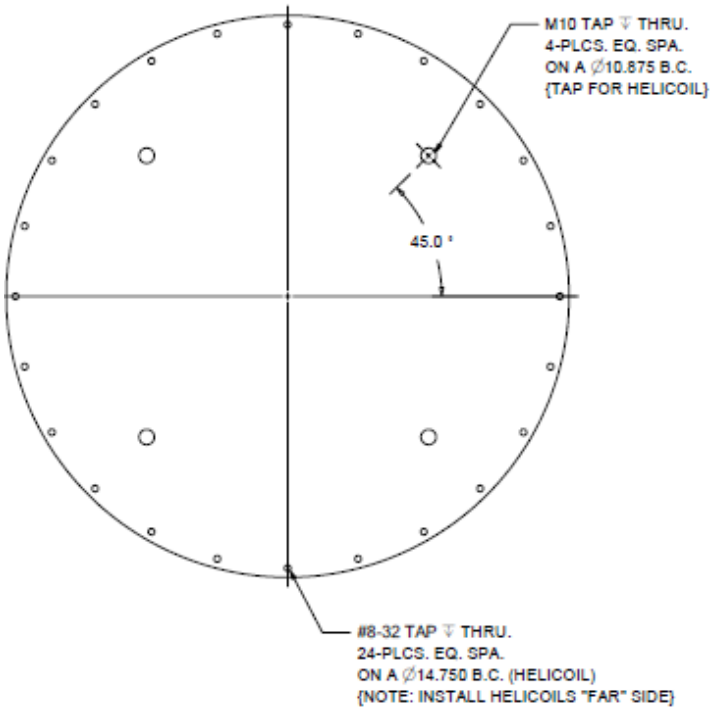

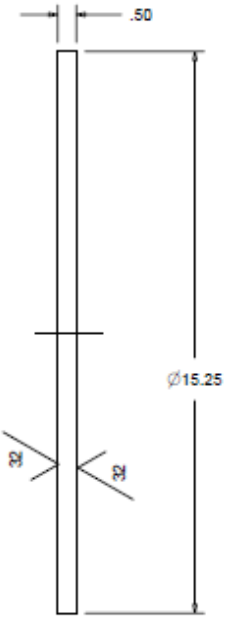

Appendix B Engineering drawings of modified heat exchange platforms

First stage:

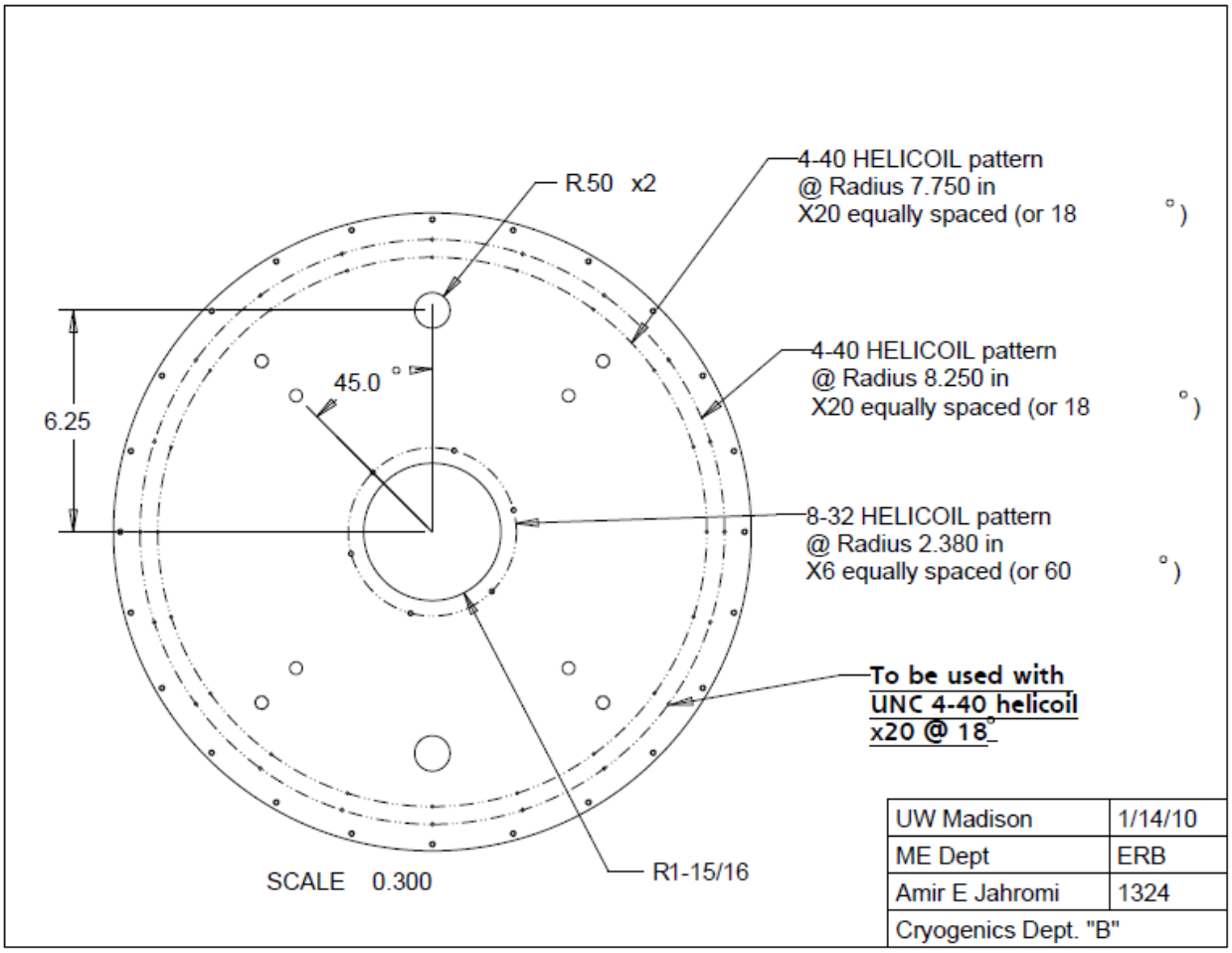

Second stage (1 of 2):

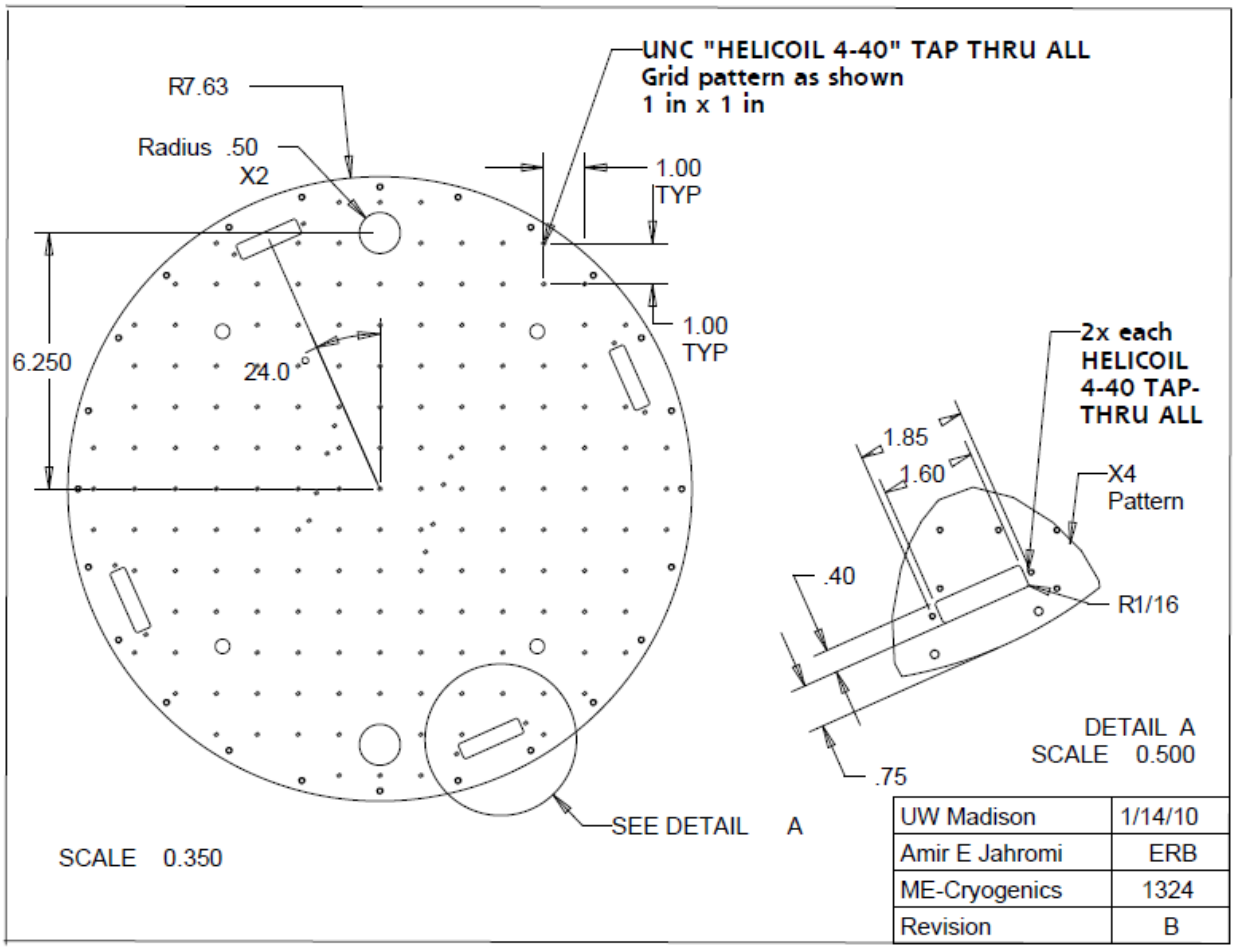

Second stage (2 of 2):

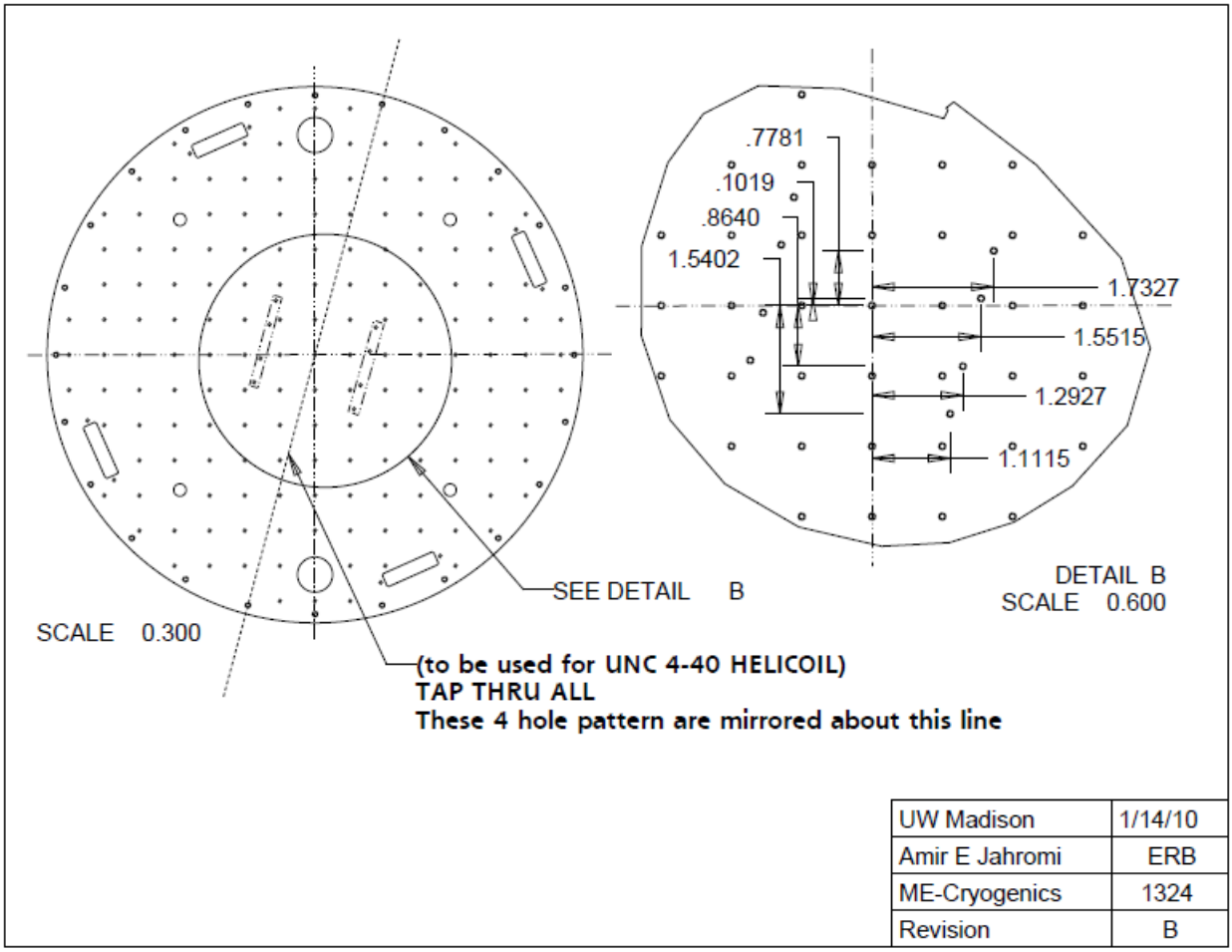

Appendix C Engineering drawing of the hermetic connector housing

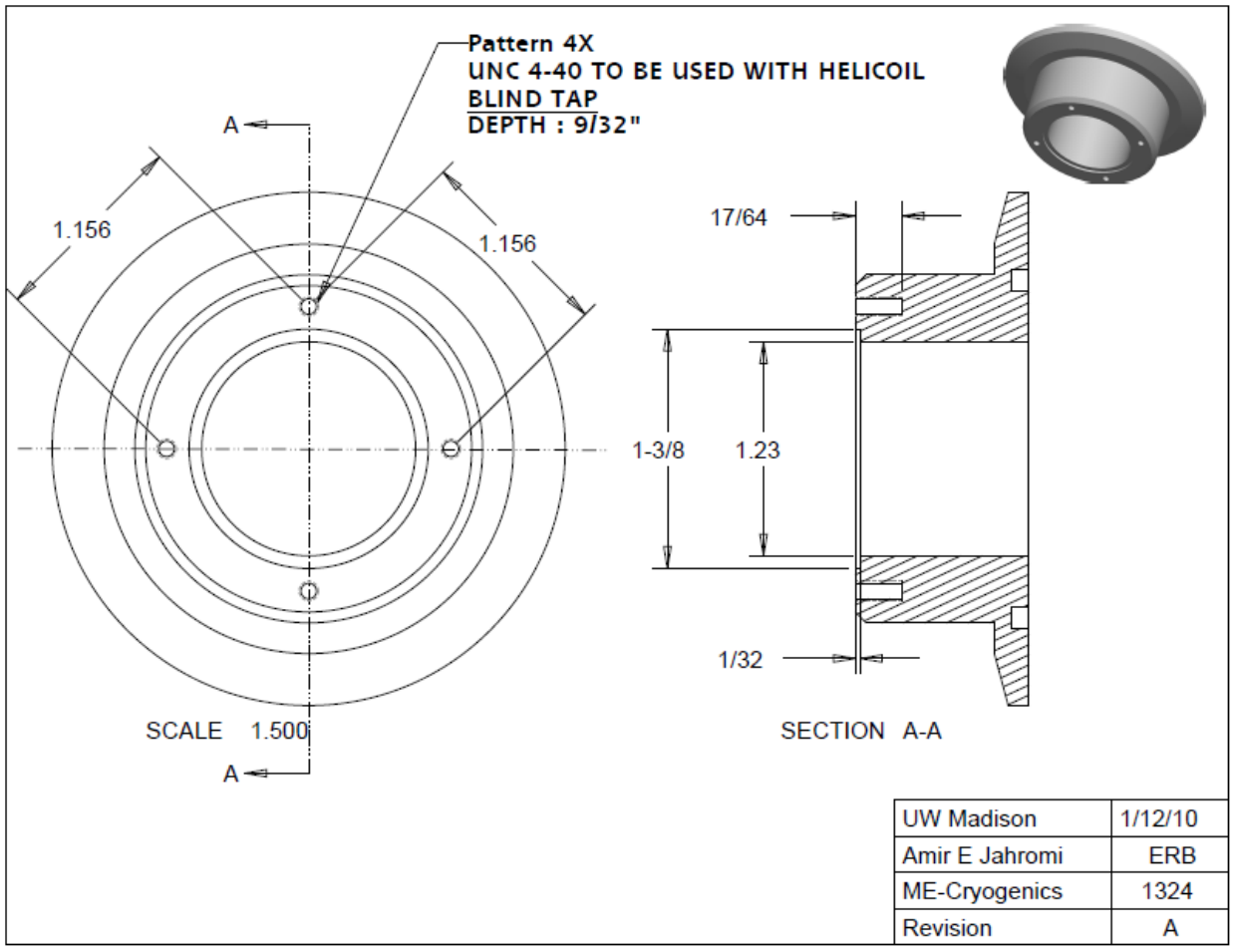

Appendix D An operation manual for the 1 K facility

Activating the system:

1. Make sure the 1 K facility line (the tubes used for the 1 K facility) are leak tight. Also ensure the 1 K heat switch loop is leak tight. Evacuating the tubes and spraying helium around the joints is not a good option for this case because it takes a long time to evacuate and detect helium through these narrow tubes. Instead, connect the leak detector to one of the ports on the Dewar and evacuate the chamber. Now pressurize the tubes with helium and see if any leak is detected. If leak is detected the detection must be localized and the leak must be repaired before running the experiment.
2. Turn on the roughing pump and start evacuating the Dewar and the tubes. The tubes need to be purged with helium several times: pressurize the tubes with helium and evacuate for 3 hours each time. Let the pump hold a vacuum through all the tubes (valves all open to vacuum).
3. Turn on the rotary vane pump to evacuate the 1 K pot.
4. Once the roughing pump becomes quiet, turn on the turbo pump; make sure the turbo pump reaches full speed at 1500 Hz. Let the turbo run until the DCU unit reads a pressure less than 10^{-4} mbar. This will be approximately 10 hours.
5. Make sure the water filter for the compressor is clean and the filter housing unit is free of debris and sediments. Turn on the water valve to the compressor unit.
6. Turn on the main brake switch on the compressor and push the green “on” button to activate the compressor. The cryocooler will start cooling.
7. Monitor the temperature. Once the temperature of the first stage and second stage reach ~40K and ~10 K respectively, turn on the heat switch by sending helium through the heat

switch loop. (Note that the temperature of the second stage is higher than it's supposed to be. This is normal because of the radiation heat load from the 1 K pot assembly to its surroundings). Also open the exhaust valve of the heat switch. Cold helium will be discharged to the ambient. Ensure adequate flow by submerging the tube in a beaker that contains water and observing the bubble formation.

8. Once the temperature of the 1 K pot assembly reaches ~40 K, pressurize the 1 K pot loop with helium. Make sure the capillary is not blocked by closing off the valve that is connected to the rotary vane pump and observing a pressure rise read by the thermocouple gauge. (Note that the thermocouple gauge is calibrated for nitrogen therefore the pressure reading is not accurate for helium. Observing a small deviation in pressure reading is enough to ensure helium flow.) Open the valve after this process.
9. Monitor the temperature of the 1 K heat exchange platform. The temperature should drop to a nominal 1 K. The 1 K pot can now be used to provide the necessary cooling for the desired experiment. To increase or decrease the flow of helium to the pot, change the inlet pressure by adjusting the knob on the regulator.

Deactivating the system:

1. BEFORE SHUTTING OFF THE CRYOCOOLER, shut off the valve that sends helium to the 1 K facility. Wait until all the liquid helium in the pot is evaporated. Ignoring this step can cause serious damage to the pot seal and the tubing joints due to rapid temperature increase and sudden pressure rise in the 1 K pot.
2. Use the heater to heat the 1 K pot assembly. Wait until the temperature of the 1 K pot increases to a temperature higher than the boiling point of helium at the specified inlet pressure.

3. Start evacuating the inlet of the 1 K pot by turning the inlet valves toward vacuum. Let the rotary vane pump evacuate the helium.
4. Shut off the cryocooler by pushing the "off" button on the compressor. Feel the water return hose from the compressor to evaluate the water temperature. Turn off the water once the return water is cold. Turn off the main switch on the compressor.
5. If quick warm up is desired instead of a natural drift then close the valve between the turbo pump and the roughing pump. Turn off the turbo pump and wait until it stops completely. Send a small amount of helium into the Dewar through one of the ports and observe the temperature rise.
6. Open the valve between the turbo pump and the roughing pump and let the roughing pump evacuate the chamber. It is now safe to send small amounts of helium, one at a time through the port.
7. Once the temperature of all the components in the Dewar is above the freezing point of water, turn off the roughing pump and the rotary vane pump. (It is extremely important to not let air enter the Dewar below the freezing point of water because the aluminized Mylar sheets have a tendency to absorb water. It is hard to extract this water out of the sheets and will take substantial amounts of time to evacuate the Dewar).

Appendix E Calibration results for the newly calibrated thermometers

Calibration results for the Cernox thermometer with **serial number X58373** is:

Temperature (K)	Electrical resistance (ohm)
290.550000	48.3650
272.420200	50.3882
270.001300	50.6751
260.008700	51.9157
250.004900	53.2449
240.013500	54.6611
230.010800	56.1831
220.026000	57.8099
210.023100	59.5689
200.026100	61.4594
190.000100	63.5114
180.019800	65.7252
170.015800	68.1401
160.019500	70.7735
150.002700	73.6602
140.003000	76.8375
130.017500	80.3395
120.012000	84.2519
110.005500	88.6358
100.017500	93.5997
95.015050	96.3448
90.010650	99.2967
85.008660	102.4794
80.003160	105.9275
75.007510	109.6775
70.001010	113.7954
65.000210	118.3190
60.007470	123.3519
55.004500	128.9895
50.001780	135.3645
48.006180	138.1567
45.008880	142.6455
42.007680	147.5574
39.004650	152.9642
36.007220	158.9200
32.002230	167.9577

29.366410	174.7402
29.366410	174.7402
27.000020	181.6783
24.500450	189.7377
22.000080	198.9574
20.000360	207.4025
18.500510	214.5169
17.000450	222.4776
15.500800	231.4971
14.000350	241.8840
12.500410	254.0745
11.008000	268.7309
9.882807	281.7406
8.895204	295.6969
7.670432	316.6837
6.562784	341.4522
5.704829	366.2901
4.955129	394.2186
4.303099	421.4909
4.175000	428.7694
4.052717	436.1382
3.952736	442.4793
3.852745	449.1189
3.751741	456.1699
3.651966	463.5154
3.552343	471.2416
3.452620	479.4207
3.352950	488.0515
3.253213	497.2087
3.153077	506.9826
3.053258	517.3445
2.953426	528.4271
2.842396	541.6833
2.745211	554.1887
2.645822	567.9374
2.546117	582.8032
2.446568	598.9338
2.346927	616.5338
2.153770	655.5123
2.091866	669.6684
1.996397	693.3228
1.897089	720.7326
1.848198	735.4598
1.799620	751.0066
1.742893	770.1554

1.721509	777.8714
1.699451	786.0425
1.676091	794.9656
1.651507	804.6740
1.631734	812.7241
1.611130	821.3560
1.589330	830.7927
1.566603	840.9754
1.542512	852.1623
1.516488	864.7374
1.497841	874.0656
1.487912	879.1455
1.473695	886.5618
1.458771	894.5296
1.448631	900.0462
1.438220	905.8146
1.421808	915.1189
1.416290	918.3001
1.410836	921.4806
1.405351	924.6993
1.392636	932.6675

Calibration results for the Cernox thermometer with **serial number X58374** is:

Temperature (K)	**Electrical Resistance (ohm)**
290.550000	51.6090
272.420200	53.8791
270.001300	54.2074
260.008700	55.6017
250.004900	57.1016
240.013500	58.7018
230.010800	60.4220
220.026000	62.2676
210.023100	64.2607
200.026100	66.4138
190.000100	68.7510
180.019800	71.2824
170.015800	74.0464
160.019500	77.0687
150.002700	80.3931
140.003000	84.0621
130.017500	88.1232

120.012000	92.6720
110.005500	97.7898
100.017500	103.6121
95.015050	106.8416
90.010650	110.3272
85.008660	114.0950
80.003160	118.1888
75.007510	122.6505
70.001010	127.5700
65.000210	133.0016
60.007470	139.0485
55.004500	145.8579
50.001780	153.5934
48.006180	156.9960
45.008880	162.4805
42.007680	168.5018
39.004650	175.1463
36.007220	182.5020
32.002230	193.7199
29.366410	202.1853
29.366410	202.1853
27.000020	210.8389
24.500450	220.9994
22.000080	232.6862
20.000360	243.4533
18.500510	252.5668
17.000450	262.8109
15.500800	274.4756
14.000350	287.9835
12.500410	303.9297
11.008000	323.2443
9.882807	340.5550
8.895204	359.2054
7.670432	387.4940
6.562784	421.2466
5.704829	451.8400
4.955129	490.7998
4.303099	535.3156
4.175000	545.6770
4.052717	556.1884
3.952736	565.2585
3.852745	574.7847
3.751741	584.9306
3.651966	595.5137
3.552343	606.6925

3.452620	618.5540
3.352950	631.1253
3.253213	644.4802
3.153077	658.7899
3.053258	674.0322
2.953426	690.3690
2.842396	710.0063
2.745211	728.6258
2.645822	749.1693
2.546117	771.4878
2.446568	795.8162
2.346927	822.5040
2.153770	882.1698
2.091866	903.9968
1.996397	940.7231
1.897089	983.5616
1.848198	1006.7136
1.799620	1031.2576
1.742893	1063.0476
1.721509	1075.2279
1.699451	1088.1540
1.676091	1102.2881
1.651507	1117.7198
1.631734	1130.5246
1.611130	1144.2836
1.589330	1159.3635
1.566603	1175.6844
1.542512	1193.6745
1.516488	1213.9437
1.497841	1229.0172
1.487912	1237.2521
1.473695	1249.2883
1.458771	1262.2268
1.448631	1271.2227
1.438220	1280.6116
1.421808	1295.8022
1.416290	1301.0057
1.410836	1306.2045
1.405351	1311.4845
1.392636	1324.5393

Calibration results for the Cernox thermometer with **serial number X58375** is:

Temperature (K)	**Electrical resistance (ohm)**

290.550000	53.3680
272.420200	55.7660
270.001300	56.1079
260.008700	57.5792
250.004900	59.1552
240.013500	60.8417
230.010800	62.6575
220.026000	64.6066
210.023100	66.7145
200.026100	68.9913
190.000100	71.4682
180.019800	74.1519
170.015800	77.0880
160.019500	80.3026
150.002700	83.8451
140.003000	87.7555
130.017500	92.0929
120.012000	96.9610
110.005500	102.4545
100.017500	108.7097
95.015050	112.1905
90.010650	115.9474
85.008660	120.0112
80.003160	124.4340
75.007510	129.2658
70.001010	134.5941
65.000210	140.4882
60.007470	147.0656
55.004500	154.4889
50.001780	162.9362
48.006180	166.6550
45.008880	172.6576
42.007680	179.2640
39.004650	186.5653
36.007220	194.6657
32.002230	207.0595
29.366410	216.4360
29.366410	216.4360
27.000020	225.8885
24.500450	237.1921
22.000080	250.2296
20.000360	262.2719
18.500510	272.4915
17.000450	284.0022
15.500800	297.1415

14.000350	312.3976
12.500410	330.4637
11.008000	352.4184
9.882807	372.3445
8.895204	393.6960
7.670432	426.1958
6.562784	465.1401
5.704829	504.8967
4.955129	550.3426
4.303099	602.5813
4.175000	614.7815
4.052717	627.1832
3.952736	637.8886
3.852745	649.1487
3.751741	661.1457
3.651966	673.6770
3.552343	686.9397
3.452620	701.0199
3.352950	715.9610
3.253213	731.8750
3.153077	748.9334
3.053258	767.1322
2.953426	786.6719
2.842396	810.1978
2.745211	832.5288
2.645822	857.2213
2.546117	884.1000
2.446568	913.4476
2.346927	945.7121
2.153770	1018.0193
2.091866	1044.6243
1.996397	1089.4118
1.897089	1141.7292
1.848198	1170.0584
1.799620	1200.1191
1.742893	1237.3989
1.721509	1252.4506
1.699451	1268.4509
1.676091	1285.9605
1.651507	1305.0492
1.631734	1320.9356
1.611130	1338.0142
1.589330	1356.7109
1.566603	1376.9517
1.542512	1399.2668

1.516488	1424.4243
1.497841	1443.1535
1.487912	1453.3695
1.473695	1468.3054
1.458771	1484.3885
1.448631	1495.5595
1.438220	1507.2410
1.421808	1526.1000
1.416290	1532.5726
1.410836	1539.0446
1.405351	1545.6104
1.392636	1561.7618